Proceeding Book of
First Conference for Engineering Sciences and Technology (CEST-2018)
(Part 1)

Communication and Information Technology

25-27 September 2018

Garaboulli - Libya

Table of Contents

Fiber-Optic Temperature Sensor Design Adapted for Libyan Environment

Mohammed Bin Saeed[1], Mohamed Otman Twati[2]
bin703m@gmail.com[1], M.twati@uot.edu.ly[2]
[1, 2] Department of Electrical and Electronic Engineering, University of Tripoli, Libya

ABSTRACT

In this work, the design of the Fiber optic Temperature Sensor has been performed using two different techniques aimed at determining the optimum design parameters of the fiber optic sensor that should work properly in the Libyan environment (temperature: -13 to 57.8 degrees Celsius). The first technique is based on Fabry-Perot Interferometer that tracks the phase change of the received light by the interferometer due to the sensitivity of the Fabry-Perot's cavity to the surrounding temperature changes. Three different substances (GaAs, Ge and Si) were used in determining the optimum design parameters of the fiber optic sensor. The optical wavelength used is 1550nm with line width of 40nm. The material selected is Si where the optimum Fabry-Perot length was found to be 20.7μm.The second technique studied is based on Fiber Coupling Actuated by a Bimetal Strip to read the change in temperature with respect to coupling power loss. Three different standard Bimetal types were used for the design of the strip, (KANTAL 200 TB20110 Ni/MnNiCu), (KANTAL 135 Ni/NiMn-steel) and (KANTAL100 TB0965 Ni/NiMn-steel). The (KANTAL 200 TB20110 Ni/MnNiCu) Bimetal material was selected for the optimal sensor design. The optimum design length, delta deflection and thickness for the strip were found to be 5.6μm, 35μm and 1.3μm respectively.

Keyword— optical fiber; temperature sensor design; fabry-perot interferometer.

1. Introduction

Over the last few decades, optical fibers have been widely deployed in telecommunication industries owing to their special performance as the best light guidance. Optical fibers have been intensively investigated at various sensor fields, owing to their unique characteristics such as multiplexing, remote sensing, high flexibility, low propagating loss, high sensitivity and low fabrication cost. Temperature is one of the most widely measured parameters within safety industry and science. In many applications, sensors are required, because of their immunity to electromagnetic interference, small in size, suitability for remoting and having lightweight. In addition, they allow operation in harsh environments to replace conventional electronic sensors due to their possibility of performing measurements in environments suffering from electromagnetic disturbance, or in environments where electronics cannot survive. Fiber optic sensors can survive offer an excellent solution to many of these challenges. Different fiber optic sensor techniques have been designed and many researches are focused on developing reliable and cost-effective fiber temperature sensors. In this work, we first describes Fabry-Perot interferometer temperature sensor that uses a reflective etalon. The etalon's optical path difference (OPD) is a temperature dependent. This is due, primarily, to the dependence of its refractive index to the temperature variations. The sensed temperature can then be determined

from the positions of the minima in the sensor's output spectrum by several simple types of spectrum analyzers, other type of sensing devices that use power coupling loss between two fibers to determine the temperature, will be described next. The designed fiber-optic temperature sensors would be used highly in high power generation rooms.

2. Materials and Methods

2.1. Fabry-Perot Interferometer

Basically, the Fabry-Perot temperature sensor (FPI) is a thin platelet of a material that has a temperature-dependent refractive index [1]. It is composed of two parallel reflecting surfaces separated by a certain distance called etalon and are classified into two categories: one is extrinsic and the other is intrinsic[2], [3]. The extrinsic FPI sensor uses the reflections from an external cavity formed out of the interesting fiber [4]. Figure 1 (a) shows an extrinsic FPI sensor, in which the air cavity is formed by a supporting structure. Since it can utilize high reflecting mirrors, the temperature-sensitive interferometer is constructed from thin films that are deposited directly onto the end of an optical fiber [5]. In other sense, when the cavity material is not the fiber itself, it is called extrinsic and it is shown in Figure 1 (b). Figure 2 shows a more detailed Fiber-optic temperature sensor using a thin-film Fabry-Perot interferometer.

(a) (b)

Figure 1: (a) Extrinsic FPI sensor made by forming an external air cavity, and (b) intrinsic FPI sensor formed by two reflecting components, R1 and R2, along a fiber.

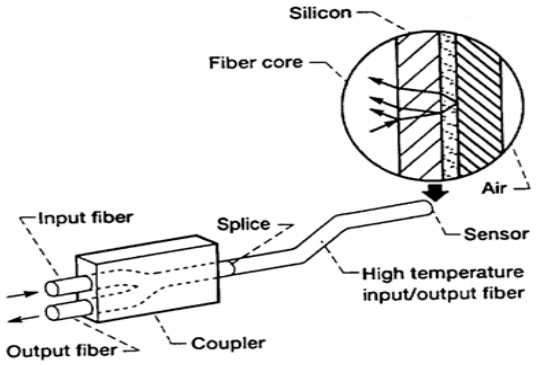

Figure 2: Fiber-optic temperature sensor using a thin-film Fabry-Perot interferometer.

2.2. Fiber Coupling Actuated by a Bimetal Strip

Coupling based intensity modulated fiber-optic sensors can be configured in basically two ways: either in a reflective arrangement as shown in Figure 3(a), or in a transmissive arrangement, using straightforward transmission from one fiber to the other, as in Figure 3 (b).

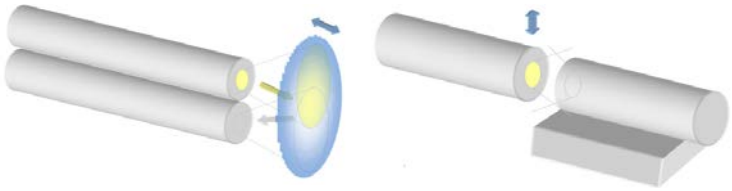

(a) (b)

Figure 3: (a) Schematic view of a coupling based intensity modulated fiber-optic sensor using a reflective configuration (b) using a transmissive configuration.

The bimetal strip Consists of different metals expand at different rates as they warm up, behave in different manner when exposed to temperature variation owing to their different thermal different thermal expansion rates. One end of straight bimetallic strip is fixed in place as the strip is heated the other end tends to curve away from, the side that has the greater coefficient of linear expansion as shown in Figure 4.

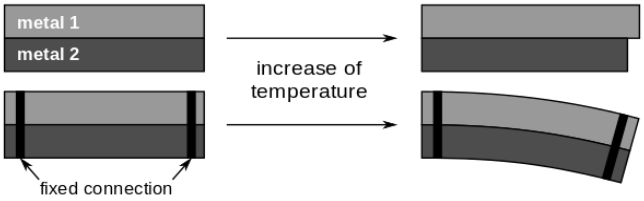

Figure 4: Shows the bimetal strip.

This part should contain sufficient detail to reproduce reported data. It can be divided into subsections if several methods are described. Methods already published should be indicated by a reference [4], only relevant modifications should be described.

3. Theory and Calculation

3.1. Fabry-Perot Interferometer

Here, the interferometer's optical path difference (OPD) is given by:

$$\Lambda_{OPD} = 2n_1 L \cos\theta_1 \quad (1)$$

And:

$$\Phi = \frac{2\pi}{\lambda}\Lambda_{OPD} \quad (2)$$

As shown if the length, L, of the cavity increases the phase shift, Φ,between two reflected light increases as well as refractive index of the material n_1. the reflectivity can be rewritten as:

$$R_F = \frac{F \sin\Phi^2}{1 + F \sin\Phi^2} \quad (3)$$

$$F = \frac{4R}{(1-R)^2} \quad (4)$$

Where:

With:

$$R = \frac{(n_1 - n_2)^2}{(n_1 + n_2)^2} \quad (5)$$

The transmissivity of the ideal Fabry-Perot interferometer is given by:

$$T_F = \frac{1}{1 + F \sin \Phi^2} \quad (6)$$

As expected, for zero loss, $T_F + R_F = 1$, Figure 5 shows that for (GaAs) for designed length as function (Φ)[7].

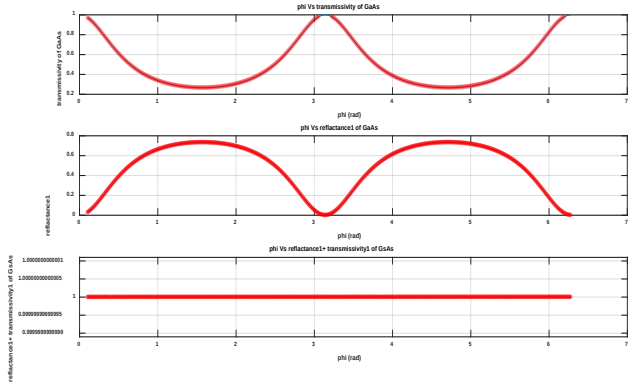

Figure 5: (Reflectance + Transmissivity) GaAs for designed length as function of (Φ).

3.2. Fiber Coupling Actuated by a Bimetal Strip

The temperature dependent deflection δ of a bimetal strip clamped at one end is given by:

$$\delta = \alpha_d . (T - T_0) \frac{L_0^2}{t} \quad (7)$$

Where α_d is the specific deflection , T represents the variable the temperature , $L_0$is the free strip length at room temperature T_0 and t represents the strip thickness. For a fiber sensor configuration according to Figure 6

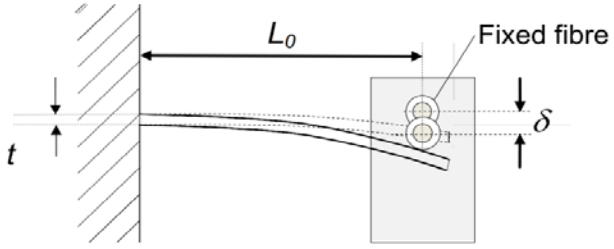

Figure 6: Temperature sensor operation principle.

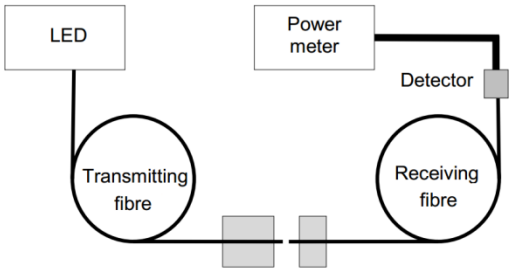

Figure 7: Temperature sensor operation principle.

In the linear temperature region of the bimetal strip , the deflection can be counted from any reference temperature T_0, which means that the reference temperature could be chosen when the moveable fiber has a zero offset to the fixed fiber . The coupled power P between two fibers as a function of temperature T[8], can thus be written as:

$$P(T) = P_0 . e^{-k(T-T_0)^2} \quad (8)$$

A Theory section should extend, not repeat, the background to the article already dealt with in the Introduction and lay the foundation for further work. In contrast, a Calculation section represents a practical development from a theoretical basis.

4. Results and Discussion

4.1. Fabry-Perot Interferometer

The design consists of the selection of a material (GaAs, Ge, Si) and the determination of the optimum thickness at for the Libyan environment range, the interferometer's reflectance is minimized at resonance, or $\Phi = \pi m$, where m is an integer. For the ideal Fabry-Perot interferometer, the minimum reflectance $[R_F]_{min} = 0$. In terms of wavelength, the resonance condition is at $\lambda = \lambda_m$where:

$$m\lambda_m = \Lambda_{OPD} \quad (9)$$

The maximum reflectance, which occurs at $\Phi = \pi(m+1/2)$ and is given by:

$$[R_F]_{max} = \frac{F}{1+F} \quad (10)$$

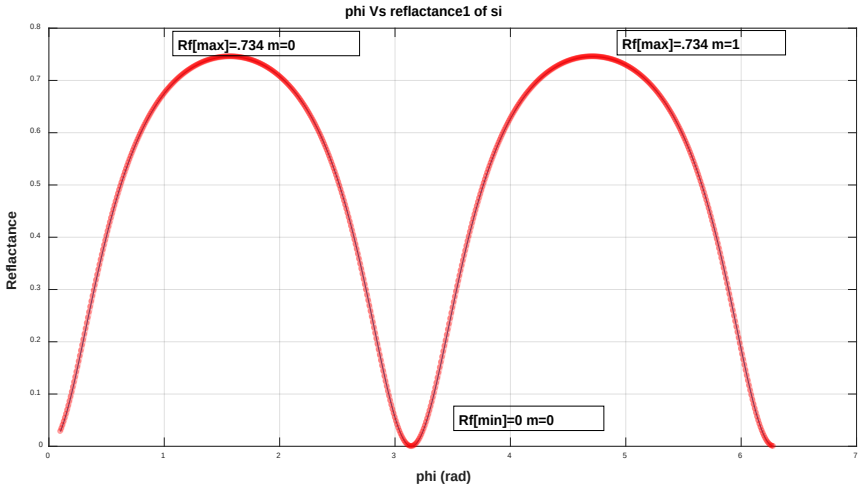

Figure 8: Shows the reflectance of (GaAs) for designed length (20.7 μm).

The maximum reflectance obtained for the designed length, L=20.7 μm, is equal 0.734, for the integers m=0, 1, 2 as shown in Figure 8. The phase sensitivity is obtained by differentiating equation (3), which gives:

$$\frac{dR_F}{d\Phi} = \frac{F \sin 2\Phi}{(1 + F \sin \Phi^2)^2} \tag{11}$$

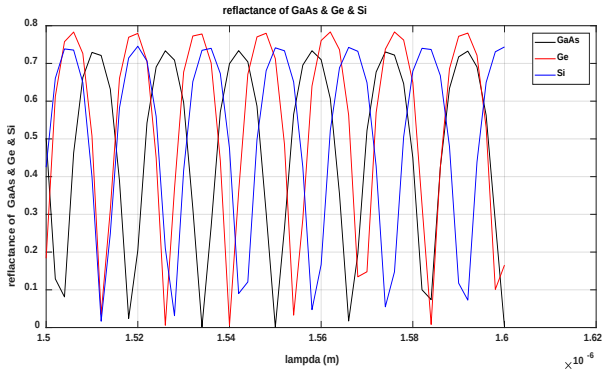

Figure 9: Comparison of phase sensitivity of (GaAs) & (Ge) & (Si) as function of (λ).

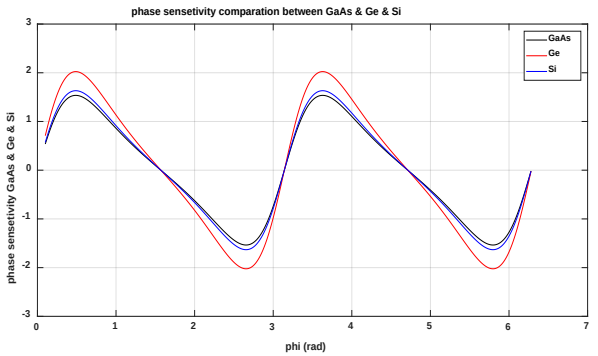

Figure 10: Comparison of phase sensitivity of (GaAs) & (Ge) & (Si) as function of Φ.

The temperature sensitivity of the Fabry-Perot's phase shift is given by:

$$\frac{d\Phi}{dT} = \pi \frac{\Lambda_{OPD}}{\lambda} \kappa_{\Phi} \quad (12)$$

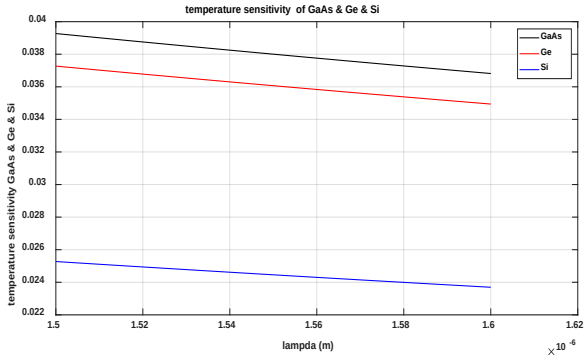

Figure 11: Comparison of temperature sensitivity of the Fabry-Perot's phase shift of (GaAs) & (Ge) & (Si) as function of λ and L=20.7μm.

By integrating both sides $\int d\Phi = \int \pi \frac{\Lambda_{OPD}}{\lambda} \kappa_{\Phi} \, . \, dT, \Phi = \pi \frac{\Lambda_{OPD}}{\lambda} \kappa_{\Phi} . T$

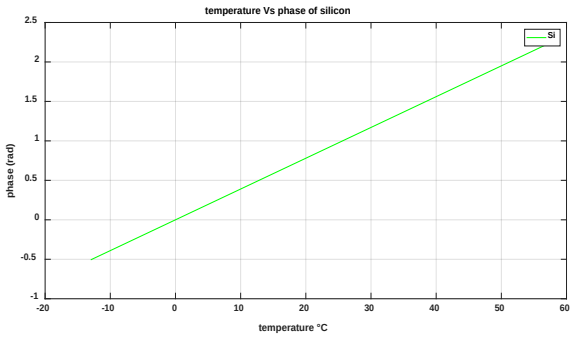

Figure 12: Phase vs. Temperature.

Where:

$$\kappa_{\Phi} = \kappa_n + \kappa_L \quad (13)$$

Here, κ_n is the thermo-optic coefficient

$$\kappa_n = \frac{1}{n_1} \frac{dn_1}{dT} \quad (14)$$

And κ_L is the thermal expansion coefficient,

$$\kappa_L = \frac{1}{L} \frac{dL}{dT} \quad (15)$$

The temperature sensitivity of the Fabry-Perot's reflectance can be determined by substituting from equations (11) and (12) into:

$$\frac{dR_F}{dT} = \left(\frac{dR_F}{d\Phi}\right)\left(\frac{d\Phi}{dT}\right) \quad (16)$$

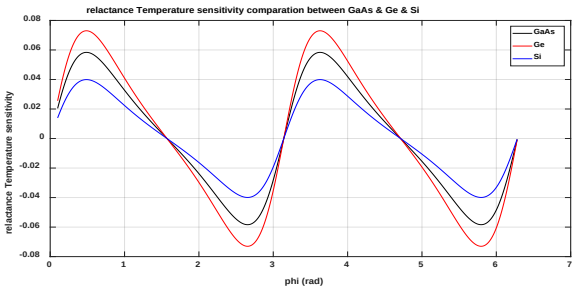

Figure 13: Comparison of temperature sensitivity of the Fabry-Perot's reflectance of (GaAs) & (Ge) & (Si) as function of (Φ).

(Ge) gave us best results for temperature sensitivity of the Fabry-Perot's reflectance because it has the largest refractive index[7].

4.2. Selection of Temperature Sensitive Material

G. Beheim has previously summarized a comparison of candidate materials for a thin-film temperature sensor. The temperature sensitivity of various candidate materials requires that sensitivity figure-of-merit be independent of the film thickness, Table1 tabulates the candidate materials in descending order of κ_Φ. This table provides n,κ_n, andκ_L, together with the wavelengths at which the optical properties were measured, all data.

Table 1: Properties of candidate Fabry-Perot materials. Units of κ_n, κ_L, and κ_Φ are 10^{-6}/0C.

Material	λ (μm)	n	κ_n	κ_L	κ_Φ
GaAs	0.9	3.6[7]	120[7]	5.7[5]	126
Ge	2.55	4.06[7]	100[7]	5.7[7]	106
Si	2.5	3.44	46[7]	2.6[7]	
	1.5	3.5	53[7]		
	1.26	3.51[7]	59[7]		
	0.78	3.695[7]	76[7]		79

So the temperature induced phase change is almost entirely caused by the change in refractive index. Of the three materials with the largest values of κ_Φ, silicon is best suited for this range application and available almost everywhere, however, it is highly absorbing at the emission wavelengths of AlGaAs LEDs. At 830nm, the absorption coefficient of germanium is $4.5\times104cm^{-1}$, so that transmission through 1 μm produces a 20-dB loss. At 1.3μm, is much lower, $0.68\times104\ cm^{-1}$, but this wavelength is outside the range of inexpensive silicon photodiodes, Silicon is preferred to germanium for this application, because its absorption coefficient is much lower at the AlGaAs emission wavelengths. At 830nm,α=$0.19\times104\ cm^{-1}$, which causes a 17% absorption in 1.0μm [6].

4.3. Determination of Fabry-Perot Sensor's Thickness

For a typical AlGaAs's LED we can choose any LED,$\frac{\Delta\lambda_{LED}}{\lambda_m} \geq \frac{\lambda_m}{2\Lambda_{OPD}}$,$\Lambda_{OPD} = m \times \lambda_m$, λ=1550nm and $\Delta\lambda_{LED}$= 40nm, which gives m≥19.3. For silicon, this correspondstoL1≥4 μm.

$$m \leq \frac{1}{\kappa_\Phi (T_{max} - T_{min})} \quad (17)$$

For a silicon sensor with a -13 to 57.80°C.

$$\Lambda_{OPD}/\lambda_m \leq \frac{1}{79\times10^{-6}(57.8-(-13))}=\frac{2\times3.695\times L\times\cos(3.1)}{1550\times10^{-9}} \leq \frac{1}{79\times10^{-6}(57.8-(-13))}$$

$$L \leq \frac{1550\times10^{-9}}{2\times3.695\times\cos(3.1)\times79\times10^{-6}(57.8-(-13))}$$=37.55μm,must be less than 178.7μm, which gives L<.37.55μm. In this case we chose L1= 20.7μm, so that L1 is within the above limiting cases so the optimization length is 20.7μm.

4.4. Fiber Coupling Actuated by a Bimetal Strip

First we should measure P_0, the coupled power, at temperature T_0, i.e., at zero offset (deflection), the moveable fiber at zero position, the design factor k is given by :

$$\mathbf{k} = (\frac{\alpha_d}{w}.\frac{L_0^2}{t})^2 \quad (18)$$

where *w* is the characteristic radius of the modulation function of the sensor and typically 25μm, the temperature dependent loss **A**of the sensor, quoted in decibels (dB), can be derived as

$$\mathbf{A(T) = 10.\log\frac{p(T_0)}{p(T)} = K.(T-T_0)^2} \quad (19)$$

Using equations (18) and (19) the design constant**K** can be written as:

$$\mathbf{K} = (\frac{\alpha_d}{w}.\frac{L_0^2}{t})^2.\mathbf{10\log e} \quad (20)$$

Using formulas (7), (19) and (20) a temperature sensor for any temperature range in the linear region of the bimetal can be designed, The sensitivity of such a sensor can be adjusted by choosing a suitable bimetal (parameters $\alpha_d$and t) and by adjusting the free strip length L_0, T_0 should therefore be chosen to be a bit lower than the minimum temperature T_{min} to be measured, or a bit larger than the maximum temperature T_{max} also to be measured. The deflection range Δ is given by:

$$\Delta = \delta_m - \delta_{min} = \frac{\alpha_d L_0^2}{t}.(T_{max}-T_{min}) \quad (21)$$

Where δ_m is the desired maximum deflection and T_{max} and T_{min} are the maximum and minimum temperatures of the measurement range, corresponding to the desired deflection range. From equation (21) the fiber position L_0can be calculated, and using this value together with $\delta=\delta_{min}$and $T=T_{min}$, equation (7) gives the zero deflection temperature $T_0$for the right slope of the modulation curve. First we take three material with linear range that can measure our Libyan environment with specific deflection (20.8×10^{-6}, 13.9×10^{-6},10×10^{-6}), as shown in Table 2.In designing and calculating sensor's parameters we take the larger deflection range to increase the sensitivity, this is because our temperature range is large.

Table 2: Some details of standard bimetal types

Thermostatic Bimetal type DIN designation added		Specific deflection [10^{-6} K^{-1}]	Specific curvature [10^{-6} K^{-1}]	Linearity range [°C]	Max operating temperature [°C]	Resistivity [Ω mm² m^{-1}] at temperature °C 0	20	100	200	300	400	Thermal conductivity [Wm^{-1} °C^{-1}]	Modulus of elasticity [103 N mm^{-2}]	Standard hardness [HV] low exp. side	high exp. side	Density [g cm^{-3}]
230		22.7	43.0	-20–+230	330	1.04	1.05	1.15	1.22	1.28		6	135	210	200	7.8
200	TB20110	20.8	39.0	-20–+175	330	1.09	1.10	1.20	1.27	1.33		6	135	210	250	7.8
155	TB1577A	15.6	28.5	-20–+250	450	0.77	0.78	0.86	0.94	1.00	1.07	13	170	210	260	8.1
145		14.8	27.7	-20–+250	450	0.78	0.79	0.85	0.93	0.99	1.06	12	170	210	240	8.1
135		13.9	25.9	-20–+200	450	0.78	0.79	0.85	0.93	0.99	1.06	12	170	210	240	8.1
130		13.2	24.8	-20–+325	450	0.72	0.74	0.82	0.89	0.95	1.02	12	170	210	240	8.1
115	TB1170	11.7	22.0	-20–+380	450	0.68	0.70	0.78	0.86	0.93	0.99	13	170	210	240	8.1
100	TB0965	10.0	18.6	-20–+425	450	0.62	0.65	0.75	0.86	0.94	1.00	15	175	210	240	8.2
94S		9.5	17.8	-0–+200	450	0.84	0.85	0.90	0.95			12	190	210	250	8.1
60		6.0	11.3	-20–+450	450	0.19	0.21	0.28	0.37	0.47	0.59	44	190	230	240	8.0
50HT		5.0	9.4	-20–+500	550	0.635	0.66	0.72	0.78	0.83		20	200	240	340	7.8

Table 3: Bimetal data and calculated sensor design parameters for minimum deflection = 5 μm,T_{min}=-13 °C and T_{max}= 57.8 °C using a fiber coupling with a typical characteristic radius of w= 25μm.

Type	α_d (10^{-6} K^{-1})	t (mm)	Δ (μm)	L_0 (mm)	T_0 (°C)	K (10^{-3}dB K^{-2})	$A(T_{min})$ (10^{-3}dB)	$A(T_{max})$ (dB)
200	20.8	1.3	20	4.2	-15	0.55	2.2	2.938
			25	4.7	-18	0.86	21.7	4.978
			35	5.6	-20	1.7	83.2	10.278
			40	5.9	*60*	*2.2*	*11819.6*	*.0107*
135	13.9	0.8	20	4	-15	0.55	2.2	2.938
			25	4.5	-18	0.86	21.7	4.978
			35	5.3	-20	1.7	83.2	10.278
100	10	1.0	10	5.3	-15	0.55	2.2	2.938
			16	5.9	-18	.86	21.7	4.978
			25	7	-20	1.7	83.2	10.278

The sensitivity of the sensor in terms of the loss change in dB per temperature degree is given by the derivative of:

$$s(T) = \frac{d(A)}{d(T)} = 2.K.(T - T_0) \quad (22)$$

By integrate both sides $\int d(A) = \int 2KTd(T) - \int 2KT_0 d(T)$

$A = KT^2 - 2KT_0T$. Fig.14 shows the sensitivity versus the temperature at different deltas, whereas the comparison between the two devices is shown in Fig. 15.

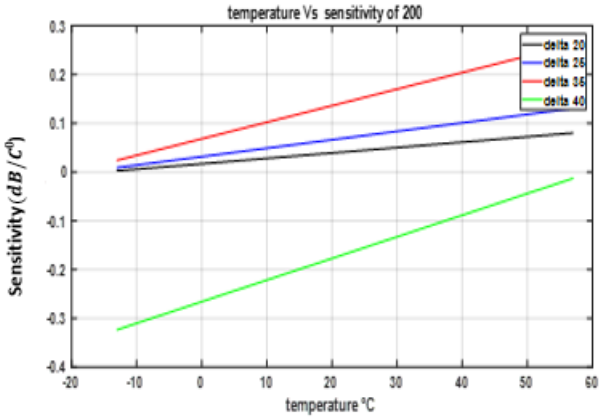

Figure 14: Sensitivity as a function of temperature for the sensor designs based on type200 bimetal listed in Table 3.

Table 3 shows the different material and the different design parameters, where the best design parameters obtained are at length of 5.6 mm and atΔ=35μm.

Clearly, Fabry-Perot technique sensor is more accurate than Intensity-type Fiber Optic Sensor, because the Fabry-Perot changing linearly with phase of silicon, so it is more suitable for our design purpose in the desired range of measurements than the other one.

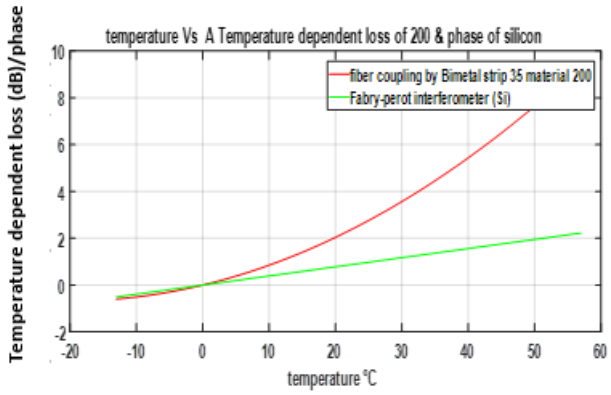

Figure 15: Comparison between two devices.

5. Conclusions

Two different types of fiber optic temperature sensors have been designed and studied. The two sensors were specially designed to be able to measure the temperature range (-13 ℃ to 57.8 ℃) that is well suited for Libyan environment. These types of fiber optics sensor are usually used in high power generators rooms, where the explosion risk factor is very high with the using of regular electric sensors. The first device is based on the Fabry-Perot interferometer with the material of silicon. The

optimum designed length obtained is 20.7μm for the operating wavelength of 1550nm. The second device designed is based on fiber coupling actuated by a bimetal strip. The designed length, delta deflection and thickness for the strip were found to be 5.6μm, 35μm and 1.3μm respectively.

From the simulation results, it is clear that the Fabry-Perot temperature sensor of silicon material changes linearly with phase while the sensor based fiber coupling by bimetal strip is not changing linearly with power loss, which would give less measuring accuracy and it is also more difficult to calibrate, however, it is more cheaper than Fabry-Perot sensor.

References

[1]. G. Beheim, "Fiber-Optic Thermometer Using Semiconductor-Etalon Sensor," Electron. Lett. 22, 238-239 (1985).

[2]. Fabry-Pérot Interferometer. Available online:

[3]. http://en.wikipedia.org/wiki/Fabry%E2%80%93P%C3%A9rot_interferometer,22/8/2017.

[4]. K. Kyuma, S. Tai, T. Sawada and M. Nunoshita, "Fiber-Optic Instrument for Temperature Measurement," IEEE J. Quantum Electron. QE-18, 676 (1982).

[5]. Kim, S.H.; Lee, J.J., Lee, D.C., Kwon, I.B. A study on the development of transmission-type extrinsic Fabry-Perot interferometric optical fiber sensor. J. Lightw. Techol. 1999, 17, 1869-1874.

[6]. L. Schultheis, H. Amstutz, and M. Kaufmann, "Fiber-Optic Temperature Sensing With Ultrathin Silicon Etalons," Opt. Lett. 13, 782 (1988).

[7]. Fu, H.Y.; Tam, H.Y.; Shao, L.Y.; Dong, X.; Wai, P.K.A.; Lu, C.; Khijwania, S.K. Pressure sensor realized with polarization-maintaining photonic crystal fiber-based Sagnac interferometer. Appl. Opt. 2008, 47, 2835-2839.

[8]. Glenn Beheim, Fiber-Optic Temperature Sensor Using a Thin-film Fabry-PerotInterferometer , Ph.D. thesis, Case Western Reserve University, Cleveland, Ohio, May 1996.

[9]. Johan Jason,"Theory and Applications of Coupling Based Intensity Modulated Fibre-Optic Sensors", Mid Sweden University,2008.

Employing Various Data Mining Techniques to Forecast the Success Rate of Information Technology Education Students

Mosbah Mohamed Elssaedi
mosbah_us@hotmail.com
Department of Computer Science, Faculty of Science, Sirte University - Libya

ABSTRACT

This study was designed to investigate the factors that affect the success rate of Information Technology Education students which composed of Computer Science and Information Technology. Several variables such as years of graduation, entrance exams, and other variables have been used for the investigation. Several data mining techniques such as linear regression, neural network, and decision tree have employed to determine the valid predictors and acceptability of the data mining technique. The results show that the best predictor taken from the entrance exams is non-verbal ability while the best forecasting using data mining is decision tree analysis with 99.19 percent accuracy. If the results taken from the system will be incorporated in entrance examinations results, admission office will be able to identify students that can graduate on-time and whose students should be taken as probationary in the program. It can also identify students not to be taken in the program to avoid waste of time in studying at the University.

Keyword— Neural network, linear regression, decision tree, forecasting, data mining.

1. Introduction

Technology is the application of scientific knowledge for practical purposes especially in industry, engineering and applied sciences. Technology can be used at work to extract materials, transportation, learning, manufacturing, creating artefacts, securing data, scaling business and more [1]. The benefits of technology in education have been a gateway to the new learning environment. Assistive technology that helps children with special needs such as an e-reader, adaptive voice software are a few good examples. The use of computers and innovation in classrooms has opened up an entirely new system for showing and successful learning. Computers generate huge amounts of information and can benefit the field of education, like helping students learn faster or make learning more interesting to some extent. With technology's rapid development, no surprise that there is an abundant of courses related to technology that is offered by different university worldwide.

The major problem is that at there is a big percentage of the unemployed with an average of 17% of college graduate came from Bachelor of Science in Computer Science and Bachelor of Science in Information Technology [2]. This sort of measurement is disturbing; it implies that colleges are delivering graduates with lacking abilities with the connection to Computer Science and IT which add to the unemployment rate. National development is every nation's goal throughout the world. A country is seen to be developed when underemployment and unemployment rates decrease if not eliminated. One of the probable reasons for this is the mismatch between education and employment.

Admission Examination or University Entrance Examination is believed to help students to select an appropriate course in college matching their aptitude and maintains a quality of education thereby, bringing national development in the country. Among the objectives of the creation of admission, examinations are to minimize aimless wastage of labour and different assets which generally could be coordinated towards more beneficial endeavours. It also assesses the capabilities and skills the students develop in their early studies which are necessary to be successful in college or even becoming an entrepreneur [3]. It can be very beneficial for students if followed but many students choose to deviate from the recommendations made by Admission by choosing another program in college. The huge amount of information and data, when analyzed can help in decision making and help to create a model that determines the success rate of Computer Science and IT student deviating their admission exams results using data mining. Data mining uses sophisticated mathematical algorithms to segment the data and evaluate the probability of future events and outputs useful information while reducing the quantity of data [4]. This study aims to develop a model that determines the success rate of computer science and IT student that deviated from a recommendation from Admission result. Furthermore, to find out the field of interest that should be improved to pass computer science or IT degree and help the academe reduce drop-outs and shifters of the program offered.

This study was designed to investigate the factors that affect the success rate of Computer Science and IT student that deviates from the recommendation of admission examination. It will also correlate to the abilities of students in the result of admission examinations to the date of graduation of Computer Science and IT students and to develop a model that determines the success rate of students. Specifically the research will be guided by the following questions: what are the predictors to be considered to determine the success rate of Computer Science and IT student that deviate from the recommendation of admission examinations?, what are the correlations of the predictors in passing On – Time the Computer Science degree? and what are the data mining techniques and algorithms will be used in the forecasting model?

2. Related Literature

Career assessment is the first step in career planning. Admission Test or College Entrance Examination is one of the career assessments given by the any University to entrants students. There is a study that aims student's performance base on information's like attendance, class test, name, age, course, and topographic location or address. In this research, they used the classification method of data mining using a decision tree. A forecasting system model was developed in a study in which the main goal is to analyze the learning behaviour of the higher education students [5]. They used the decision tree, a popular classification method of data mining that results in a flowchart-like a tree structure where each node denotes a test on an attribute value. Another forecasting system model was developed which the main goal is to understand student data such as name, age, address, student's grades and course for career selection and job absorption rate after graduation [6]. There is research that finds out whether natural talents and interest of 116 students based on admission exams result match the program that the students have enrolled in. In this study, the researcher employed a

qualitative research design. There are eight potentials/inclinations of students measured: scientific ability, reading comprehension, verbal ability, mathematical ability, clerical ability, manipulative skills, nonverbal ability and entrepreneurial skills [7]. In the conducted study, the results show that the respondents have varied occupational interest based on an admission exam. Based on this research, most of the respondents choose not to enrol in the program that matches respondent's field of interest that leads to the respondent's failure on some of the respondent's subject while the respondents that enrol in the program that matches the respondent's field of interest were seen to have become successful.

3. Methods

In building the forecasting model, student data such as admission examination field of interest, occupational Interests and the student's date of graduation were used to find the relationship by feeding to the data mining analyzing tool. The data sets that were used to develop the forecasting model are the records of these students of Computer Science and IT degree. The data of Computer Science and IT student batch 2011–2015served as the training data of the forecasting model and the Computer Science student batch 2016served as the test data that evaluate the model The data used were combined data from the admission office of one University in the Philippines and compared to the data of Sirte University. The data was laballed according to the data to conform with Sirte University. Rapidminer, a data mining tool is used to process data and create a forecasting model. Certain algorithms are used in creating the forecasting model and to find out the best ability in admission exams that best affect the performance of the Computer Science and IT students.

Descriptive Correlation. The correlation measures the strength and direction of a linear relationship between two variables. The value correlation is always between +1 and -1. The following are an interpretation of values in correlation:

- Exactly -1. A perfect downhill linear relationship.
- – 0.70. A strong downhill linear relationship.
- – 0.50. A moderate downhill linear relationship.
- – 0.30. A weak downhill linear relationship.
- 0. No linear relationship.
- + 0.30. A weak uphill linear relationship.
- + 0.50. A moderate uphill linear relationship
- + 0.70. A strong uphill linear relationship.
- Exactly +1. A perfect uphill linear relationship.

3.1 Conceptual Framework

A conceptual framework was used by the researchers to outline the courses of action or to present a preferred approach to the developed system. Asshown in Figure1, there are five phases in the proposed forecasting model:

1. *Data Gathering* – this is the first phase of the model where data such as the admission examination result were extracted which contains the different fields of interest, the occupational interest of the student and the student graduation date. This data will be saved in the repository.
2. *Data Pre-Processing* – the second phase of the model this is where the data cleansing, estimating of missing values and normalization of database takes place.
3. *Modelling*– the third phase of the model is where the building of the model takes place. The data mining tool will analyze all the data and outputs all data mining algorithms results for each technique.
4. *Determine the Success Rate* – the fourth phase of the model is the entry point of the test data to evaluate the model's accuracy.
5. *Result* – the last phase of the model is where the output will be displayed in a dashboard which is the success rate of computer science and IT students that deviates from the admission results.

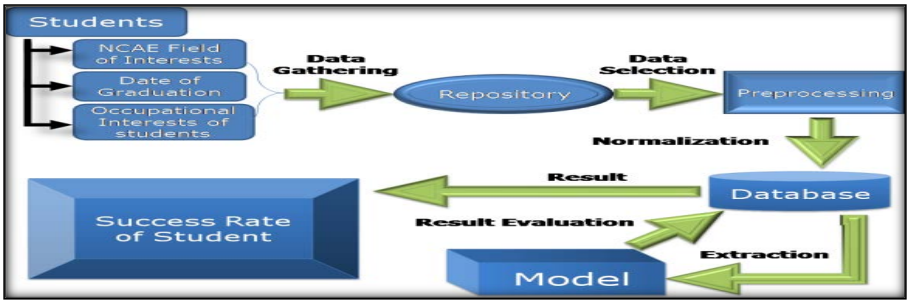

Figure1: Phases of the model

4. Results and Analysis

4.1 Predictors for Success Rate

The variables used in the study are the data of Computer Science and IT students from the school year 2011– 2015 with 368. The data setis put in the outliner detection to minimize the noise of the actual datasets and to increase the accuracy of the forecasting model before measuring the significance of each predictor.

Table 1: Predictors and variables

Dependent Variable	Independent Variable	Optimize Selection
Date of graduation	Clerical Ability	Clerical Ability
	Nonverbal ability	Nonverbal ability
	Scientific Ability	Scientific Ability
	Mathematical Ability	Mathematical Ability
	Manipulative skills	Manipulative skills
	Verbal ability	Reading Comprehension
	Reading Comprehension	Entrepreneurial Skills
	Entrepreneurial Skills	

Table 1 shows the predictors and the variables used in the study. The researcher used the date of graduation of the students as the dependent variable because the student's date of graduation defines if the student is successful in the course that the students take during college. After the detection of outliners, the researchers used the optimize selection operator in Rapid Miner. It selects the most relevant attributes of the given datasets. Two deterministic greedy feature selection algorithms

(forward selection and backward elimination) are used for feature selection. It eliminated the Verbal Ability using backward elimination from the seven dependent variables.

4.2 Correlation of Predictors to Graduate On-Time in Computer Science Degree

The researchers used the correlation of Rapid Miner to measure the relationship and strengths of the variables after feeding and using correlation in the tool. Table2shows the correlation between On-Time graduations of a student with Abilities extracted from admission exams. The scientific ability has a moderate uphill linear relationship with On-Time graduations of Computer Science and IT student with 0.430, meaning it has a moderate effect on the success rate of passing the degree. Table 3 shows that the most important ability in admission exam to pass Computer Science and IT program is the Non Verbal Ability.

4.3 Data Mining Techniques and Algorithms

The researcher used three data mining techniques and compared each result to find out what are the best data mining techniques that best suits the data sets that the researchers gathered namely regression, neural network, and decision tree analysis.

4.3.1 Regression

The researcher used linear regression to be able to forecast the success rate of computer science student in passing the computer science degree using the abilities presenting NCAE. After applying the model to the Rapid Miner tool, the researcher came up and produced the following output:

Table 2: Correlation predictors

First Attribute	SecondAttribute	Correlation
On-Time	ScientificAbility	0.430
On-Time	Manipulative Ability	0.057
On-Time	VerbalAbility	0.034
On-Time	NonVerbalAbility	1
On-Time	ReadingComprehension	0.024
On-Time	ClericalAbility	0
On-Time	MathematicalAbility	0.172
On-Time	EntrepreneurialSkills	0.083

Table 3: Linear regression output

Attribute	Coefficient
Clerical Ability	-0.002
ScientificAbility	0.005
Non-VerbalAbility	0.031
MathematicalAbility	0.005
Intercept	-2.383

Table3 was the result after using the linear regression from the Rapid Miner tool, the coefficients are used for Linear Regression Model which is:

Y = -2.383 + (-0.002) (Clerical Ability) + (0.005) (Scientific Ability) + (0.031) (Non Verbal Ability) + (0.031) (Non Verbal Ability) + (0.005) (Mathematical Ability)

To get the forecasted value, the intercept should be subtracted to the sum of products of abilities in admission exams to their respective coefficient values. If the value is equal to 1, the student will pass, and if it is 0, the student will not pass the CS degree.

4.3.2 Neutral Network

The researcher used a neural network for the next test and Table 4 shows the three layers under Multilayer Perception of the neural network. In able to map the following input, The researcher uses the predictors as the input layer or factors consists of Non-Verbal Ability, Clerical Ability, Mathematical Ability, Scientific Ability, Manipulative Skills, Verbal Ability, Reading Comprehension and Entrepreneurial skill. The hidden layer consists of Number of units, Number of Hidden Layers, Number of Units in the hidden layer, Activation Function, Dependent Variables and Number of Units. The last year or the output layer consists of Rescaling Method for Scale Dependents, Activation Function, and Error Function. The neural network normalized the data and was used to map and get the input layer, hidden layer, and output layer. It was developed to measure the frequency of action potentials.

Table 4: Neural network analysis

Neural Network Information

Network Information			
Input Layer	Factors	1	Non Verbal Ability
		2	Clerical Ability
		3	Mathematical Ability
		4	Scientific Ability
		5	Verbal Ability
		6	Manipulative Skill
		7	Reading Comprehension
		8	Entrepreneurial Skills
	Number of Units		2913
Hidden Layers	Number of Hidden Layers		1
	Number of Units Hidden Layers		7
	Activation Function		Hyperbolic Tangent
Output Layers	Dependent Variable	1	On-Time
	Number of units		
	Rescaling Method for Scale Dependents		Standardized
	Activation Function		Identity

4.3.3 Decision Tree Algorithm

Figure 2 shows the result of the decision tree using CHAID algorithm with the predictors are the child and the dependent variable was the parent. The researchers used a classification tree to classify the nodes of the predictors according to the data. The Node 0 which is Non Verbal ability is the highest factor or the best predictor to determine if the student will pass the Computer Science or IT degree. The node of the Non-Verbal Ability was the computed quantitative measurement of the data of graduates of computer science and IT program in the University.

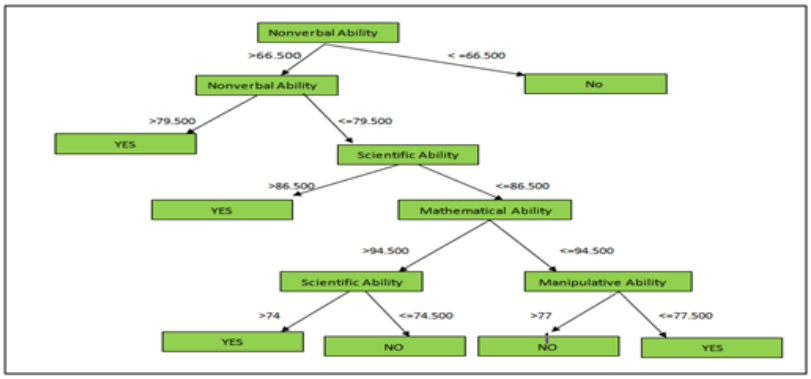

Figure 2: Decision tree analysis

4.4 Level of Acceptability of the Forecasting Model.

Accuracy or decision effectiveness is the main factors in evaluating a forecasting model[8]. The Rapid Miner tool has a performance evaluator whocan display the accuracy, precision, and area of the curve in each model created using the tool.

Table 5: Sample measure of forecasted result: linear regression

(A) Student	(B) Actual	(C) Forecasted	(D) (A-F) Error	(E) |Error|	(F) |Error|²	[A/B] *100
A	1	1.078	-0.078	0.078	0.006	7.8
B	1	0.845	0.155	0.155	0.024	15.5
C	1	0.815	0.185	0.185	0.034	18.5
D	1	1.147	-0.147	0.147	0.021	14.7
E	1	1.076	-0.076	0.076	0.005	7.6
F	1	1.044	-0.044	0.044	0.001	4.4
G	0	0.4	-0.4	0.4	0.16	0
			%Error		8.81428%	
			Accuracy		91.18572%	

Table 5 shows the actual and forecasted value in the batch 2011 of Computer Science and IT student of the University, the percentage of error of student's actual value and the accuracy of the predicted value. The research used different measures such as MAD (|Error|) which weights all errors evenly, MSE (|Error|²) which weights errors according to their squared values, and MAPE ([|Error|/Actual]*100) which weights according to relative error. The percent error computed is 8.81428%, almost equal to 91.18572%, which means that the result for the model is accurate and therefore the admission exams occupational interest was relative in the success rate of the students.

Table 6: Sample measure of forecasted result: decision tree

Student	AV	PV	CA	SA	MS	VA	NVA	RC	MA	EA
A	YES	YES	75	81	91	83	91	81	77	83
B	YES	YES	78	81	92	83	84	77	75	78
C	YES	YES	93	76	82	92	88	80	80	75
D	NO	NO	85	78	78	87	79	76	76	78
E	YES	YES	82	88	76	94	88	95	91	92
F	YES	YES	98	83	87	75	88	92	96	78
G	YES	YES	96	85	94	79	72	94	99	93
% error	123/124	=	0.81							
Accuracy	100-0.81	=	99.193%							

From the given table, the accuracy of decision tree mode is the difference of the percent error which is 0.81 and 100 percent as shown in Table 6. After solving the level of acceptability, the result is 99.193%, which means that the result for the decision tree was accurate and can be used as evidence of relevance to the study.

Table 7: Sample measure of forecasted result: decision tree

Student	AV	PV	CA	SA	MS	VA	NVA	RC	MA	EA
A	YES	YES	75	81	91	83	91	81	77	83
B	YES	YES	78	81	92	83	84	77	75	78
C	YES	YES	93	76	82	92	88	80	80	75
D	YES	YES	82	88	76	94	88	95	91	92
E	YES	YES	98	83	87	75	88	92	96	78
F	NO	NO	85	78	78	87	79	76	76	78
G	YES	YES	96	85	94	79	72	94	99	93
% Error		120/124		=	3.225					
Accuracy		100-3.225		=	96.774%					

The accuracy of the neural network model is the difference of the percent error which is 3.225 and 100 percent. After solving the level of acceptability, the result is 96.774%, which means that the success rate of the students is valid with the help of admission exams occupational interest. Basedon the result and observations from the model together with data that was being gathered, here are the findings of the researcher.

1. Predictors that are considered to determine the success rate of Computer Science student from the recommendation of Admission Exams. Based on the gathered data the predictors that are considered in predicting the success rate of Computer Science students are Non-Verbal Ability, Verbal Ability, Clerical Ability, Reading Comprehension, Manipulative Skills, Mathematical Ability, Scientific Ability and Entrepreneurial Skills. The abilities that are present in NCAE results are used as a dependent variable or the input to forecast the outcome or independent variable. The researcher used the date of graduation of Computer Science students as the independent variable because this will determine if the student is successful in the Computer Science degree if the student was able to finish the degree within four years, then the student is said to be successful.

2. Relationship of the predictors in passing Computer Science degree. The researcher used the Rapid Miner tool to be able to find the value of correlation of the predictors to the success rate of Computer Science student. After feeding the data in the tool, the researcher found out that the Non-Verbal Ability is the best predictor to determine the success rate because it has a perfect linear relationship with the success rate of Computer Science student in passing the degree. Followed by the Scientific Ability which has a moderate uphill linear relationship with the success rate.

3. Data mining techniques and algorithms that were used in the forecasting model. The data mining techniques that were used by the researcher during the study are Linear Regression, Neutral Network, and Decision Tree. Linear regression estimates the value of the target as a function of the predictors for each case. The neutralnetwork which consists of an interconnected group of artificial neurons, and it process information using a connectionist approach to computation. Decision tree shows how one choice leads to the next, and the use of branches shows that every alternative or option is mutually exclusive. The researcher used the different measures such as MAD(|Error|)which weights all errors evenly, MSE(|Error|) which weights errors according to their squared values, and Physical Education[|Error|/Actual]*100 which weights according to relative error. The researcher used Physical Education or Linear Regression; the researchers found out that physical education is the most popular aggregate measure of forecasting accuracy. The percent error computed is 8.81428% or

equal to 91.18572% accurate. For the remaining models which are the neural network and decision tree, the researcher used the performance evaluator of Rapid miter. The neural network got an accuracy of 96.774% while the decision tree got an accuracy of 99.193%.

5. Conclusion and Recommendation

1. The proposed study could be a great help to the Admission Office or Registrar of the University students in enhancing their basic forecasting skills especially using Data Mining.
2. The researcher considered that the forecasting model that was made efficient if it will be used to determine the success rate of Computer Science and IT student in passing the degree.
3. There is a significant relationship between the date of graduation of Computer Science and IT student and predictors in forecasting the success rate of the students in passing the Computer Science degree.

The researcher recommends that there should be a separate section for students that have a low score on Non-verbal ability to give more attention or supervision in teaching them because these students have a high chance in failing the Computer Science degree.

References

[1] Fildes, R. and Kourentezes, N. (2010). Validation and Forecasting Accuracy in Models of Climate Change.
[2] Ramey. (2012). Use of Technology.
[3] Mallorca, R. (2008). Student's Natural Aptitudes and the Required Skills in their Chosen Program."
[4] Gupta. S., Adhay Bnasal, and RetishRastogi. (2012). Learning Behaviour of Analysis of Higher Studies Using Data Mining.
[5] Saurab Pal. (2012). "Mining Educational Data to Reduce Drop-out Rates of Engineering Students.
[6] Torres, T. (2015). I8 percent of unemployed collegegraduates – NSO.
[7] Tuffrey Stephane (2011). Data Mining and Statistics for Decision Making Statistic for Dummies.
[8] Wilma L. Labrador. (2009). National Career Assessment Examination (NCAE) As It Influences The TV System.

Multiple Noises Removal from Computed Tomography (CT) Images

Abdelkader Salama Alrabaie[1*],Marwan M M El marmuri[2], Emhimed Saffor[3]
[1]kadersalama1@gmail.com , [2]marwanelmarmouri@yahoo.com, [3]Amh.saffor@sebhau.edu.ly
[1]Department of Physics, College of Education /Brack, Sebha University, Libya
[2]Department of X-ray Diagnostic &Radiotherapy, College of Medical Technology, Zawia University, Libya
[3]Department of Physics, College of Sciences, Sebha University, Libya

ABSTRACT

Noise is seen in images during image acquisition and transmission. This is characterized by noise model. Image enhancement through noise reduction is a fundamental problem in image processing. Noise filtering is a necessary action and has become one of the indispensable components of image processing operation. In this work, we have applied different filtering techniques (arithmetic mean filtering, median, and Weiner) to remove multiple mixed noises such as; (speckle, Gaussian, salt and pepper) from Computed Tomography (CT) images. Performance metrics such as; Peak Signal to Noise Ratio (PSNR), and Mean Square Error (MSE) were used to evaluate filtering techniques. The results showed that the median filter had worked more effectively to remove these noises. All the above mentioned techniques were implemented using MATLAB environment. It should give some results showing the values of PSNR and MSE for these flirters to indicate the differences between them.

Keyword— CT, MATLAB, MSE, Noise, PSNR.

1. Introduction

Medical images such as magnetic resonance imaging (MRI), computed tomography (CT), ultrasound (US), and X-ray images are subject to a wide variety of distortions, during acquisition, processing, compression, storage, transmission and reproduction, any of which may result in a degradation of visual quality. Medical images are collected by different types of sensors and they are contaminated by different types of noises. Generally speckle; Gaussian, salt and pepper noises mostly occurred in the MRI, CT, and US images.[1]Noise tells unwanted information in digital images. Noise produces undesirable effects such as artifacts, unrealistic edges, unseen lines, corners, blurred objects and disturbs background scenes. In medical image processing many methods are used for noise reduction.[2]Noise filters generally attempt to smooth the corrupted image by neighbourhood operations. To measure the performance and image quality of the noise removal techniques several parameters are available for the comparison. Common parameters are Peak Signal Noise Ratio (PSNR), Root Mean Squared Error (RMSE), Mean Squared Error (MSE) etc.[1][3]

A). Noise Models:

i) Gaussian Noise: Gaussian noise caused by natural sources such as thermal vibration of atoms and discrete nature of radiation of warm objects. Gaussian noise generally disturbs the gray values in digital images. That is why Gaussian noise model essentially designed and a characteristic by its probability density function (PDF) or normalizes histogram with respect to gray value and it is given as:[2][4]

$$P(g) = \sqrt{\frac{1}{2\pi\sigma^2}} e^{-\frac{(g-\mu)^2}{2\sigma^2}} \qquad (1)$$

Where: g = gray value, σ = standard deviation and μ = mean

ii) Speckle Noise: This noise is multiplicative noise. Their appearance is seen in a coherent imaging system such as laser, radar and acoustics etc. Speckle noise can exist similar in an image as Gaussian noise. Its probability density function follows gamma distribution, and given as:[2]

$$F(g) = \frac{g^{\alpha-1} e^{\frac{-g}{a}}}{(\alpha-1)! a^{\alpha}} \qquad (2)$$

Where a^2 is the variance, α is the shape parameter of gamma distribution and g is the gray level.

iii) Impulse Valued Noise (Salt and Pepper Noise): Salt and pepper noise is represents itself as randomly occurring white and black pixels. Salt and pepper noise creeps into images in situations where a quick transient, such as faulty switching, takes place.[5] Image pixel values are replaced by corrupted pixel values either maximum or minimum pixel value i.e., 255 or 0 respectively. Although in noisy image, there are possibilities of some neighbours do not changed as shown in Figure 1 for an example.

254	207	210
97	212	32
62	106	20

→

254	207	210
97	0	32
62	106	20

Figure 1: The central pixel value is corrupted by Pepper noise

The (PDF) of this noise is shown in the Figure 2.

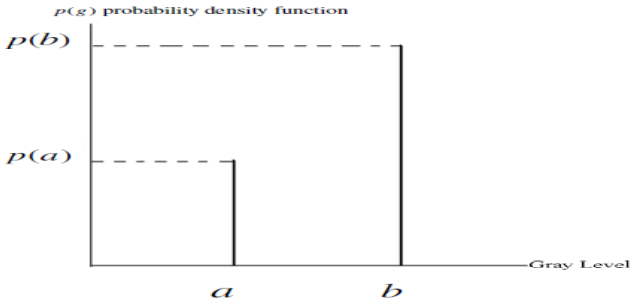

Figure 2: PDF of Salt and Pepper noise

$$p(g) = \begin{cases} pa & \text{for } g = a \\ pb & \text{for } g = b \\ 0 & \text{otherwise} \end{cases} \qquad (3)$$

Salt and Pepper noise generally corrupted the digital image by malfunctioning of pixel elements in camera sensors, faulty memory space in storage, errors in digitization process and many more.[2]

(B) Filters:

i). Arithmetic Mean Filtering (AMF): This is one of the simplest of the mean filtering techniques. It expressed as AMF by the equation (4).[6]

$$f(x,y) = \frac{1}{mn} \sum_{(a,t)\in S_{xy}} g(s,t) \qquad (4)$$

S_{xy} represent the set of coordinates in a rectangular space that is image window of size m x ncentred at given point (x,y).The AMF technique calculates the average value of the corrupted image g(x,y) in the area defined by S_{xy}. The value of restored image f at any point (x,y) is Arithmetic Mean computed using the pixels values in the image that is in the region defined by S_{xy}.

ii). Median Filter: the median filter replaces the value of the pixel by the median of the gray levels in the neighbourhood of that pixel [1] i.e.

$$Z_{(x,y)} = median_{(s,t)\in S_{xy}}\{g(x,y)\} \qquad (5)$$

The value of the pixel at (x,y) is included in the computation of the median.[7-9]

iii). Weiner filter: It is an adaptive low-pass filter which uses a pixel-wise adaptive Wiener method based on statistics estimated from a local neighbourhood of each pixel.[7] Adaptive filters are a class of filters which change their characteristics according to the values of the grey scales under the mask. Such a filter can be used to clean Gaussian noise by using local statistical properties of the values under the mask. One such filter is the minimum mean-square error filter; this is a non-linear spatial filter; and as with all spatial filters, is implemented by applying a function to the grey values under the mask. The output value can be calculated by following equation.[6]

$$m_f + \frac{\sigma f^2}{\sigma f^2 + \sigma g^2}(g - m_f) \qquad (6)$$

Where; g is the current value of the pixel in the noise affected image, mf is the mean, σf2 is the variance in the mask and σg2 is the variance of the noise over the entire image. The wiener2 function applies a Wiener filter which is a type of linear filter to an image adaptively, tailoring itself to local image variance. Where the variance is large, wiener2 performs little smoothing. Where the variance is small, wiener2 performs more smoothing. This approach often produces better result than linear filtering.[8] The technique that is implemented in MATLAB is Weiner filter. It is an adaptive low-pass filter which uses a pixel-wise adaptive Wiener method based on statistics estimated from a local neighbourhood of each pixel [7].

2. Materials and Methods

Brian and Chest Computed Tomography (CT) images of sizes (225x225) pixels are used in this study. These images are corrupted by multiple and different noises (speckle, Gaussian, salt and pepper). Filtering techniques (AMF, Median, and Weiner) are used to remove these noises. To evaluate filtering techniques quality metrics like Mean Squared Error (MSE), and Peak Signal to Noise Ratio (PSNR) were used. Algorithms were implemented in MATLAB with default setup parameters. The structure of methodology used in this study can be shown in Figure (3).

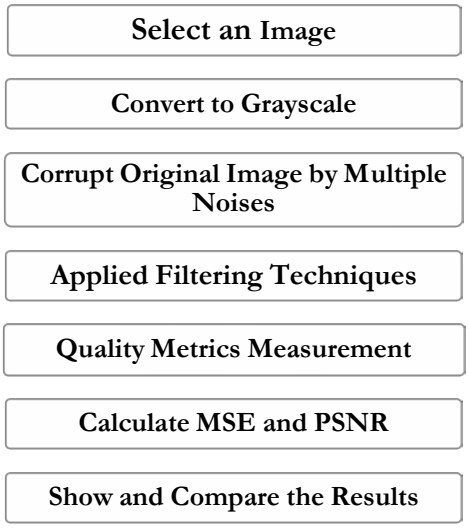

Figure 3: Methodology Structure

The (PSNR) is evaluated in decibels and is inversely proportional the Mean Squared Error. The PSNR can be calculated form equation (7) :[1]

$$PSNR\,(dB) = 10\log\left(\frac{(255)^2}{MSE}\right) \qquad (7)$$

Where (MSE) used to calculate by taking difference between two images pixel by pixel, and it is defined as:[3]

$$MSE = \frac{1}{MN}\sum_{i=1}^{M}\sum_{j=1}^{N}(x(i,j) - y(i,j))^2 \qquad (8)$$

Where x(i,j) represents the original (reference) image and y(i,j) represents the distorted (modified) image and i and j are the pixel position of the M×N image. MSE is zero when x(i, j) = y(i,j).

3. Results and Discussion

The visualization results of MATLAB simulation are shown in Figure (4).

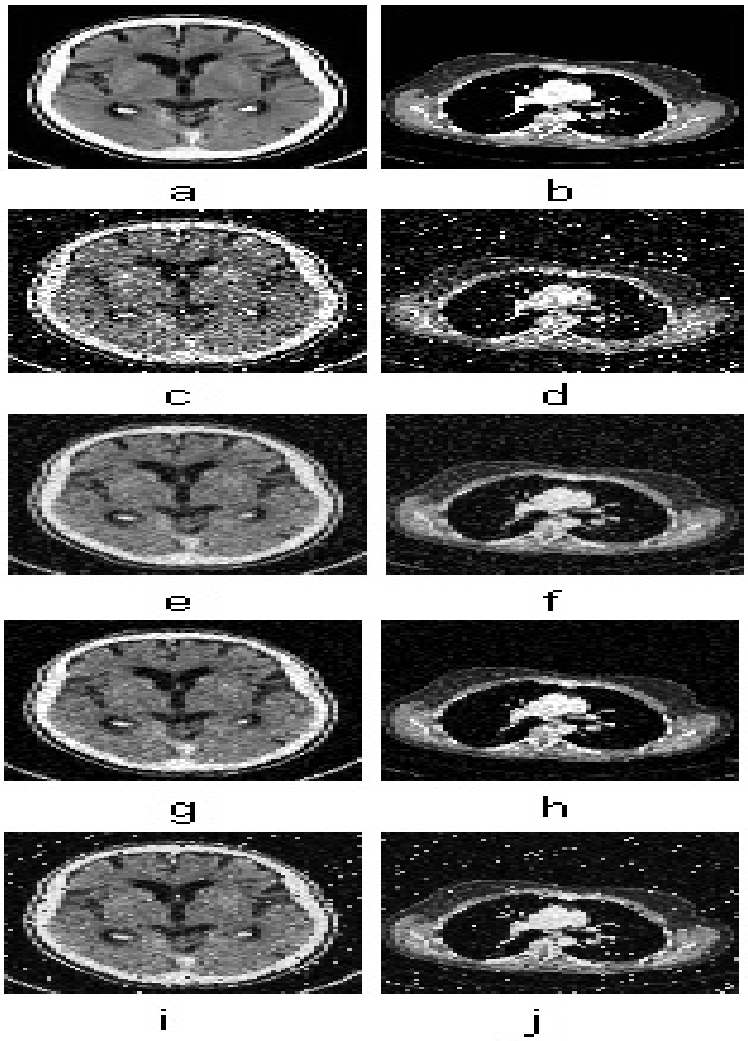

Figure 4: Filtering noisy (CT) images
(a) and (b)original images(Brain & Chest)(c) and (d) noisy images(e) and (f) Average filter applied (g) and (h) Median filtering applied (i) and (j) Weiner filtering applied

The values of (MSE & PSNR) for applied filter techniques are tabulated in Table (1) to evaluate and compare the filtered (CT) images. The comparison has been made amongst (AMF, Median, and Weiner) filters.

Table (1), Figure (4),and Figure (5).show the experimental results and illustrate a thorough comparison of all the filtering techniques for brain and chest (CT) image used in this study.

Table 1: MSE and PSNR values

Image	Brain		Chest	
Filter	**MSE**	**PSNR**	**MSE**	**PSNR**
Average	572.77	20.55	742.16	19.42
Median	412.41	21.97	435.38	21.74
Weiner	886.03	18.65	1.10×10^3	17.69

Through finding the noises (speckle, Gaussian, salt and pepper) noises in both (CT) images by filtering techniques it is found that the median filter works better for the removing multiple noises from (CT) images. The highest values of (PSNR) are given by Median filter 21.97 and 21.74 for Brain and Chest (CT) images respectively. Therefore the output images is greater denoised. The median filter is more effective in removing different noises (speckle noise, Gaussian noise, salt and pepper). Whereas the Weiner filter can be used to clean Gaussian noise by using local statistical properties of the values under the mask, and it fails for salt and pepper noise. The median is much less sensitive than the mean to extreme values. Since the median value must actually be the value of one of the pixels in the neighbourhood, the median filter does not create new unrealistic pixel values when the filter straddles an edge. These advantages aid median filters in suppressing the uniform noise as well as other noises. Median filtering is therefore better able to remove this outlier without reducing the sharpness of the image.[7-9]

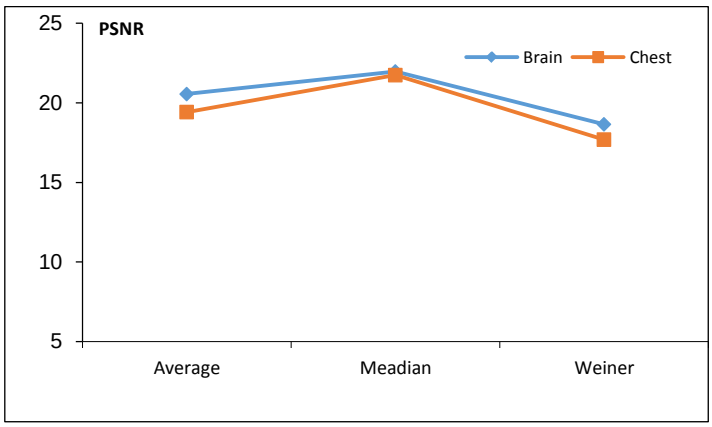

Figure 5: PSNR values

4. Conclusions

During image acquisition and transmission, noise is seen in images. This is characterized by noise model. Image denoising is necessary action in image processing operation. Noise models also designed by probability density function using mean, variance and mainly gray levels in digital images. In this work, we have applied different filtering techniques (AMF, Median, and Weiner) to remove multiple noises (speckle noise, Gaussian noise, salt and pepper). The simulation results found that the median filter is more effective in removing different noises. Through this work we have observed that the choice of filters for denoising the medical images depends on the type of noise and type of filtering technique, which are used. These filters are very useful in many applications. These results are more useful for medical diagnostic.

References

[1] S. Senthilraja, P. Suresh, and M. Suganthi, "Noise Reduction in Computed Tomography Image Using WB – Filter", International Journal of Scientific & Engineering Research, Volume 5, Issue 3, pp. 243-247, March-2014.

[2] Ajay Kumar Boyat, and Brijendra Kumar Joshi, "A Review Paper: Noise Models in Digital Image Processing", Signal & Image Processing : An International Journal, SIPIJ, Vol. 6, No. 2, pp. 63-75, April- 2015.

[3] C. Sasi varnan, et al, "Image Quality Assessment Techniques on Spatial Domain", International Journal of Computer Science and Technology, Vol. 2, Issue 3, pp. 177-184, September 2011

[4] K. Somasundaram, and P. Kalavathi, "Medical Image Denoising using Non-Linear Spatial Mean Filters for Edge Detection", National Conference of Signal and Image Processing, (NCSIP), pp.149-153, 2012.

[5] SONALI R. MAHAKALE & NILESHSINGH V. THAKUR "A Comparative Study of Image Filtering on Various Noisy Pixels", International Journal of Image Processing and Vision Sciences, Vol. 1, Issue 2, pp. 69-77, 2012.

[6] Gururaj P. Surampalli et al, "Adaptive Approach to Retrieve Image Affected by Impulse Noise", International Journal of Research in Engineering and Technology, Vol. 3, Special Issue 3, pp. 218-221, May- 2014.

[7] Ajay Kumar Nain, et al "A Comparative Study of Mixed Noise Removal Techniques", International Journal of Signal Processing, Vol. 7, No. 1, pp.405-414,2014.

[8] Bhausaheb Shinde, Dnyandeo Mhaske, and A.R. Dani, "Study of Noise Detection and Noise Removal Techniques in Medical Images", I.J. Image, Graphics and Signal Processing, pp. 51-60, 2012.

[9] Sukhwinder Singh, and Neelam Rup Prakash, "Modified Adaptive Median Filter for Salt & Pepper Noise" International Journal of Advanced Research in Computer and Communication Engineering, Vol. 3, Issue 1, pp. 5067-5071, January 2014.

A New Technique to Encrypt-Decrypt Digital Color Images Using One-Dimensional Matrix

Khdega A.Yosef Galala
kdebh@yahoo.com
Department of Computer Science, College of Education, Al Jufrah University, Libya

ABSTRACT

Due to digital technologies, the usage of images in modern industrial life is increasing rapidly. Therefore, the security of digital image has been a major issue in the modern digital world. Image encryption methods are one of the strong techniques recommended in this domain. These techniques try to convert an image to another image that is difficult to recognize and to understand. This art aims fundamentally to achieve the storage and transmission of image securely over the network. In this study a new image security technique is presented. As first step, the new technique extracts the red, green, and blue (RGB) components from the original color image. Then the XOR operation is used to change the RGB values of each pixel and then the RGB pixel positions are also changed randomly according to the key matrix. MATLAB R2012a was used to get the experimental results. The evaluation of this technique was done using some color images which differ in size and type. Simulation results show that, the performance of the proposed technique is high and the original image was retrieved without any distortion.

Keyword— image encryption; image decryption; color images; network security.

1. Introduction

In recent years, with the explosive growth of both computer and internet technology, a huge amount of sensitive and valuable data is being exchanged over unsecured networks. Data not just text it also includes digital images, video, graphical objects, audio and other the multimedia data [1]. Digital image is the most important multimedia data, it is widely used for many aspects of our daily life such as online personal photograph album, internet communication, pay-per-view TV, digital signatures legal, medical imaging systems, military image systems, etc [2]. Digital images are sent, treated automatically and shared across the internet. So the protection of these images from unauthorized access is offering a great challenge to governments, individuals and companies alike[3].

To meet this challenge, various image security techniques such as encryption, stenography, secret sharing, watermarking, etc were proposed. Among these all, image encryption (IE) become one of eminent technique especially using over the internet. These techniques try to convert an image to another image that is difficult to recognize and to understand; while the image decryption is the result of retrieving original image from the encrypted one [4]. Generally, the image encryption applies two basic methods: replacement methods or scrambling methods [5]. Digital image scrambling is a useful method for providing high protection to image data by scrambling image into an unintelligible format [6].

Since 1990s, many existing image encryption techniques have been developed based on scrambling techniques like key based scrambling techniques, Rubik Cube matrix transformation, image

scrambling based on 2D, etc [7]. One of them was proposed by [8] to encrypt image by generate random key sequence. Then the rows and columns of the image are scrambled using this key and then circular shifting of the rows and columns are done using the same key. The authors of [5] also uses scrambling method to encrypt the grey level image based on random number generation as matrix. In [9], a new technique based on one-dimensional random scrambling and combined with XOR operation is developed.

Although, there are various image encryption techniques available for executing images encryption but, there is still a lack of appropriate techniques for images encryption [10]. So we still need to develop more and more powerful techniques. Therefore, the main goal of this paper is to propose a new image encryption technique based on one-dimensional scrambling method. Thus, the rest of the paper is organized as follows: in section 2 the proposed technique is discussed in details; section 3 focuses on the experimental results of the new technique; section 4 gives explains the features of proposed technique and conclusion is presented in section 5.

2. The Proposed Technique

The new image encryption technique is based mainly on true color images, free from image size and type. It consists of two main phases which are encryption and decryption phase as shown in figure 1 below. The first phase can be described as follows:

2.1. Encryption phase

The proposed method of encryption consists of ten main steps as shown below:

Step 1. Input original color image and get its size.

Step 2. Based on the size of the original image, generate a random single array with unique values varies from 1 to the original image size (i.e. If an image is 150×120 then the array will have 18000 elements). Save it as the secret key matrix 'SKM' which will be used later for image scrambling.

Step 3. Extract red 'R', green 'G', and blue 'B' components of the original image.

Step 4. Apply the XOR operation between the red matrix 'R' and the green matrix 'G' to get the new green matrix 'G1' , ' G1= R ⊕G '.

Step 5. Apply the XOR operation between the red matrix 'R' and the blue matrix 'B' to get the new blue matrix 'B1', ' B1= R ⊕B '.

Step 6. Apply the XOR operation between the red matrix 'R' and the matrix obtained in the previous step to get the new red matrix 'R1', ' R1= R ⊕ B1 '.

Step 7. Reshape the three matrices obtained in steps (4,5,6) to three one-dimensional arrays.

Step 8. Scrambling the pixel position in each matrix obtained in the previous step in the order of randomness of SKM key.

Step 9. Reshape each matrix obtained in the previous step to 2-dimensional array which is the same size as the original one.

Step 10. Finally re-combine separate color channels obtained in step 9 into a single RGB color image to get encrypted image.

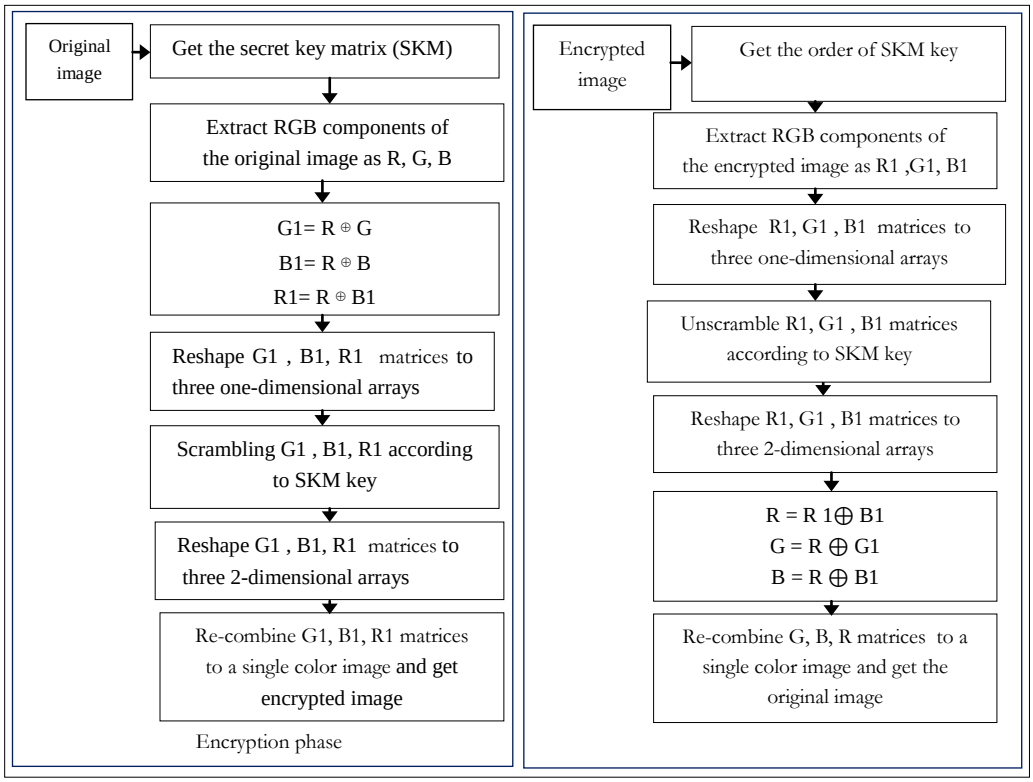

Figure 1: The proposed technique phases

2.2 Decryption phase

The decryption stage can be performed according to following steps:

Step 1. Load the encrypted image and get its size.

Step 2. Get the random matrix, sort its elements in ascending order. Get the order of the key matrix by comparing elements of matrix before and after sorting. According to the obtained order of the key matrix 'SKM', we change positions of pixels in the input image to get back the original image.

Step 3. Extract red 'R1', green 'G1', and blue 'B1' components of the encrypted image.

Step 4. Reshape each matrix obtained in the previous step to three one-dimensional arrays.

Step 5. Unscrambling pixels in each matrix obtained in the previous step using SKM key.

Step 6. Convert each matrix obtained in the previous step to 2-dimensional array which is the same size as the original one.

Step 7. Apply the XOR operation between the red matrix' R1' and the blue matrix 'B1' obtained in the previous step to get the original red matrix ' R', ' R = R1 ⊕ B1'.

Step 8. Apply the XOR operation between the red matrix obtained in the previous step and the green matrix obtained in step 6 to get the original green matrix ' G', 'G = R⊕G1'.

Step 9. Apply the XOR operation between the red matrix obtained in step7 and the blue matrix obtained in step 6 to get the original blue matrix ' B', 'B = R⊕B1'.

Step 10. Finally re-combine separate color channels obtained in steps (7,8,9) to a single RGB color image to get back the original image.

3. Experimental Results

The simulation of the above technique has been achieved by using MATLAB R2012a. The test images applied in this work was analyzed using histogram and operational speed of technique. The details of those processes as described below:

3.1. Histogram

At this stage, two images were used in this performed analysis. They are 300 * 300 RGB image named 'Ahmed Al Bashir' and 600 * 450 RGB image named ' Tree'. Figure 2 and figure 5 show the original images with the histogram of each channel of the original color image. Figure 3 and figure 6 show encrypted images with the histogram of each channel of the encrypted color image while figure 4 and figure 7 show the decrypted images with the histogram of each channel of the decrypted color image.

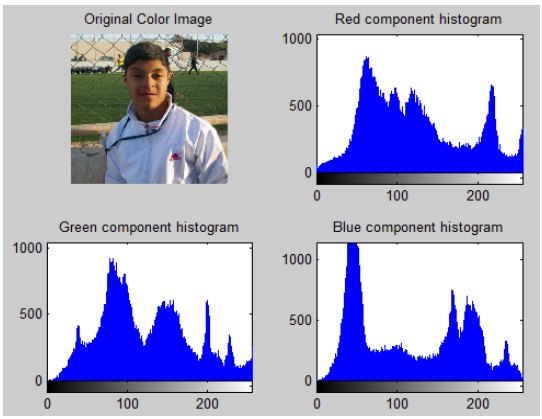

Figure 2: Original image of Ahmed

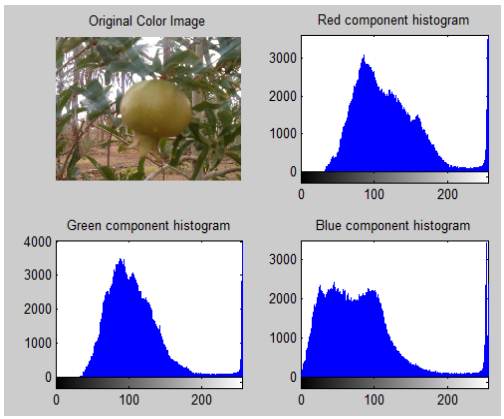

Figure 5: Original image of tree

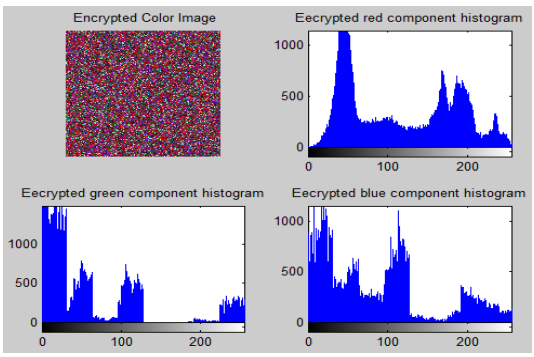

Figure 3: Encrypted image of Ahmed

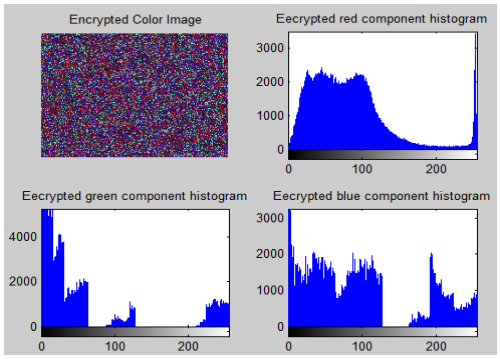

Figure 6: Encrypted image of tree

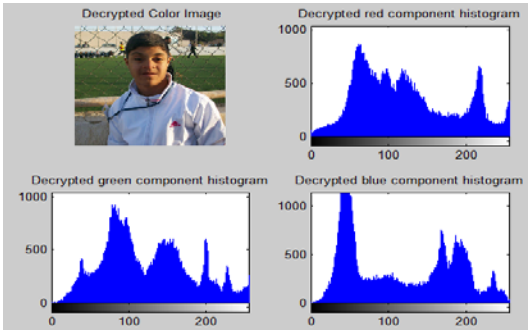

Figure 4: Decrypted image of Ahmed

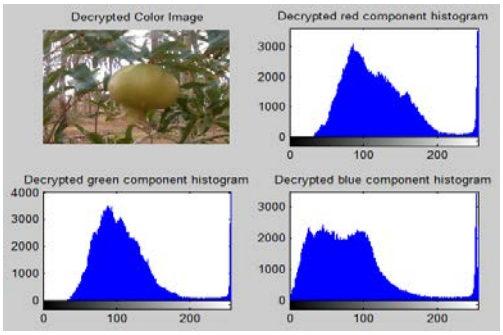

Figure 7: Decrypted image of tree

The histogram analysis indicates that, for both images the original image and its encrypted image has different statistics. As we see, the histograms of encrypted images are great different from the histograms of the original images, which will make it difficult to apply any statistical attack on the image encrypted.

3.2. Operational Speed Analysis

This work also measures the CPU time taken by the new technique to encrypt and decrypt color images. Seven different image sizes are selected to be used in this test. Table 1 shows the results of compared the CPU time to encrypt and its decryption for each image.

TABLE 1: CONSUMED TIME FOR ENCRYPTION AND DECRYPTION PROCESSES

Image size	Encryption time (sec.)	Decryption time (sec.)	Total time (sec.)
259*194*3	0.003495	0.013511	0.017006
276*182*3	0.003214	0.012671	0.015885
299*168*3	0.003232	0.014378	0.01761
300*200*3	0.004063	0.014976	0.019039
300*300*3	0.005545	0.027047	0.032592
600*450*3	0.018416	0.083314	0.10173
940*627*3	0.040704	0.188611	0.229315

As can be seen in the table 1 above, the proposed technique gives the best speed to encrypt and decrypt color images and has been observed a slight increase in execution time of technique with the increase in image size.

The consequences disclose that, the proposed technique was implemented successfully and all original images were recovered without any loss. So it could be used effectively to encrypt any color image.

4. Features

A prominent features of the new technique are:

The proposed technique is a very effective and simple technique to encrypt color images.

It is adaptable to encrypt images differ in size and type.

It has high operation speed to execute both encryption and decryption processes.

5. Conclusions

In this work, a new technique to encrypt digital color images has been introduced. Statistical analysis was done using histograms and operational speed analysis to get the experimental results. Simulation results confirmed that the new technique has been successfully implemented and it could be used effectively for encryption purposes. For the future work the proposed technique could be used to encrypt other images types such as binary images and gray images.

References

[1]. W. Lee, T. Chen and C. Chieh Lee, "Improvement of an encryption scheme for binary images, " *Pakistan Journal of Information and Technology*, Vol. 2, pp. 191-200, 2003.

[2]. Rojo, M.G., G.B. García, C.P. Mateos, J.G. García and M.C. Vicente, "Critical comparison of 31 commercially available digital slide systems in pathology," *International journal of surgical pathology*, Vol. 14, pp. 285-305, 4 October 2006.

[3]. Mitra, Y V. Subba Rao and S. R. M. Prasnna, "A new image encryption approach using combinational permutation techniques, " *Journal of computer Science*, Vol. 1, pp.127, 2006.

[4]. Madhu B., Ganga Holi and Srikanta Murthy K., "An overview of image security techiques, " *International Journal of Computer Applications,* Vol.154, pp. 37- 46, November 2016.

[5]. Makera M Aziz and Dena Rafaa Ahmed, "Simple image scrambling algorithm based on random numbers generation, " *International Journal of Advanced Research in Computer Science and Software Engineering*, Vol. 5, pp. 434 - 438, September 2015.

[6]. Prarthana Madan Modak and Vijaykumar Pawar, " A comprehensive survey on image scrambling techniques, " *International Journal of Science and Research (IJSR)*, Vol. 4, pp.814 -818, December 2015.

[7]. Sandeep Kaur and Sumeet Kaur, "Four level image encryption using scrambling and key based methods, " *IJCSC*,Vol. 3, pp. 187-190, 2012.

[8]. P. Premaratne and M. Premaratne, "Key-based scrambling for secure image communication, " *Emerging Intelligent Computing Technology and Applications, P. Gupta, D. Huang, P. Premaratne & X. Zhang, Ed. Berlin: Springer*, Vol. 304, pp.259-263, 2012.

[9]. Qiudong Sun, Ping Guan, Yongping Qiu and Yunfeng Xue, "A Novel digital image encryption method based on one-dimensional random scrambling," *9th International Conference on Fuzzy Systems and Knowledge Discovery*, pp. 1669-1672, May 2012.

[10]. T. Bhaskara Reddy, Hema Suresh Yaragunti, T. Sri Harish Reddy and S. Kiran, "An effective algorithm of encryption and decryption of images using random number generation technique, " International Journal of Computer Technology & Applications, Vol. 4, pp. 883-891, 2013.

The performance of Space Time Block Coding (STBC) in MIMO relay network

Hamza Eldenferia[1*], Jamal Elbergali[2]
[1]hamza.ham1985@gmail.com, [2]jelbergali@yahoo.com
[1,2] Electronic Engineering Department- College of Industrial Technology Misurat- Libya

ABSTRACT

This paper is presenting the performance analysis of a cooperative MIMO(Multiple-Input-Multiple-Output) relaying system with a single relay based on Alamouti scheme. It examines the Space Time Codes (STC) techniques where the focus is on the Space Time Block Coding (STBC). The MIMO system is built on Alamouti Space Time Block Coding (STBC) over Rayleigh flat fading channels. The source and destination nodes are equipped with two transmit antennas while the relay node is equipped with multiple antennas and Amplifiers-and-Forwards (AF). In addition the receiver uses the Zero Forcing (ZF) equalizer. The system reliability will be evaluated by using of bit error rate (BER) performance.

Keyword— MIMO relay network**;** Alamouti scheme; Space Time Block Coding (STBC); Zero Forcing (ZF) equalizer; bit error rate (BER)

1. Introduction

Wireless communications have recently turned to a technique known as Multiple Input Multiple Output (MIMO) to improve the quality (bit-error rate) and data rate (bits/sec). MIMO technology has attracted attention in wireless communications, because it offers significant increases in data throughput and link range without additional bandwidth or increasing transmit power [1]. This is done by using multiple transmit and receive antennas, as well as suitable coding techniques. They take benefit of spatial and temporal diversity to combat the random fading induced by multi-path propagation of the signal and maximize efficient use of bandwidth. There is also a fundamental gain in transmitting data over a matrix rather than vector channel. Transmission of data over MIMO channels has traditionally focused on data rate maximization or diversity maximization [2].

Recently, Cooperative communication[3] has attracted a lot of attention because of its ability to enhance the system performance. Cooperative communication concerns a system where users share and organize their resources to improve the transmission quality and enhance the power allocation. The combination of MIMO processing with cooperative relaying helps to improve the capacity of the overall cooperative system [4]. In recent times, it has been revealed that cooperation based on Space-Time Block Codes (STBC) gives an effective method to present spatial diversity in various wireless scenarios [5][6].

1.1. Multi - Antenna Transmission Methods

To transmit information over a single wireless link, different transmission and reception strategies can be applied. Which one of them should be used depends on the knowledge of the instantaneous MIMO channel parameters at the transmitter side. If the Channel State Information (CSI) is not available at the transmitter, Spatial Multiplexing(SM) or Space-Time Coding(STC) can be used for transmission. If the CSI is available at the transmitter, beam forming can be used to transmit a single data stream over the wireless link. In this way, spectral efficiency and robustness of the system can be improved [1]. It can be concluded that the choice of the transmission model depends on three entities important for wireless link design, namely bit rate, system complexity and reliability. STC has low complexity and promises high diversity, but the bit rate is moderate. SM provides high bit rate, but is less reliable. Beam forming exploits array gain, is robust with respect to channel fading, but it requires CSI at both transmitter and receiver. In this research only STC transmission has been considered.

Let us consider a point-to-point MIMO system with n_t transmit and n_r receive antennas. The block diagram is given in Figure 1. Let $h_{i,j}$be a complex number corresponding to the channel gain between transmit antenna j and receive antenna i[2][3].

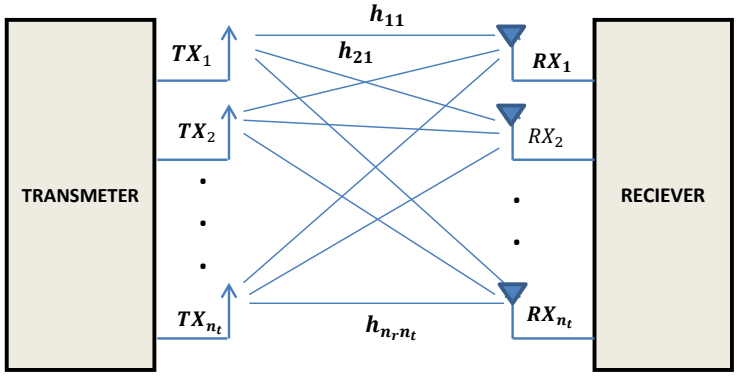

Figure 1. MIMO model with n_t transmit antennas and n_r receive antennas.

If at a certain time instant the complex signals $\{x_1, x_2, \cdots, x_{n_t}\}$are transmitted via n_t transmit antennas, the received signal at antenna i can be expressed as [7]:

$$y_i = \sum_{j=1}^{n_t} h_{i,j} x_j + n_i \qquad (1)$$

Where n_i is a noise term. Combining all receive signals in a vector *Y*, this equation can be easily expressed in matrix form [7]:

$$Y = Hx + n \qquad (2)$$

Y is the $n_r \times 1$ receive symbol vector, H is the $n_r \times n_t$MIMO channel transfer matrix, x is the $n_t \times 1$ transmit symbol vector and n is the$n_r \times 1$ additive noise vector.

1.2. Wireless Relaying Systems

The main advantages of using relay are to increase coverage and decrease the need to use high power at the transmitter [8][9][10]. Essentially, in relaying systems the source terminal uses other terminals or relays to forward its information to the destination terminal. Generally, there are two types of relaying systems, Decode-and-Forward (DF) relaying systems, and Amplify-and-Forward (AF) systems. In this paper AF system is used to implement the Model. Recently, with a good understanding of the benefits of MIMO systems, scientists have suggested some methods that could help to achieve the advantages of both MIMO and wireless relaying systems.

2. System Model

In this paper, we present performance analysis of a MIMO relaying system based on Alamouti scheme. As shown in Figure 2, the system considered two antennas at source and destination and one relay centred exactly between the source and destination. BPSK signal modulation is used to generate equal probability of '0's and '1's at the transmitter side.

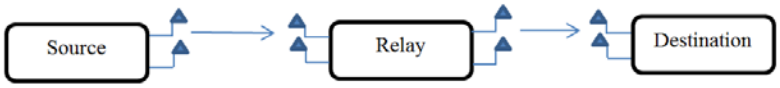

Figure 2. 2×2 MIMO relaying system.

At the relay node, we have used AF algorithm. The system channel between source, relay and relay destination are simply used as Rayleigh flat-fading channel with Additive White Gaussian Noise (AWGN) with zero mean. Also the Zero Forcing (ZF) technique has been used as equalizer at the receiver side.

2.1. Space Time Block Coding scheme

In this paper, two transmit and receive antennas is used. The input information stream $\boldsymbol{x}(t)$ is encoded by STBC encoder. Alamouti suggested that group the symbols into groups of two. In the first time slot, send $\boldsymbol{x}_1$ and $\boldsymbol{x}_2$ from the first and second antenna. In second time slot send $\boldsymbol{x}_1^*$and $-\boldsymbol{x}_2^*$from the first and second antenna. Where $(.)^*$ denoted to complex conjugate function. Thus, at two time slots the input symbols are given by [10]:

$$x(t) = \begin{pmatrix} x_1 & -x_2^* \\ x_2 & x_1^* \end{pmatrix} \qquad (3)$$

The encoded information is transmitted through Rayleigh fading channel and AWGN as addition noise. The received signal vector at the receiver can be given like:
In the first time slot, the received signal is [7]:

$$\begin{pmatrix} y_1^1 \\ y_2^1 \end{pmatrix} = \begin{pmatrix} h_{11} & h_{12} \\ h_{21} & h_{22} \end{pmatrix} \begin{pmatrix} x_1 \\ x_2 \end{pmatrix} + \begin{pmatrix} n_1^1 \\ n_2^1 \end{pmatrix} \quad (4)$$

In the second time slot, the received signal is:

$$\begin{pmatrix} y_1^2 \\ y_2^2 \end{pmatrix} = \begin{pmatrix} h_{11} & h_{12} \\ h_{21} & h_{22} \end{pmatrix} \begin{pmatrix} -x_2^* \\ x_1^* \end{pmatrix} + \begin{pmatrix} n_1^2 \\ n_2^2 \end{pmatrix} \quad (5)$$

Combining the equations at time slot 1 and 2.

$$\begin{pmatrix} y_1^1 \\ y_2^1 \\ y_1^{2^*} \\ y_2^{2^*} \end{pmatrix} = \begin{pmatrix} h_{11}h_{12} \\ h_{21}h_{22} \\ h_{12}^* - h_{11}^* \\ h_{22}^* - h_{21}^* \end{pmatrix} \begin{pmatrix} x_1 \\ x_2 \end{pmatrix} + \begin{pmatrix} n_1^1 \\ n_2^1 \\ n_1^{2^*} \\ n_2^{2^*} \end{pmatrix} \quad (6)$$

2.2. Relay Procedure

The received signal y_r at relay node is amplified by matrix $\boldsymbol{F}$ and retransmitted to the destination node. The relaying matrix $\boldsymbol{F}$ can be expressed by [10][11][12]:

$$F = \beta_r I_{N_r} \quad (7)$$

Where β_r is the amplifying factor of the relay and $\boldsymbol{I}_{N_r}$ is the $N_r \times N_r$ identity matrix. The amplifying factor is calculated by [11][12]:

$$P_a = {\beta_r}^2 tr\{F(H_r H_r^H + I_{N_r})F^H\} \quad (8)$$

Where P_a is the transmit power in relay node, $(.)^H$ represent the Hermitian complex conjugate transpose and tr(.) denotes to trace of a matrix[9][8].

2.3. Zero Forcing (ZF) Algorithm

The ZF equalizer is used in receivers to alleviate the effects of ISI. Therefore, to reach reasonable system performance and to decrease the complexity of the equalizer, ZF equalization technique has been used in this research [7]. The equivalent channel matrix with noise given by [11][12]:

$$H = H_{r,d} F H_r \quad (9)$$

$$n = H_{r,d} F n_r + n_{r,d} \quad (10)$$

Where $H_r$is the channel between source and relay and $H_{r,d}$is the channel between relay and destination.

The estimated received signal $\hat{x}$ can be determined as following:

$$\hat{x} = W_{ZF} Y \quad (11)$$

Where $W_{ZF} = H(H^H H)^{-1}$,is known as the ZF pseudo-inverse for a general $m \times n$ matrix and $(.)^{-1}$indicates simple matrix inversion.

3. Results and Discussion

In this research two-hops MIMO relay network with STBC is simulated by MATLAB software. The MATLAB program used to highlights the performance of STBC MIMO relay compared with STBC

MIMO without using relay (Direct connection). In addition, we have examined the optimum location of the relay, by fixing the Signal to Noise Ratio (SNR) at 20dB and make the distance varied.
In this program the BPSK modulation is used to modulate the information, and also STBC encoder and decoder is used at the source and destination sides. The backward channel (source to relay) and the forward channel (relay to destination) are Rayleigh fading channel with zero mean complex circular AWGN. In addition, the ZF relay scheme is used at the receiver side as equalizer to alleviate the effects of ISI. At the relay node the AF technique has been used because it's easy to implement and the results near to practice one. The results have been divided to two sections:

Section I: The performance is measured by means of calculating the Bit Error Rate (BER) and plotting against the SNR between the source and destination, where the SNR is varied between 0 to 30dB. The MIMO network is used, with and without using relay. The distance in this section has been fixed as D for source-relay and relay destination, and 2D for direct connection (without aid of relay) as shown in Figure 3.

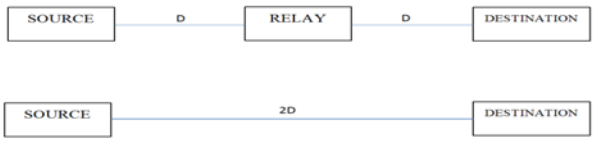

Figure 3. The distance considerations.

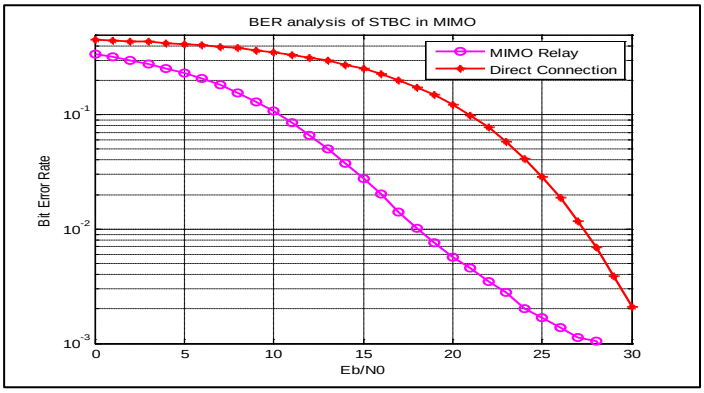

Figure 4. BER for MIMO using relay (MIMO relay) and MIMO without relay (Direct Connection).

As can be seen from Figure 4, the curves show the performance of MIMO using relay (MIMO relay) and MIMO without using relay (Direct Connection) between the source and destination using ZF algorithm for both. It can be observed that the BER performance for (MIMO relay) network is much better than the performance of MIMO(Direct Connection) network that's because the relay amplify and forward the information at distance D and retransmitted it again while in direct connection the source transmit the information directly over distance 2D with the same transmitted power. So, when we compare the BER plot, we can see that (Direct Connection) network has around **3dB poorer** performance than (MIMO relay) network. That's introducing the relay network in the MIMO system minimize the BER which is more constructive in practical communication systems.

Section II: In this section the SNR has been fixed at 20dB and the distance between the source and relay is varied. This step has been taken to find out the optimum location for the relay between the

source and destination. In this part, we estimate the distance between the source and destination as unit function equal to 1, so the distance between source to relay is D and relay destination B=(1-D). Therefore, the relay location starts at 0.1 and ends at 0.9.

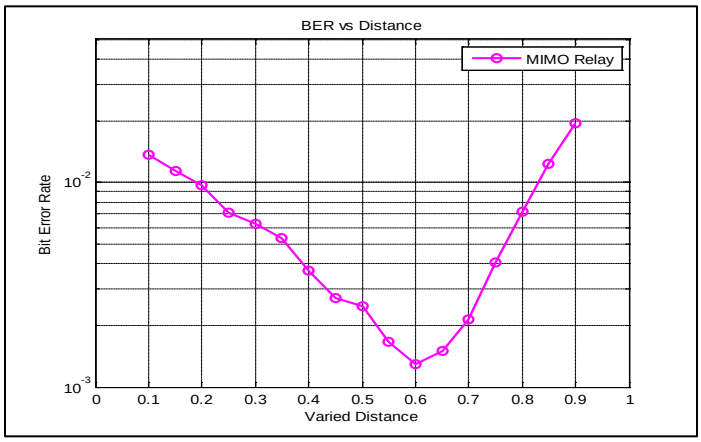

Figure 5. Find out the optimum location of the relay between the source and destination.

As can be seen from Figure 5 the curve shows optimum location of the relay between source and destination and the effects of changing the relay location. The curve shows the best location for the relay between source and destination. As can be seen from output performance the best place for relay is almost in the middle distance between source and destination. In addition, the worst case when the relay was near to the destination.

4. Conclusion

In conclusion, the aim of this paper was the performance of Space Time Block Codes (STBC) in MIMO relay communication systems. The research showed the relevant theories for MIMO relay network and STBC coding in order to get the appreciation for the theoretical predictions of the performance of the MIMO relay network systems. The simulation used the STBC based on multi-antenna cooperative systems and provided the corresponding simulated performance under Rayleigh fading channel AF algorithm and ZF equalizer. The system performance is improved more with the (MIMO relay) network than the MIMO system without the aid of relay network (Direct connection). In addition, to get the best performance of the MIMO relay network the relay has to be at the middle distance between the sources and destination.

References

[1] M. Alamouti, "A Simple Transmit Diversity Technique for wireless communications", *IEEE Journal on seleareas in communications*, Vol. 16, No. 8, October 1998.

[2] D. Gesbert, M. Shafi, D.S.Shiu, P.Smith and A.Naguib, " From Theory to Practice: An Overview of MIMO space-time coded wireless systems".

[3] A. Stefanov, E. Erkip, On the performance analysis of cooperative space-time coded systems, in: *IEEE Wireless\ Communications and Networking*, 16–20 March 2003, vol. 2, pp. 729–734.

[4] Y.Wang, F.Liu, S. Xu, X.Wang, Y. Qian and P.Wang, "Performance Analysis of Multi-hop MIMO Relay Network", *IEEE Communications society*, ICC 2008 workshop proceedings.

[5] A. Nosratinia, E. Hunter and A. Hedayat, "Cooperative Communications in Wireless Networks", Adaptive Antennas and MIMO Systems for Wireless Communications, *IEEE Communications Magazine*, October 2004.

[6] J. N. Laneman, D. Tse, and G. W. Wornell, "Cooperative diversity in wireless networks: Efficient protocol and outage behavior," *IEEE Trans.on Information Theory*, vol. 50, no. 12, pp. 3062–3080, Dec 2004.

[7] N.Ngajikin, W.N.Ahmad, N.Fisal and S.K.Yusof, "Simulation on Performance of Space time Block Code", *RFand Microwave Conference*, October 2004.

[8] Y.fan and J. Thompson, "MIMO Configurations for Relay Channels: Theory and Practice", *IEEE Transactions on wireless communications*, Vol. 6, No. 5, May 2007,

[9] S. Behbanhani and R. Merched, M. Eltawil, "Optimizations of a MIMO Relay Network*", IEEE transactions on signal processing*, Vol. 56, No. 10, October 2008,

[10] S. Atapattu and N. Rajatheva, "Exact SER of Alamouti code transmission through amplify-forward cooperative relay over Nakagami-m fading channels," in *Proc. IEEE International Symposium on Communicationsand Information Technologies ISCIT '07*, 2007, pp. 1429–1433.

[11] Y. Song, H. Shin, and E. Hong, "MIMO cooperative diversity with scalar-gain amplify-and-forward relaying," *IEEE Trans. Commun.*,vol. 57, no. 7, pp. 1932–1938, Jull 2009.

[12] Y. Ding, J. K. Zhang and K. M. Wong, "The Amplify and Forward Half Duplex Cooperative System: Pairwise Error Probability And Precoder Design", *IEEE Transaction on Signal Processing,* Vol. 55, No. 2, pp. 605-617, February 2007.

Building English Vocabulary Schema and Words Retention using Review Value Calculation for English as Secondary Language Students

Burnhan Mustafa Tanis[1*], Melvin A. Ballera[2], Mosbah Mohamed Elssaedi[3]
[1]burnhanmt@outlook.com, [2]melvin.ballera@tip.edu.ph, [3] mosbah_us@hotmail.com
[1] AMA University - School of Graduate Studies, Philippines
[2] Technological Institute of the Philippines - Manila, Philippines
[3]Faculty of Science - Computer Science, Sirte University, Libya

ABSTRACT

Vocabularies, the core of any language, is probably the most challenging and time consuming part of learning a foreign language in a diverse and disperse community of learners. This study proposes an approach that can help a learner build up his/her English vocabulary volume by intensive article reading, the inclusion of Google Cloud Natural Language API and Glosbe Dictionary API, the use of review value calculation computing technique. The review vale calculation were able to determine the number of days were the new words should be reviewed and be part of the long-term memory. Result shows that students were able to increase their words acquisition skills by applying technology and computing. Students were able to retain words fast and understand better, by employing an interactive monitoring process. If the system will be implemented carefully, it is hypothetically produce a faster technique in acquiring new vocabularies for foreign students.

Keyword— Vocabulary schema, review value calculation, short term memory, long term memory, assessment interval

1. Introduction

E-learning has been used to help students learn the English language in their own convenient time and place [1]. It has become a large industry offering online lessons to students with the use of video-conference system. Video conferencing fosters communication and collaboration and trainee-teachers and can jointly dissect the newly acquired knowledge [2][3]. The author [4] concluded that video conferencing is a "powerful tool" to give students confidence in innovative teaching practices. More students view it as a great alternative to learning the English language outside the classroom. They see it as new age education systems that can bring knowledge in an updated form. Vocabulary is one of the critical part of learning English language. It is a fundamental way to comprehend whatever the student hears, reads and most importantly, how the person communicates to the world. It is known to be one of the hardest of acquiring the knowledge to speak the English language but it is often overlooked. With more teachers and learners giving priorities to Grammar and Reading Skills, students have a hard time learning and retaining the words that they have learned. They immediately forget the words after the teacher has given them the meaning or even after looking at the dictionary.

A lot of studies suggested on how students can improve their vocabulary. One of the best would be through reading.

A long-term habit of extensively reading articles that are appropriate for a learner's English ability can greatly improve the vocabulary and command of a learner of English. However, this strategy may be difficult to implement for a learner with no extensive vocabulary because the learner may have problems either in choosing appropriate levels of articles in accordance with her/his needs and interests or in figuring out the meaning of unknown words using the semantics of familiar words in an article that is obtained. Dictionaries are always helpful; however, the need to continually look up unknown words, which once learned may be forgotten in a few days as per learning curve theory, might also easily discourage a learner. Several studies have also developed language tutoring systems in order to assist learners in learning language and have also proposed different personalization strategies [5]. With regard to an e-learning system, it is also hard to select appropriate articles for such learners if details on or precise profiles of learners are never established.

This study proposes an approach that can help a learner build up his/her English vocabulary volume by intensive article reading, during which meanings of unknown words are understood in the context of articles, assessment test and the used of evolutionary computer science technique, the review value calculation for determining vocabulary memory retention. The intention is to obtain the vocabulary from articles more affective, so learners will not easily forget the words.

2. Related Literature

Vocabulary learning is the area in which learners use learning strategies most frequently [6]. Oxford defines learning strategies as "operations employed by the learner to aid the acquisition, storage, retrieval and use of information". Vocabulary learning has been classified into two ways the traditional vocabulary learning and technology savvy vocabulary learning. Traditional vocabulary learning prepare selected vocabulary lists to assist learners and claim that such lists can reinforce students' memories and understanding of the words. However, it is impossible to compile a vocabulary list that is appropriate for all the students in a class with different English levels [7]. Another study used keyword method as the best memory technique for learning concrete words but not abstract words [8]. Another suggests that the use of vocabulary notebook/index cards can be an effective shortcut to achieve [9]. Ideally, the words recorded in the notebook/index cards are chosen according to the need of individual learners, thus learner autonomy is raised. As a matter of fact, learner autonomy and its effectiveness have been widely recognized. One way to aid vocabulary acquisition is through the use of technology in pedagogically sound manner [10]. Semantic mapping is a popular strategy used in classrooms. Learners are encouraged to use concepts and relationships to create a semantic map in which keywords are highlighted. Linkage is formed between the above information and the new word so as to reinforce the memory of the new word. Researchers have both positive and negative comment toward this method [11]. It is also interesting to note that both traditional and technology savvy technique is worthy to mention however there still a need to address

and develop new innovative ways to improve learning in vocabulary acquisition using deterministic peer review calculation that deals with words retention and acquisitions.

3. Vocabulary Architecture and Methods

Figure 1 shows the English vocabulary schema building processes which are composed of four phases: assessment phase, practicing phase, vocabulary acquisition phase, and the actual acquisition phase. During assessment phase, the level and interest of the learner will be initially assessed to create learner's vocabulary schema, profiles and a personalized learning process. The establishment of interest and level of the student (based on European standard), the system is capable of rendering 25 – 40 articles, depending on the information taken during the initial assessment. As the learning process progress, short quizzes will be given based on the learner's vocabulary schema to determine learner's comprehension.

Practicing phase on the other hand is capable of helping learners through human English native speakers subject to the availability of online Instructor. Usually, learners will request an online instructor for actual mentoring and tutoring. Results will then be recorded for profiling the learner's vocabulary schema. When the user requested to speak to a native speaker, the system will find a teacher that is available at that time in the system. The native speaker will then be given enough time to review the student's level and vocabulary schema before speaking to the student.

Vocabulary acquisition phase is a stage where an article will be presented based on learner's level, interest and profiles. The article is directly link to the Google Cloud Natural Language Application Programming Interface (API) to determine parts of speech and grammars rules, lemmatization and stemming while Instructor define vocabularies that needs to be learned by the learners. Actual acquisition stage define the meaning of the vocabularies, employing Glospe Dictionary API to define the vocabulary according to the localized definition of words and language conversion from language to another e. g. English to Spanish and to other recognized languages.

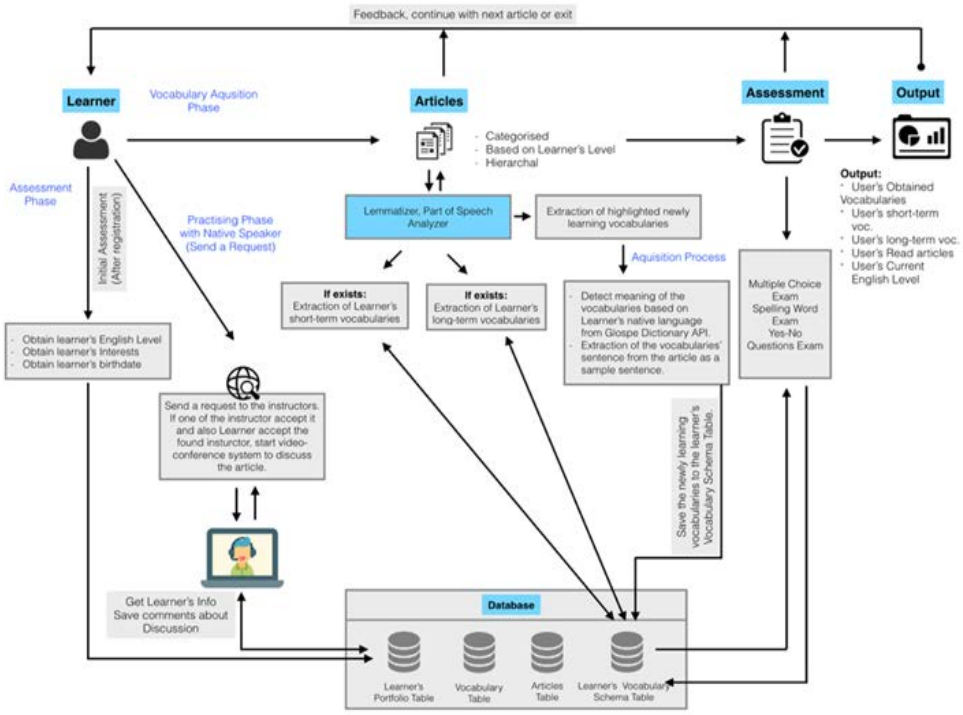

Figure 1: The vocabulary learning processes of the system

In the learning process and acquiring new words, the review value calculation will dynamically computed to determine reinforcement (reading related articles), adjustment (quizzes) to make sure that new vocabularies will be learned. The higher the value of review value calculation the higher its memory retention. There are four essential table that will keep the progress and assessment of the leaner: learner's portfolio table, learner's vocabulary schema table, general vocabulary table and article table. These tables will contain the entire learner's information such as interest, level and articles which will be saved automatically. This is where Review Value Calculation Module will get all the information before giving the user the appropriate articles to read, vocabulary to use in the articles and quizzes to give.

Looking at the conditions, if the learner gets lower than 3 out of the given 4 questions, learner stays in the same level, but on the other hand, if the learner gets 3 or more he would then move on to the next succeeding questions until the system finds his rightful level. To determine the acquisition of a new vocabulary, short-term and long–term should be determined using the concepts of review value calculation or *rvc*. Short-term refers to any newly obtained vocabulary in the system. When user obtains a new vocabulary it will be marked as a default short-term. Each newly obtained vocabulary is ranked as 1 in the user's vocabulary schema. As the words continuously appearing in the quizzes its rank increases. The system will compute the assessment interval or *Ai* as shown in (1). The lower the rank of the word, the more it would appear in assessment so the learner could master that particular word. If the words reaches rank 4 then it will be transferred to long term memory.

$$Ai = \left(round(0.5 * rc) + (2 * sp) + (2 * riec)\right) * rg \quad (1)$$

The assessment interval, *Ai* is computed in terms of days. The next assessment for that particular vocabulary is after 36 days. A quiz containing that word would then appear and if the learner gets it correctly, a new assessment interval would then take places and it could appear – depending on the system's calculation, a month, a year or so. Nevertheless, after 36 days interval and an assessment happen, if the user got it wrong, it would be degraded again into short-term.

4. Results And Discussion

For brevity, figures and tables have been restructured; only 20 out of 50 learners have been used for discussion. A total of 50 students were extracted from 1000 possible learners of the company. Table 1 shows the initial level of learners from different countries doing online courses of English Communication, mostly from Turkish, Russian, European and Central Asian. The age average is 24.5 with standard deviation of 1.25. The area of interest is adventure while English level is ranging from beginners level A1 to B1.

Table 1: Users' profile and initial assessment result

#	Name	Family Name	Initial Level	Vocabulary Area	Age	User's Native Lang.
1	Kubilay	Künç	A2	Adventure	34	Turkish
2	Numan	Numan	A1	Adventure	42	Turkish
3	Mücella	Çelik	A2	Adventure	20	Turkish
4	Zeynep	Pampal	A1	Adventure	17	Turkish
5	Ömer	Mindivanli	B1	Adventure	22	Turkish
6	Ahmet Turan	Bakır	A2	Adventure	23	Turkish
7	Furkan	Pehlivan	A1	Adventure	21	Turkish
8	Selman Kasim	BAĞIRICI	A2	Adventure	17	Turkish
9	İbrahim	Özsürücü	B1	Adventure	19	Turkish
10	Adalet	Arıkanoğlu	B1	Adventure	20	Turkish
11	Uğur	Özdemir	A2	Adventure	25	Turkish
12	Ahmet	Söyler	A2	Adventure	26	Turkish
13	Öznur	Karakılınç	A1	Adventure	30	Turkish
14	Яна	Елфимова	A1	Adventure	24	Russian
15	Barış KARSLI	KARSLI	A1	Adventure	22	Turkish
16	Лёша	ЯН	A2	Adventure	21	Czec Rep.
17	Mustafa	Onat	A1	Adventure	19	Turkish
18	Leopoldo	Datuin	B1	Adventure	33	Moldova
19	Orxan	Ismayilov	A1	Adventure	19	Azerbaijan
20	EMRE	ULAKÇI	A2	Adventure	32	Turkish

It has shown that the participants have almost the same level considering their age and nationalities. This may be probable due to less exposure of English language on these countries. The development process of vocabulary schema was divided into three parts, namely: will be obtained, newly obtained and obtained vocabulary words.

Table 2 shows the status of the 20 learners with their corresponding records given the articles in the area of adventures. The third column corresponds to the target vocabulary or will be obtained vocabularies. For student number 1 for example, it requires to have a 110 to be obtained vocabularies but 78 were obtained with rendered 10 articles out of 15 articles and etc. All these are all part of showing the students' progress throughout their journey in enhancing their vocabulary schema and learning English.

Table 2: Learners profile on target vocabulary and number of articles

#	Name	Family Name	Target Vocabulary	Vocabulary Area*	Obtained Vocabulary	User's Native Lang.	Article Level	Total Article	Finished Article
1	Kubilay	Künç	110	Adventure	78	Turkish	A2	15	10
2	Numan	Numan	100	Adventure	80	Turkish	A1	22	18
3	Mücella	Çelik	110	Adventure	80	Turkish	A2	15	18
4	Zeynep	Pampal	100	Adventure	50	Turkish	A1	20	10
5	Ömer	Mindivanli	113	Adventure	45	Turkish	B1	20	7
6	Ahmet Turan	Bakır	115	Adventure	45	Turkish	A2	15	8
7	Furkan	Pehlivan	100	Adventure	45	Turkish	A1	20	12
8	Selman Kasim	BAĞIRICI	115	Adventure	70	Turkish	A2	15	11
9	İbrahim	Özsürücü	113	Adventure	50	Turkish	B1	20	7
10	Adalet	Arıkanoğlu	113	Adventure	60	Turkish	B1	20	9
11	Uğur	Özdemir	115	Adventure	70	Turkish	A2	15	13
12	Ahmet	Söyler	115	Adventure	50	Turkish	A2	15	9
13	Öznur	Karakılınç	100	Adventure	40	Turkish	A1	25	12
14	Яна	Елфимова	100	Adventure	40	Russian	A1	22	12
15	Barış KARSLI	KARSLI	100	Adventure	60	Turkish	A1	22	15
16	Лёша	ЯН	115	Adventure	80	Czec Rep.	A2	22	18
17	Mustafa	Onat	100	Adventure	90	Turkish	A1	22	20
18	Leopoldo	Datuin	113	Adventure	50	Moldova	B1	20	10
19	Orxan	Ismayilov	100	Adventure	70	Azerbaijan	A1	22	17
20	EMRE	ULAKÇI	115	Adventure	60	Turkish	A2	22	11

Apart from the front-end of the system, another major component to consider as to how review value calculation algorithm is implemented to support improving the learner's vocabulary schema is considering the back-end, formula used in finding the assessment of interval. Assessment interval defines the schedule on when that particular vocabulary should appear in the quiz. Considering the performance during exam counter, how many times the word appeared in the articles and did the learner conduct a speaking practice with the lecturer online, are the components of finding the assessment interval. For discussion, student number 2 were taken and extracted for discussion.

Applying the formula discussed in previous section, Table 3 derived the attributes of *vocabulary_id* 62, and the assessment interval of the vocabulary will be assessed after 4 days. Looking at the *created_at* entry, this shows when the vocabulary was first seen and if it appears in other articles *updated_at* will be refreshed. But based on the assessment interval, if the particular word was created last 2017-11-29, a quiz will be given to the learner four days later (2017-12-03) regarding the vocabulary.

This approach is actually seen in General English Proficiency Test, GEPT, in Taiwan as early as 2000. Same vocabulary and articles used in different levels of GEPT for different levels of English abilities. In addition to adjusting memory cycles of vocabulary (Wang, 2012), it also infers the relationships between words in an article and intelligently adjusts the memory cycles of those words that do not appear in the after-reading quizzes but are known to a learner. This approach does not only enhance the learner's vocabulary schema but also checks the learnt word from time-to-time with assessment interval.

Table 3: The assessment interval of a particular student

id	user_id	av_id	vocabulary_id	ranking	review_counter	review_in_exam_counter	speaking_practice_counter	assessment_interval	next_assessment_dt	created_at	updated_at
85	2	66	62	1	3	1	0	4	2017-12-03	2017-11-29 18:i:46	2017-11-29 18:i:19
87	2	65	61	1	1	1	0	3	2017-12-02	2017-11-29 18:i:46	2017-11-29 18:i:46
88	2	64	60	2	1	2	0	5	2017-12-04	2017-08-10 18:i:19	2017-11-29 18:i:19
89	2	63	59	1	1	1	1	5	2017-12-04	2017-11-29 18:i:46	2017-11-29 18:i:46
84	2	58	55	1	5	1	1	7	2017-12-06	2017-11-29 18:i:46	2017-11-29 18:i:19
86	2	57	54	2	3	2	1	8	2017-12-07	2017-08-10 18:i:19	2017-11-29 18:i:19
83	2	56	53	1	3	1	1	6	2017-12-05	2017-08-10 18:i:19	2017-11-29 18:i:46
78	2	55	52	1	2	1	1	5	2017-12-04	2017-08-10 18:i:19	2017-11-29 18:i:46
82	2	53	50	3	1	3	1	9	2017-12-08	2017-08-10 18:i:19	2017-11-29 18:i:46
81	2	52	49	1	2	1	0	4	2017-12-03	2017-08-10 18:i:19	2017-11-29 18:i:46
80	2	51	48	1	3	1	0	4	2017-12-03	2017-11-29 18:i:46	2017-11-29 18:i:46
77	2	50	47	3	1	3	0	7	2017-12-06	2017-11-29 18:i:46	2017-11-29 18:i:46
79	2	49	46	1	1	1	0	3	2017-12-02	2017-11-29 18:i:46	2017-11-29 18:i:46
76	2	48	45	1	1	1	0	3	2017-12-02	2017-11-29 18:i:46	2017-11-29 18:i:46

Figure 2 shows the monitoring of individual progress of the user in terms of his/her vocabulary schema. It includes the number of gained short-term and long-term vocabularies. This graphic illustration is presented for visual and vivid purposes. Out of 67 new acquired vocabularies 10 of which were converted into long-term while the other is currently active based on read articles. Clicking the show button in Figure 2 will show all the new vocabularies learnt by the learner. The vocabulary, type of figure of speech and its translation are all shown to serve as if a dictionary of its own and refer as the vocabulary schema. Learners can easily track his/her own progress with a click in his/her most convenient time. The used of review value calculation provide essential factor to support improving the learner's vocabulary schema is through the promotion of the learner from one level to another. For instance, the system can shows and monitor students who makes progress by increasing its level. For example student 2 was able to obtain 100 new vocabularies and after taking a handful of quizzes; he would be promoted to A2.

Figure 2: Long-term vs. short-term vocabulary

Vocabulary, the core of any language, is probably the most challenging and time consuming part of learning a foreign language. It takes time and flows like a continuous process, once you have settled the fundamentals of a language (pronunciation, orthography and basic grammar). Throughout this process, learners become familiarized with the words they come across. It is the frequency of usage and the number of encounters in different forms and contexts that determine the acquisition of new vocabulary. When teaching vocabulary, the context is really important that is why some authors underlines the important words that can be used for real communication [12]. The great challenge for

teachers to design individual and group activities using the Internet resources is how to explore different cultures more directly and effectively [13]. University language learners studying English as additional subject, still have problems in acquiring vocabulary. The assumption is that this might be due to the strategies used in teaching vocabulary. Thus, language teachers and researchers started considering technology as an option to teach more effectively. It seems that learners show very little effort to deal with their problems about newly learned words when technology is involved. During the lesson teachers often assume that students will deal with this problem of vocabulary building outside the class on their own. However, learners do not have enough knowledge about the vocabulary learning techniques and they have difficulty in dealing with this problem themselves [14].

5. Conclusion

Learning new vocabulary is one of the most challenging and time eating processes of foreign learners. Several vocabulary type of researches have navigated this area of tutoring and successfully implemented in different manners. The study focus on learning new vocabulary by rendering articles for reading based on the user interest and entry level thereby progressing in due time. To make sure that the acquisition of vocabulary will happen, a computing mechanism has been incorporated into the system using review value calculation. By it used, learners were able to monitor their progress and vocabulary acquisition by transferring to long-term memory from short term memory. Based on the results many foreign students were able to demonstrate fast comprehension and understanding. Almost all the student increased their English level according to European English Level Framework. Although the study is successfully implement, computing mechanism in words acquisition, there is a need to have an intelligent system to help the learners to advance in words acquisition. For example, a presence of an artificial intelligence to teach the student and encourage them to continue is needed for faster words acquisition. Another proposal is to transform the learning process into a game based tutoring system in acquiring new vocabularies.

References

[1]. Kritikou, Yioli (2013).Cognitive Web-Based Vocabulary Learning System: The Results Of A Pilot Test Of Learning Greek As A Second Or Foreign Language. Procedia - Social and Behavioral Sciences 141 (2014) 1339 – 1345.

[2]. Johnson, T.E, Maring, G.H., Doty, J.H., & Fickle, M. (2006). Cyber mentoring: Evolving High-End Video Conferencing Practices to Support Preservice Teacher Training. Journal of Interactive Online Learning 5(1), 59-74.

[3]. Hu, C. & Wong, A. F. L. (2006). Video Conferencing by Student Teachers: Does it Make Any Difference? New Horizons in Education, (53), 42-56.

[4]. Kent, A. M., Simpson, J. L. (2010). Interactive videoconferencing: Connecting theory to practice for pre-service teachers. Journal of Digital Learning in Teacher Education, 27(1), 12–21.

[5]. Atkinson J. (2009). Designing a feedback component of an intelligent tutoring system for foreign language. Knowledge-Based Systems, 22(7), 496-501.

[6]. Klapper, J. (2008) 'Deliberate and incidental: vocabulary learning strategies in independent second language learning', in Hurd, S. and Lewis, T.,(eds.) (2008) Language Learning Strategies in Independent Settings, vol. 33, Clevedon, Multilingual Matters.

[7]. Graham, S.,Harris, K.R., and Loynachan, C. (1993). *Journal of Educational Research* 86 (6): 363-368.

[8]. Stoller, F.L., &Grabe, W. (1993). Implications for L2 vocabulary acquisition and instruction from L1 vocabulary research in Huckin T., Haynes, M., and Coady, J. (eds.), *Second language reading and vocabulary learning*, pp.24-45. Norwood, New Jersey: Ablex.

[9]. Schmitt, N. & Schmitt, D. (1995). Vocabulary notebooks: theoretical underpinnings and practical suggestions.*ESL Journal* 49(2): 133-143.

[10]. Sahin, Mehmet. (2009). Computer Assisted Instruction in Aiding Second- Language Learners. Eurasian Journal of Educational Research. Issue 34. Pp. 115-132.

[11]. Nation, I.S.P. (1990). *Teaching and learning vocabulary*. Boston. Heinle and Heinle Publishers.

[12]. Warschauer, M. (1995). E. Mail for English Teaching. Alexandra, VA: TESOL Publications. The role of using Facebook in improving English, TOJSAT : The Online Journal of Science and Technology- July 2013, 3 (1).

[13]. Nadar, R. (1996) Digital democracy in action, Forbes. 2 December: 49, The role of using Facebook in improving English TOJSAT : The Online Journal of Science and Technology- July 2013, Volume 3, Issue 1

[14]. Monica S., &Mirabela P. A. (2014). The Impact of Social Media on Vocabulary Learning Case Study Facebook. http://steconomiceuoradea.ro/anale/volume/2014/n2/013.pdf

Using Triple Modular Redundant (TMR) Technique in Critical Systems Operation

Samira Abu Shernta[1], Ali A. Tamtum[1*]
[1]sss191278@gmail.com, [1*]aamtamtum@yahoo.com
[1,1*]Department of Electrical and Computer Engineering, Elmergib University, Libya

ABSTRACT

Many computing systems used in applications of critical systems utilize fault tolerance criteria for normally continuing to operate. Operating in the presence of faults is required in many applications for safety and reliability such as in electric power distribution systems, telecommunications, medical life-support, nuclear reactor control, transportation, automotive, aircraft, and space vehicles. Such systems require continuity and reliability of service. One of the used techniques for meeting the severe reliability requirements inherent in certain future computer application is the use of Triple Modular Redundant (TMR) configuration. Essentially, this technique depends on voting two out of three system output levels. In this paper a fault-tolerant system is proposed using TMR configuration for processors and memory modules with spare model for - line self- reconfiguration. A voter is designed to pass reliable data and signals between processors and memory modules. The voter has the capability to analyze the error and stop the system on the proper time. The proposed system is designed at register level and tested using MATLAB simulation. A set of different faults are injected in different modules of the system in different data pater. The simulation results present the accuracy and capability of the proposed system with respect to faults as well as the ability of errors handing.

Keyword— Triple Modular Redundant (TMR); Critical systems; Voter; Computing systems.

1. Introduction

Many systems require continuity and reliability of service while operating in the presence of limited faults. The ability to deliver highest quality of service for which it is intended is very important criteria in critical systems. To fulfil these primary requirements, fault tolerant techniques are necessary to make sure these systems are fault-tolerant systems which continue to operate satisfactory in the presence of faults[1]. One of the used techniques for meeting the severe reliability requirements inherent in certain future computer application is the use of Triple Modular Redundant (TMR) configuration. The author in [2] stated that the TMR technique required tight synchronization between different units which achieved by using a single and very reliable clock to insure continuity of operation in fault tolerant systems. A fault tolerant system is a system that its behaviour is compatible with its specification in presence of faults in some of its components [3]. Faults in different operating systems are presented in many publications such as in [4] and [5] which represent detailed information regarding fault time latency and transient faults. The choice of error detection, fault handling techniques and their implementation as well as the classes of faults are presented in [6].
Multi-Version techniques based on the use of two or more versions or "variants" of a piece of software, executed either in sequence or in parallel are presented in [7]. Dynamic recovery is generally more hardware-efficient than voted systems, and it is, therefore, the approach of choice in resource-

constrained systems especially in high performance scalable systems.. Its disadvantage is that computational delays occur during fault recovery where fault coverage is often low and special operating systems may be required [8].

Error detection checks that are employed in computer systems can be of different types, depending on the system and the fault of interest. Most error detection mechanisms are presented in [9]. Error coverage and mechanisms of error prediction and of latent errors are presented in [5, 10, 11]. Error detection methods such as Watchdog timers have been used since the early days of digital systems especially in embedded systems [12, 13].

The concept of redundancy implies the addition of information, resources, or time beyond what is needed for normal system operation. The redundancy can take one of four forms, including hardware redundancy, time redundancy, software redundancy, and information redundancy. The concept of hardware redundancy became more common and more practical, the cost of replicating hardware within a system is decreasing simply because the cost of hardware are decreasing. The Hardware redundancy means the addition of extra hardware, usually for the purpose either detecting errors or tolerating faults[14].

The most known hardware fault tolerance technique is triple modularity redundancy (TMR), which has been used in many fault tolerant systems. The use of TMR technique and its advantages as well as the use of multistage TMR with replicate voters are presented in [15] and [16]. In [17], a commodity chip multiprocessors (CMP) design with features for providing system-level soft error protection, is described with dual modular redundant (DMR) and triple modular redundant (TMR) systems. In [18], A hypothetical triple-modular redundant computer is subjected to a Monte Carlo program on the IBM 704, which simulates component failures. Two types of namely duplex and triple modular redundancy (TMR) systems are presented in [19]. More application and representations of TMR are presented in [20-22]

In this paper a fault-tolerant system is proposed using TMR configuration for processors and memory modules with spare model for –line self- reconfiguration. A voter is designed to pass reliable data and signals between processors and memory modules.

2. The Proposed TNR System

2.1. TMR Technique Review

The most known hardware fault tolerance technique is triple modularity redundancy (TMR), which has been used in many fault tolerant systems. The hardware unit (M) represented in Figure1 is triplicated and all three units work in parallel. The outputs of these three units are given to the voting element (V). The voting element accepts the outputs from the three modular and delivers the majority vote as output.

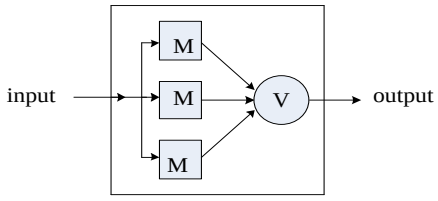

Figure 1: Triple Modularity Redundancy (TMR) organization

Clearly, the TMR organization can completely mask the failure of the one hardware unit. One of the features of TMR is that no explicit actions need to be performed for error detection, recovery, etc, TMR is particularly suitable for transient faults, since in the basic TMR the voter does not "remove" the faulty unit after an error occurs. This scheme cannot handle the failure of two units. In fact, once one unit fails, it is essential that both units should be work correctly (so that the voter can get a majority voted output). Due to this, the reliability of the TMR system becomes lower than a simplex system once a failure occurs.

The TMR scheme depends on the voting element. However, the voting element is typically a simple and highly reliable circuits. Another implementation aspect of TMR is that it requires tight synchronization between the different units. This has been frequently achieved by using a single clock. This requires the clock to be very reliable.

2.2. The Proposed System

Triple Modular Redundancy (TMR) configuration is the most efficient method to tolerate many types of faults and masking many types of errors at the system level. It is suitable for real time applications and online system reconfiguration where instant maintenance is not possible such as in Autopilot and unmanned space vehicles. This configuration tolerates the following set of faults:

- Faults effecting the operation of processors, memory modules and system buses.
- Faults produced from programs, compilers used to produce those programs
- Design and manufacturing faults in processors modules and memory modules.

Whereas the set of occurred errors that can be masked by this configuration includes the following classes:

- Processors internal transient errors.
- Processors internal intermittent errors.
- Data bus errors.
- Address bus Errors.
- Control and timing bus errors.
- Memory transient errors.
- Memory intermittent errors.
- Memory buses errors.

In a TMR configuration permanent errors caused by any faulty module are detected but not tolerated. Therefore the faulty module has to be replaced by a good one in order to resume system functions. Real-Time applications cause long down-time and increases Mean Time To Repair MTTR. In such a system the MTTR should be zero in order to recover from those errors and to continue system operations to achieve a high reliability.

To overcome a wide range of those errors and to tolerate that set of faults, a good configuration is proposed for a high reliable and available system with Self-Reconfiguration. In this proposed configuration, processors modules are treated separately from memory modules and the memory modules form also TMR subsystem. Another feature of this configuration is that voting is done at the signals level (data, address and control signals) between the processors modules and the memory modules.

According to this proposed configuration, the three processors (1,2,3) work in parallel and execute the same code and perform the same task. All signals outgoing from these processors are passed through a voter that compares these signals and passes the majority matched ones. If one processor does not match with the other two then the selected majority output from the voter is passed to the memory modules (or to the external I/O devices). Then that processor or its system bus is considered faulty and is given a time to recover from transient faults. If the same processors shows faulty outputs for more than a pre-specified attempts, it is considered as permanent faulty module and the whole system enters a reconfiguration procedure by bringing the spare processor to replace the faulty one.

The same process is done with the memory modules when data is read from memory to the processors. The voter is introduced with two sides: one side for the processors modules and the other side for the memories modules. The voter should also be designed in such a way to work as a comparator and by pass buffer. The voter should also have the mechanism to reconfigure the system by isolating (disconnecting) a faulty module and invoking (connecting) the spare module. The other task of the voter is to load the invoked processor with the current state of the other two processors by a roll-forward recovery procedure and resuming the system operation.

2.3. System Operation

The following assumptions are considered for the proposed system:

1 System is at start state.
2 All named model are loaded with the same copy of the program.
3 All three processors are ready to execute the same program.
4 The spare processor is physically connected but logically and electorally disconnected.
5 Give all general block diagram to used voter, three processors and three memories.

The block diagram of the voter are shown in Figure 2 which represents the composition of the Voter.

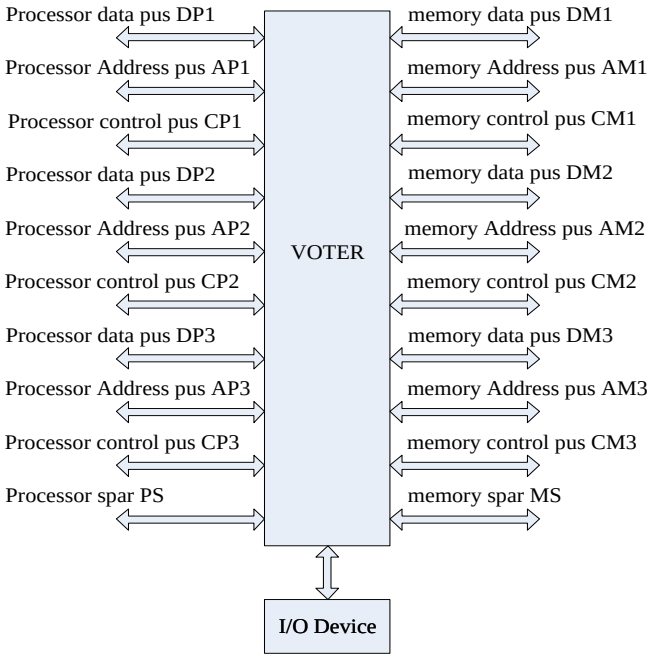

Figure 2: Block Diagram of the voter

In the input side of the Voter there are three processors (Data, Address, and Control) as well as a spare processor. Similarly, in the output of the Voter there are three memories (Data, Address, and Control) as well as a spare memory. Data will be transferred to the I/O devices in case of data saving fail.

Figure 3 represents operating flow chart in which the system starts working by applying either Read or Write command. The system is then tested whether it is working or not. If the system working, a check is made on Address, Control and Data. If not, processors are added to the system and the system is tested again. Then, the three processors are tested. In case of error detection, the damaged processor is specified and repaired and the system continues working. Then data writing and saving in the memory is done. On the other side the process of reading data from the memory is running. Then a test is made. In case of an error is detected, error is located and repaired. This process continues until finishing the desired job.

The operation starts in " write cycle" by entering data to pr1,pr2 and pr3. After that ,the operation is tested to know if there is an error or not?

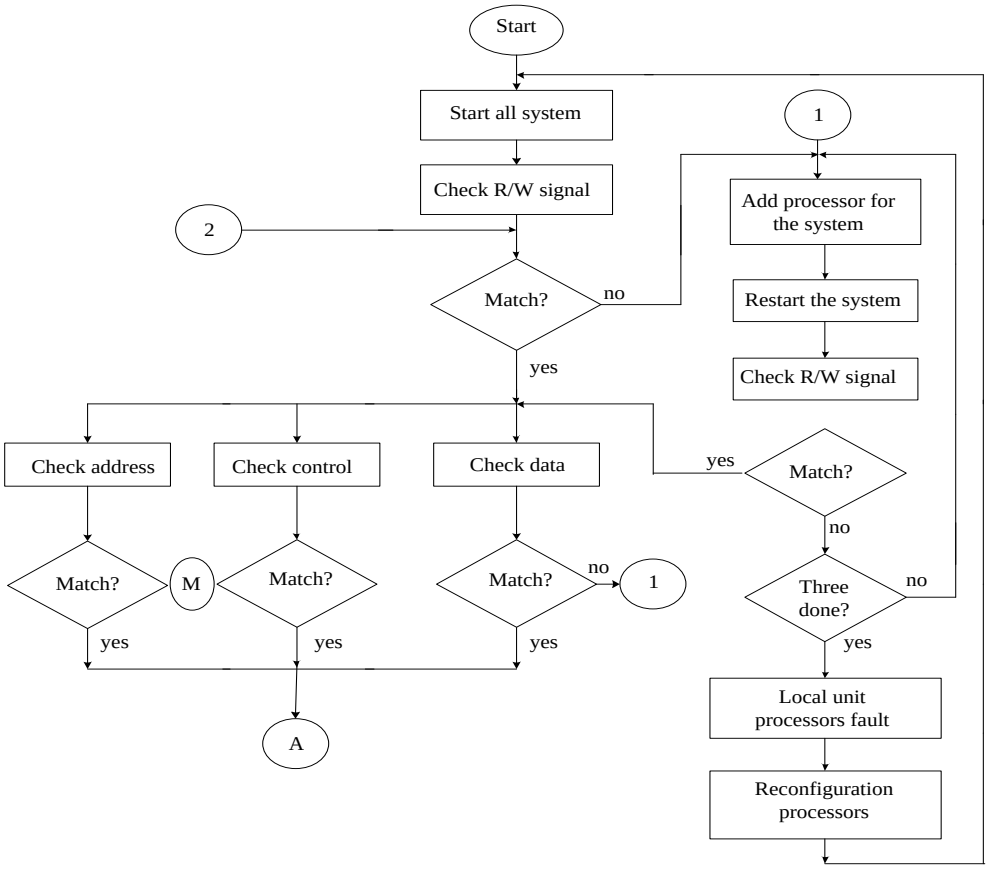

Figure 3: Operating flow chart

There are two cases "Yes" or "No".

"yes" means there is an error and another test will start to know whether the error is permanent or not. The voter will know in which process the error occurs.

" no" means that the error is transient and it may be regain by doing the operation again. Once the faulty process is known, it will be changed by a spare process to continues the operation .

Case II: If "NO" we need to know where the results will be sent. There are two options. Either the results will be sent to the memory and the data will be saved into "me1,me2 and me3 " or the data will be sent into the input ,output devices.

Regarding read cycle, the data will be read from the memory and the operation will continue to the end of the cycle in similar manner.

3. Numerical results

The results can be summarized in Tables 1, 2, 3,4, 5 and 6 which represent Processor Data Bus, Memory Data Bus, processor address Bus, memory address Bus, Control processor Bus and Control memory Bus including total time latency.

Table 1: Processor Data Bus

Module	Injected faults	Detected faults	Time Latency (Second)	Coverage	System Recovery (Y,N)
Dp1	0	0	2.7375e-005	0	N
Dp2	0	0	2.7375e-005	0	N
Dp3	4	3	2.7375e-005	75%	Y
Total	4	3	8.3991e-005	75%	Y

The system considered healthy when DP3 recorded failure two consecutive times. When number of errors =3,a permanent error in DP3 is recorded and changed with the spare one (DPs).

Table 2: Memory Data Bus

Module	Injected faults	Detected faults	Latency (Second)	Coverage	System Recovery (Y,N)
DM1	2	2	2.9241e-005	100%	Y
DM2	0	0	2.9241e-005	0	N
DM3	0	0	2.9241e-005	0	N
Total	2	2	8.7724e-005	100%	Y

A permanent error in DM1is recorded with latency time = 2.9241e-005 sec; and total latency time = 8.7724e-005sec;The error in DM1 is temporary and a 100% recovered.

Table 3: Processor address Bus

Module	Injected faults	Detected faults	Latency (Second)	Coverage	System Recovery (Y,N)
Ap1	0	0	3.2352e-005	0	N
Ap2	3	3	3.2352e-005	100%=100%	Y
Ap3	0	0	3.2352e-005	0	N
Total	3	3	9.7055e-005	100%	Y

The number of injected errors equal to 3, and the error in AP2 is permanent and changed with the spare one (Aps).

Table 4: Memory address Bus

Module	Injected faults	Detected faults	Latency (Second)	Coverage	System Recovery (Y,N)
AM1	0	0	2.8152e-005	0	N
AM2	0	0	2.8152e-005	0	N
AM3	6	3	2.8152e-005	3/6*100%=50%	Y
Total	6	3	8.4457e-005	50%	Y

Number of errors =3 and permanent error in AM3. The spare AMs replaces the mean AM3 with 50% coverage.

Table 5: Control processor Bus

Module	Injected faults	Detected faults	Latency (Second)	Coverage	System Recovery (Y,N)
Cp1	2	2	2.8774e-005	2/2*100%=100%	Y
Cp2	0	0	2.8774e-005	0	N
Cp3	0	0	2.8774e-005	0	N
Total	2	2	8.6323e-005	100%	Y

The error in CP1 is temporary with 100% coverage.

Table 6: Control memory Bus

Module	Injected faults	Detected faults	Latency (Second)	Coverage	System Recovery (Y,N)
CM1	0	0	2.9863e-005	0	N
CM2	3	3	2.9863e-005	3/3*100%=100%	Y
CM3	0	0	2.9863e-005	0	N
Total	3	3	8.9589e-005	100%	Y

The number of errors =3 and the error in CM2 is permanent. The spare CMs is utilized instead of using the mean CM2.

4. Conclusions

The principles and concepts of fault tolerance were introduced and investigated. The analysis was devoted to the online error detection and mainly focused on the use triplication techniques. According to the outcome from the survey of the online error detection techniques and investigation of some previous systems, a TMR system configuration was proposed to increase system reliability and availability for self – reconfigurable application. In this system both the processor and memory module are triplicated with one spare module. A voter was designed to pass reliable data and singles between processors module and memory modules. The voter has the capability to stop the system and analysis the error. It enters the system for roll- back procedure in case of transient error or it replaces the faulty module with the spare one in case of permanent error. Thus system is recovered and resumes its operation on line which achieves the target objective. To verify the capabilities and the behaviour of proposed system and voter design, the system is simulated using MATLAB package. A set of faults are injected in different information paths and the response of the system was monitored.

References

[1]. N. Kim and S. Gupta "Testing of Digital Systems" , *Cambridge University press 2003*.

[2]. Chris Weaver , Todd Austin, "A Fault Tolerant Approach to Microprocessor Design" *Advanced Computer Architecture Laboratory University of Michigan*, July 2001.

[3]. Teijo Lehtonen ,Juha Plosila, Jouni Isoaho, "On Fault Tolerance Techniques towards Nanoscale Circuits and Systems " *Turku Center for Computer Science*, TUCS Technical Report, August2005..

[4]. Ali H. Maamar ,Asma y. Elhawadi, "Self Checking Register file" *Computer Department HigherInstitute of Electronics, Beni- Waled*, APRIL 1999.

[5]. Lisboa, C. A. Erigson, M.I. and Carro, l.andcarro ,L, "System level approaches for mitigation of long duration transient fanlts in future technologies", *12th IEEE EuropeanTcst Symposium (ETS,07),* 2007.

[6]. Januu Sosnowski, "Transient fault Tolerance in Digital System", *Warsaw University of technology, IEEE*, 1994.

[7]. Subhasish Mitra, "Diversity Techniques for Concurrent Error Detection" *Technical Report , Center for Reliable Computing* , may 2000.

[8]. Parg K Lala "Sef- checking and fault –Tolerance Digital Design", *Morgan Kaufmann Publisher*,2001.

[9]. Manoj Franklin , "A Study of Time Redundant Fault Tolerance Techniques for Superscalar processors", *Department of Electrical &computer Engineering , Clemson Universty ,Clemson, USA*, 1995 IEEE.

[10]. Stanislaw J. Piestrak," Design of fast self -testing checkers a Class of Berger Codes", *IEEE Transaction on Computer*, MAY 1987.

[11]. [11] Kim and K. G. Shin , "Evaluation of Fault Tolerance Latency from Real -Time Application 's Perspectives", *IEEE Transactions on Computers*, vol . 49 No 1,Jan. 2000.

[12]. Robert Redinbo, " Generalized Algorithm-Based Fault Tolerance: Error Correction via Kalman Estimation", *IEEE Transactions on Computers*, Vol. 47, No. 6, June 1998.

[13]. Robert Redinbo, " Generalized Algorithm-Based Fault Tolerance: Error Correction via Kalman Estimation", *IEEE Transactions on Computers,* Vol. 47, No. 6, June 1998.

[14]. Constantinescu, "Teraflops Supercomputer : Architecture and Validation of the Fault Tolerance Mechanisms", *IEEE Transactions on Computers*, Sep 2000.

[15]. Karri, K. Kim, and M. Potkonjak, " Computer Aided Design of Fault-Tolerant Application Specific Programmable Processors", *IEEE Transactions on Computers*, Nov 2000.

[16]. Dutt and N. R. Mahapatra, "Node-Covering, Error Correcting Codes and Multiprocessors With Very High Average Fault Tolerance*", IEEE Transactions on Computers*, Sept 1997.

[17]. James E. Smith, " Motivating Commodity Multi-Core Processor Design For System-Level Error Protection", *Kewal K. Saluja* 2006.

[18]. George W. Grosline, "The Use of Triple-Modular Redundancy to Improve Computer Reliability", *IBM Journal*, April 1962.

[19]. Rami Melhem, "Energy-Efficient Duplex and TMR Real-Time Systems Appeared in the IEEE Real-Time Systems Symposium", *Computer Science Department, University of Pittsburgh*, Dec 2002.

[20]. Dmitry Burlyaev, Pascal Fradet, Alain Girault, "Verification-guided voter minimization in triple-modular redundant circuits", *Automatin& Test in Europe Conference & Exhibition (DATE),* Year: 2014.

[21]. Jeffrey Prinzie, Michiel Steyaert, Paul Leroux, Jorgen Chrisiansen, Paulo Moreira, "A single-event upset robust, 2.2 GHz, to 3.2 GHz, 345fs jitter PLL with triple-modular redundant phase detector in 65 nm CMOS", *IEEE Asian Solid-State Circuits Conference (A-SSCC),* Year: 2016..

[22]. Pang Zh, Qi Zheng, Zhankui Zeng, Liman Yaung, "The single integrity design and simulation of triple-modular redundant (TMR) computer", *IEEE International Conference on Cybernetics and Intelligent Systems (CIS) and , IEEE Conference on Robotics, Automation and Mechatronics (RAM),* Year: 2017.

Handwriting Arabic Words Recognition Based on Structural Features

Salim Aloud
salemali416@yahoo.com
Department of Computer Science, College of Sciences
Azzaytuna University, Libya

ABSTRACT

Handwriting recognition technology is the ability of a computer to recognize characters, words and other symbols that have been written by hand in natural handwriting. This study presents a method for recognition of Handwritten Arabic Words (HAW) through expanding in the way of structural features extraction by relying on geometrical information (straight lines, loops, points, and curve). The input to the system is binary images written by hand by number of people. The features are to convert the image from two dimensional into one dimensional as a victor that is to be used as a signature for the image the experiments have been conducted on a database of a thousand words representing names of a hundred Libyan cities at a rate of ten patterns for each city. Classification of the words was dependence on Artificial Neural Networks (ANN) of Multiple Layers Perception (MLP) type. Wherein half of the words were used to train the network and the other half to test the network. The ratio of recognition was 80.4 %.

Keyword— recognition, features extraction, structural information.

1. Introduction

Words and characters recognition methods have been improved since many years. These methods used for printed or handwritten scripts and used two different approaches of processing which are online and offline. It has been gaining more interest lately due to the increasing popularity of handheld computers, digital notebooks, and advanced cellular phones. These devices nowadays are commonly used worldwide that encouraged companies to improve their products to support multi languages. These devices can deal with many languages spoken by billions of people around the world. Arabic language is the main language of all Arabic countries with more than 280 million people are speaking this language as a first language and by 250 million as a second language. Arabic language comes as the fifth rank of most commonly used languages in the world. There are some other languages related to Arabic language. These languages have some similarities with Arabic language whence from the characters shapes or from the pronunciation [1] .the progress in Arabic language is slower than the progress in developing solutions for Latin and Asian languages [7].There are many other applications for analysis of human handwriting such as writer recognition and verification, form processing, interpreting handwritten postal addresses on envelopes and reading currency amounts on bank checks etc. The main problem encountered when dealing with handwritten Arabic characters is that characters written by different persons representing the same

character are not identical but can vary in both size and shape. unlimited variation in human handwriting styles similarities of distinct character shapes, character overlaps, and interconnections of neighboring characters. In addition, the mood of the writer and the writing situation can have an effect on writing styles [2][4][6] Handwritten recognition starts with image preparation stage by transforming it from a color image into grayscale image. Then convert it into a binary image. . The preparation stage is followed by features extraction stage during which the image is converted into a group of features in order to change them from two dimension data to one dimension data or a victor of the features. In general the features come in three main parts statistical features, structural features and global transformation. [1]. In this study the structural features are used which depend on the word's geometrical information as ratio of the length to the width, the loops, branching points, straight lines and the curve or slopes in the various directions. The process of separation of the features of each word connected with it, occurs by relying on the ANN of the MLP type. The training process takes place by allowing the network to practice on half of the number of patterns at a rate of 5 models, or patterns for each word. The training algorithm place by way of back propagation (BP) which is used to train the MLP type network [8]. The testing process was conducted on the other half of the patterns which amount to 500 words. The recognition rate was over 80%.This paper is organized as follows: Section 1 gives a brief description of Arabic Alphabet Characteristics. Section 2 explained Features extraction stage. Section3 explaining classification stage by ANN. Section 4 gives Experiments and results.

2. Arabic Language Alphabet Characteristics

The Arabic language has a lot of advantages which make it different from the other ones in terms of shape, and way of writing and direction of the writing and which are clarified as follows:

1. Arabic text (machine printed or handwritten) is written cursively and in general from right to left.
2. Arabic writing uses letters, punctuation marks, spaces, and special symbols.
3. An Arabic letter might have up to four different shapes, depending on its relative position in the word: 1: isolated, 2: connected from the left, 3: connected from the right and 4: connected from both right and left according to its place in the word like the letter (ع). Table 1.
4. Some letters exist as a combination of two letters in some certain situations, like the letter (lamelif لا) which is created by combining two letters , the letter(lam ل) and (alif ا).
5. Sixteen Arabic letters have from one to three secondary components. The type and position of the secondary components are very important features of Arabic letters. For example, Tah (ط) and Thah (ظ) differ only by the number of dots above the main body, Seen (س) and Sheen (ش), Sad (ص) and Dad (ض).

Table 1: show four different shapes for letter (ع)

(a) isolated	(b)connected from the left	(c)connected from the right	(d)connected from both right and left
ع	عـ	ـع	ـعـ

6. Arabic writing contains many fonts and writing styles. The letters are overlaid in some of these fonts and styles.
7. Ligatures are combinations of two and sometimes three letters into a single shape [4].

In general, the Arabic writing is written by using different writing techniques, or styles which result in letters and words having different shapes which in turn cause obscurity in any recognition system.

In general the Arabic writing may be classified into three different styles:

Typewritten: This style is generated by computer. It is the simplest one because the characters are written without overlaps or ligature.

Typeset: This style is more difficult than the typewritten because it has many ligatures and overlaps. It is used to write newspapers and books. Nowadays, this style may also be generated using computers.

Handwritten: This style is the most difficult because of the variation of writing the Arabic alphabets from one writer to another [3].

3. Features Extraction

The first step in features extraction stage is preprocessing stage. In this step the image convert from gray scale into binary image which means it has only two levels zero (0) level which represents a background, and level (1) which represents foreground. The change process occurs by using the threshold technique. And then extract connected components through convert it into labelled image [9]. Then the features extraction stage comes. The features extraction stage is considered as the most important stage of the study and the capability of any recognition system to differentiate any writing depends to a large degree on the exactness of the features extracted from the image. In this study the structural features are used.

Structural features describe the geometrical and topological characteristics of a pattern by describing its global and local properties. The structural features depend on the kind of pattern to be classified. For Arabic characters, the features consist of (ratio of the length to the width, the loops, branching points, straight lines and the curve or slops in the various directions).In this study; the structural features have been used where a word is divided as in the Figure 1. Features of each area are extracted by analyzing the connected components existing in each area.

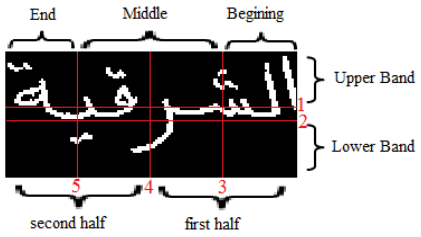

Figure 1: show sample of the name (الشرقية)

The letter alif (ا)usually appears in the upper part of a word and its height is twice as large as its width or more Figure 2. And the loops: each part of the binary image that has the color of the background, and whose edges have the color of the foreground, and falls within the connected components is regarded as a loop Figure 3.

Figure 2: detect letter alif

Figure 3: detect loop

The calculation of one point is found out through calculation of the area, of each component, and case where the area is less than the threshold, it is considered as a point Figure 4. And in case where the width of the component is bigger or equal to twice its length (-) then the component is considered as two points Figure 5.

And in case there is a curve in the point falling above a word, the component is then regarded as three points (ـٮـ) Figure 6.

Figure 4: detect one point

Figure 5: detect two points

Figure 6: detect three points

The features that are possible to obtain in the lower part of the image are:
The letters of Arabic language that may appear underneath a word are
(ج ح خ ر ز س ش ص ض ع غ ل ن و ي) detect this features by tracing the number of crossings from the background to the foreground horizontally (h) and vertically (v) at middle connected component if h =1 and v = 1 return (curve ر) Figure 7. If h = 2 and v = 1 return (curve ن) Figure 8. if h = 1 and v = 2 return(curve ح) Figure 9.

Table 2: shows details of features vector

element	Description
1	Number of straight lines(ا) in beginning of word
2	Number of straight lines(ا) in middle of word
3	Number of straight lines(ا) in end of word
4	Number of loops in beginning of word
5	Number of loops in middle of word
6	Number of loops in end of word
7	Number of points(•) up the word
8	Number of points(•) down the word
9	Number of (curve ر)in first half of word
10	Number of (curve ر) in second half of word
11	Number of (curve ن)in first half of word
12	Number of (curve ن) in second half of word
13	Number of (curve ح)in first half of word
14	Number of (curve ح) in second half of word
15	Number of (letters kaf ک) in the word

Figure 7: detect curve ر

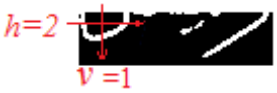

Figure 8: detect curve ن

Figure 9: detect curve ح

-

The letter kaf calculated either by calculating the width of the component Figure 10.

Or by tracing the number of crossings from the background to the foreground vertically Figure 11.

Figure 10: detect character kaf

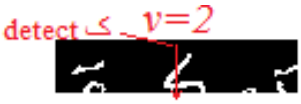

Figure 11: detect character kaf

In this study a features vector containing 15 elements has been set up each of which expresses a feature of the word in a way that each image is represented by a vector containing 15 elements. This vector is the one that is used in the process of training and testing of the ANN. This vector is shown in Table 2. For example the word (توكرة) Figure 12 its features vector was as follows:

Features vector = [0 0 0 1 0 1 4 0 1 1 0 0 0 0 1]

Figure 12: word (توكرة)

The first, second and third elements are 0, 0, 0 and they mean that they don't contain the straight lines neither on the beginning of the word nor the middle or end of the word. The fourth component (1) means existence of a loop at the beginning of the word, the fifth nonexistence of a loop in the middle of the word, the sixth which is (1) existence of one loop at the end of the word, the seventh (4) meaning existence of four points over the word, the eight (0) nonexistence of points under the word and the ninth which is (1) meaning existence of a (curve ر) in the first half of the word and the tenth (1) which means existence of an (curveر) in the second half of the word. The eleventh and twelfth which are (0), mean nonexistence of (curve ن) in the first nor second half of the word. The thirteenth and fourteenth which are (0) mean the) curve ح) without its curve in the first half or the second one. The fifteenth (1) means existence of the letter (Kaf ک) in the word.

4. Classification Stage

The process of separation of the features of each word connected with it occurs by relying on the ANN of the MLP type which is used to separate any data even if they are not linear. The MPL network contains three layers input, hidden and output layer and in each layer there is a number of nodes Figure 13 [4]. The number of nodes in the input layer is equal to the number of elements in the features vector (15 elements). But the number of the nodes in the output layer depends on the number of the words which are to be separated (100 words). The hidden layer lies between the input and output layers. The training algorithm place by way of back propagation (BP) which is used to train the feed forward network MLP type network with supervised learning [8].

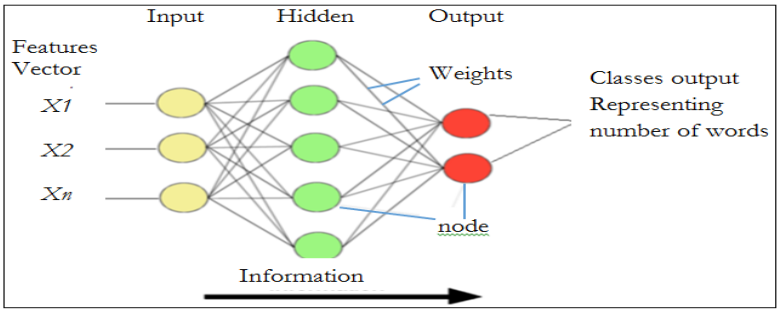

Figure 13: ANN of the MLP type

5. Experiments

5.1. Training Mode

In the training mode the first half of the data was selected and such a half represents 500 words at a rate of 5 forms for each word .The number of the names is 100 which requires to be 100 classes. And as the features vector includes 15 components, the number of the input layer nodes becomes 15. The number of the hidden layer's nodes was 22. As the required number of the classes is 100, the number of the output layer's nodes was 7. And the learning rate was 0.2 the network has been trained by counting on iteration in a way that the number of the iteration was determined to be at 30000, a number that reached to $8.222 * 10^{-5}$ by the average of the errors.

5.2. Recall Mode

In this mode the values of the weights are fixed. The neural network works to determine only the input data in each class. The values of the weights are not changed nor there a calculation for the error. In the recall mode, the other half of the patterns, totaling 500 words and representing an extra 5 models for each word, have been used.

6. Results

Out of the 500 words, the result was that the ANN classified, 402 correct words while 98 words were identified incorrectly, which means the rate of recognition was 80.40 % as in the Table 3.

Table 3: shows the results of study

Number of words	Correct words	Incorrect words	rate of recognition
500	402	98	80.4%

7. Conclusion

In this research, the way the features are extracted has been expanded upon to involve more details on the geometrical features connected with the word written by hand, which is to discover the curve, underneath the word which appears to lean to the left or to the bottom, thereby leading to more accurate features which in turn contributed in the enhancing rate. It remains a difficult task to try to recognition of Arabic handwriting due to difference in writing styles from one person to another and to various kinds of handwriting and what accompany them in terms of overlapping and interconnection. As such, the main concern is to upgrade the capability to recognition to the maximum extent possible. And the enhancing relies in the main on the way the features are extracted, that is to say, the more exact, or accurate the features are the more better the capability to recognition becomes.

In addition, the recognition enhancing rate depends on the separation method. Through the findings of this research it was found that some errors were attributed to the network not being trained on some patterns, thus not being capable to recognition those patterns. The solution lies in increasing the patterns, or in other words, in training the network on as much patterns as possible. In the future

work, the same methods connected with the findings of this research will be employed in recognizing texts written by hand.

References

[1]. M.A Abuzaraida and A.M Zeki and A. M Zeki " Feature Extraction Techniques of Online Handwriting Arabic Text Recognition " 5 th International Conference on Information and Communication Technology for the Muslim Word 2013.

[2]. H.EL Moubtahij, A.Halli and K.Satori " Review of Feature Extraction Techniques for Offline Handwriting Arabic Text Recognition " International Journal of Advances in Engineering & Technology, Mar.2014. Vol.7,Issue 1,pp.50-58.

[3]. A. Lawgali, A. Bouridane, M. Angelova, Z. Ghassemlooy "Handwritten Arabic Character Recognition: Which Feature Extraction Method? " International Journal of Advanced Science and Technology Vol.34,September, 2011.

[4]. Rafael M. O. Cruz, George D. C. Cavalcanti and Tsang Ing Ren "Handwritten Digit Recognition Using Multiple Feature Extraction Techniques and Classifier Ensemble "IWSSIP 2010 - 17th International Conference on Systems, Signals and Image Processing.

[5]. Ashoka H.N. , Manjaiah D.H. , Rabin dranath Bera " Feature Extraction Technique for Neural Network Based Pattern Recognition" International Journal on Computer Science and Engineering , Vol. 4 No. 03 March 2012.

[6]. Fenwa Olusayo Deborah, Omidiora Elijah Olusayo , Fakolujo Olaosebikan Alade," Development of a Feature Extraction Technique for Online Character Recognition System" Innovative Systems Design and Engineering , ISSN 2222-1727 (Paper) ISSN 2222-2871 (Online)Vol 3, No 3, 2012.

[7]. G. Abandah, K. Younis, M. Khedher " HANDWRITTEN ARABIC CHARACTER RECOGNITION USING MULTIPLE CLASSIFIERS BASED ON LETTER FORM" In Proc. 5th IASTED Int'l Conf. on Signal Processing, Pattern Recognition, & Applications (SPPRA 2008), Feb 13-15, Innsbruck, Austria.

[8]. A. Lawgali, A. Bouridane, M. Angelova, Z. Ghassemlooy "Handwritten Arabic Character Recognition: Which Feature Extraction Method? " International Journal of Advanced Science and Technology Vol.34,September, 2011.

[9]. Rafael C. Gonzalez and Richard E. Woods "Digital Image Processing " Second Edition. Prentice Hall 2002.

A Novel Chaotic Uniform Quantizer for Speech Coding

Osama A. S. Alkishriwo[1*]
[1]alkishriewo@yahoo.com
[1]Department of Electrical and Electronic Eng., College of Eng., University of Tripoli, Libya

ABSTRACT

Quantization is an essential step in the analog-to-digital conversion process and it is very important in all modern telecommunication systems. In this paper, a novel chaotic uniform quantizer is proposed and its application for speech coding is presented. The proposed system consists of three stages: two PCM coders separated by an XOR operation with a chaotic sequence, where the first step is used for continuous signal sampling and second stage performs data encryption, while the third stage provides additional data compression. The performance of the presented quantizer for Laplacian distributed signals and real speech signals is investigated and compared with that of the well-known uniform and non-uniform quantizers. Simulation results show that the proposed quantizer provides secured data with higher levels of SQNR compared to others.

Keyword— Quantization; Uniform quantization; Non-uniform quantization; Source coding; Encryption; Chaotic systems.

1. Introduction

In all modern telecommunication systems, the analog–to–digital conversion is very important phase in the way of processing analog signals. It consists of two main steps which are quantization and coding. Quantization provides a means to represent signals efficiently with acceptable fidelity for signal compression, while coding decides exactly which code–words to assign to each distinct quantization level [1].

Existing quantization schemes can be classified into two categories, namely, uniform quantization and non uniform quantization [2]. Uniform quantization is widely used due to its simplicity of implementation, but not optimal for signals with non uniform distribution in terms of mean square error. While nonuniform quantization is much more complex, it is in general causes less information loss than uniform quantization, especially for small quantization resolutions. Lloyd–Max quantization is a major type of nonuniform quantization [3, 4]. It is optimal in the sense of mean squared error (MSE), but it is computationally intensive. Companding, which consists of nonlinear transformation and uniform quantization, is a technique capable of trading off quantization performance with complexity for nonuniform quantization [5].

In literature, many nonuniform quantizers have been developed to meet the challenge of designing a low complexity and high signal–to–quantization noise ratio (SQNR). In [6, 7] sophisticated compression models based on fixed–rate scalar quantizer for Laplacian probability density function have been recently proposed. The problem of support region optimization has been extensively considered in the field of scalar quantization [8]. The optimization of the support region of the product polar companded quantizer is presented in [9]. This resulted in SQNR increase, but in a

more complex encoding/decoding procedure. Although a great number of quantizers have been developed to provide an additional enhancement of the quantized signal quality, there is still a need to continue the research in this field.

In this paper, a novel chaotic uniform quantizer is proposed. It consists of three stages: two PCM coders separated by an XOR operation with a chaotic sequence. The first step is used for continuous signal sampling using rough quantization with a large number of quantization levels. After that, encoded data are XORed with a uniformly distributed random sequence which is generated from chaotic dynamic system to perform data encryption. The encrypted data are decoded to obtain discrete samples, which are further quantized using a quantizer with a small number of quantization levels in order to provide additional compression. The proposed quantizer is evaluated by means of a computer simulation using synthetic Laplacian source signals and real speech signals. The presented quantizer provides gain in the signal to quantisation noise ratio, encryption of the quantized samples, and compression over the conventional uniform quantizer as well as companding quantizer. This indicates the possibility of practical application of the chaotic proposed quantizer in the contemporary transmission of speech signals.

The rest of the paper is organized as below. Section II presents the preliminaries of chaotic uniform quantizer. Section III describes the proposed chaotic uniform quantizer. Simulation results, comparison and discussion are given in Section IV. Finally, conclusions are summarized in Section V.

2. Preliminaries of Chaotic Uniform Quantizer

2.1. Chaotic Dynamic System

Chaos systems are considered suitable for practical use because of its complex dynamic behaviors. They provide a good combination of speed and high security. They have many excellent intrinsic properties, such as high sensitivity to initial conditions and control parameters, which are the desired properties in the application of encryption. The three dimensional discrete chaotic system, which are presented in [10], is defined as follows

$$\begin{aligned} x_{n+1} &= \left[\frac{\alpha \times (x_n - x_n^2)}{(y_n - y_n^2)}\right] \ mod\ 1 \\ y_{n+1} &= \left[\frac{\beta \times (y_n - y_n^2)}{(z_n - z_n^2)}\right] \ mod\ 1 \\ z_{n+1} &= \left[\frac{\gamma \times (z_n - z_n^2)}{(x_n - x_n^2)}\right] \ mod\ 1 \end{aligned} \qquad (1)$$

The chaotic behaviour of the system is observed when the control parameters are chosen as $0.5 < \alpha, \beta, \gamma < 4$ with the initial conditions x_n, y_n, and $z_n \epsilon$ [0, 1].

2.2. Uniform Quantizer

A uniform quantizer splits the mapped input signal into quantization steps of equal size. If X is a random variable with the probability density function $p_X(x)$ at input of the quantizer is converted to

one of $\boldsymbol{Q}$ allowable levels, $\boldsymbol{m_1}$,$\boldsymbol{m_2}$,..., $\boldsymbol{m_Q}$and $\boldsymbol{Y}$ is a discrete random variable at outputof the quantizer. Then, the quantizer $\boldsymbol{q}$ maps $\boldsymbol{X}$ to $\boldsymbol{Y}$ as follows:

$$\boldsymbol{Y = q(X) = m_i}\,, \qquad \boldsymbol{i = 1, 2, 3, \dots, Q} \tag{2}$$

Thus the quantization error, $\boldsymbol{e_q = x - y}$, is a random variablewith pdf $\boldsymbol{p_{e_q}(e_q)}$ and the average distortion is,

$$\boldsymbol{D = E\{e_q^2\} = \int_{-\infty}^{+\infty} (X - Y)^2 p_X(x)\, dx} \tag{3}$$

where $\boldsymbol{E\{.\}}$ is the expectation value. The signal to quantization noise ratio ($\boldsymbol{SQNR}$) is obtained by dividing the input source variance $\boldsymbol{\sigma^2}$over the average distortion ($\boldsymbol{D}$) as follows:

$$\boldsymbol{SQNR = 10\ \log_{10}\left(\frac{\sigma^2}{D}\right)} \tag{4}$$

3. Proposed Chaotic Uniform Quantizer

The configuration of the proposed chaotic uniform quantizer is shown in Figure 1. The quantization process can be achieved using three main steps. In the first step, analog-to digital (A/D) conversion is performed using a quantizer with a high number of quantization levels $\boldsymbol{Q_1}$, whose purpose is to convert analog signal to discrete samples. Then, the quantized samples are encoded and XORed with a uniform random sequence generated from chaotic system. The resulted data are decoded to obtain an encrypted discrete time signal which has a uniform probability density function. The aim of the second stage is to provide additional signal compression by using a low number of quantization levels $\boldsymbol{Q_2}$ where ($\boldsymbol{Q_2 < Q_1}$). The key stream in the chaotic system is composed of controlparameters $\boldsymbol{\alpha}$, $\boldsymbol{\beta}$, $\boldsymbol{\gamma}$ and initial values $\boldsymbol{x_0}$, $\boldsymbol{y_0}$, $\boldsymbol{z_0}$.

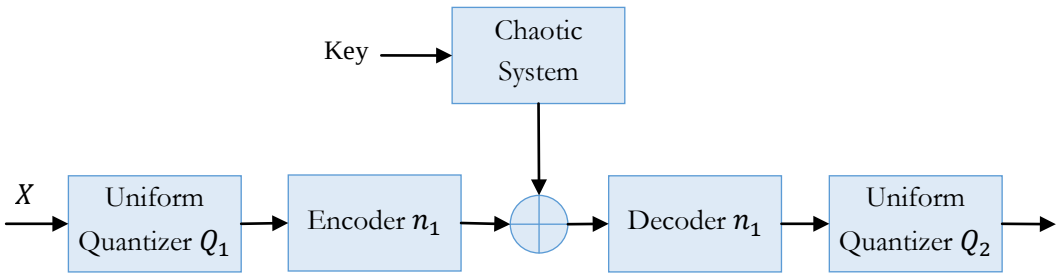

Figure 1: Proposed chaotic uniform quantizer.

4. Simulation Results

The input–output characteristics of uniform quantizer, nonuniform quantizer, and chaotic quantizer are shown in Figure 2. It is known that uniform quantizer has fixed step size and fixed output level as given in Figure 2(a), while nonuniform quantizer has variable step size and fixed output level as

illustrated in Figure 2(b). However, chaotic quantizer has fixed step size and variable output level as shown in Figure 2(c).

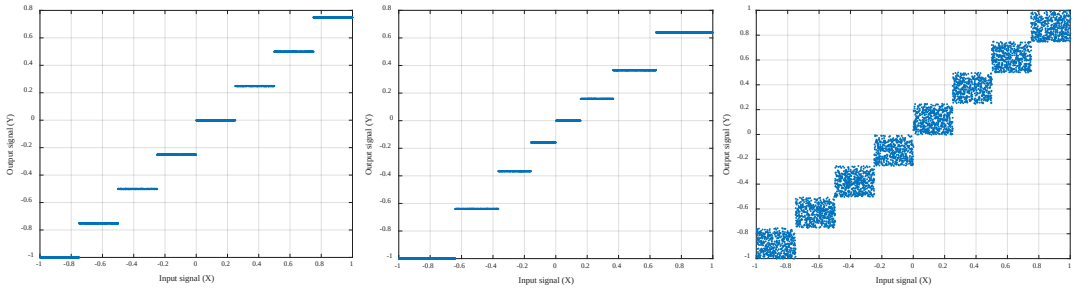

(a) (b) (c)

Figure 2: Quantizer characteristics : (a) Uniform quantizer, (b) Nonuniform quantizer, (c) Chaotic quantizer.

The performance of the proposed chaotic quantizer in quantization of signals having Laplacian probability density function is shown in Figure 3(a). The choice of Laplacian distribution is made so as to match the data typically found in speech coding problem. The results of chaotic quantizer are compared with the results presented by conventional uniform and nonuniform quantizers. As a direct application of the proposed chaotic quantizer for speech coding, it has been applied to a speech signal and the results are reported in Figure 3(b). In both cases, the performance of chaotic quantizer in terms of SQNR is superior to the performances of traditional uniform and nonuniform quantizers. For instance, for the case of Laplacian source, the chaotic quantizer produces $\mathbf{3}\ \boldsymbol{dB}$ and $\mathbf{1}\ \boldsymbol{dB}$ SQNR on average higher than uniform and nonuniform quantizers, respectively. Similarly, for the case of speech signal the improvement on the values of SQNR are $\mathbf{2.5}\ \boldsymbol{dB}$ and $\mathbf{0.8}\ \boldsymbol{dB}$.

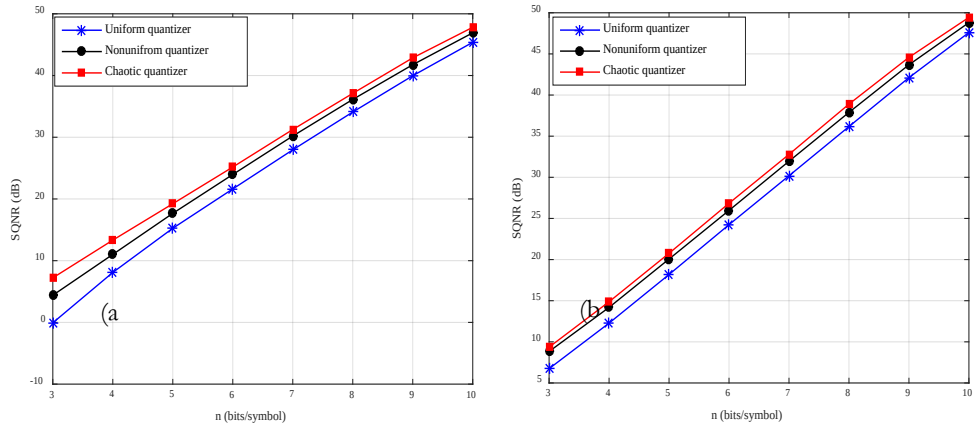

Figure 2: Signal to quantization noise ratio versus number obits per symbol for, (a) Source with Laplacian probability density function, (b) Speech signal.

An important advantage of the proposed chaotic quantizer is the quantization of samples and encrypting them at the same time. The used chaotic system given in (1) has three initial values and three control parameters. Thus,if the precision is set to be $\mathbf{10^{-15}}$, the key space can reach $\mathbf{10^{6\times15}} \approx \mathbf{2^{299}}$, which can efficiently resist the brute-force attack.

5. Conclusions

In this paper, the chaotic uniform quantizer is proposed and its performance for input signal with Laplacian distribution and its application for speech signal processing are explored. Experimental results demonstrate that the chaotic uniform quantizer is superior to the conventional uniform and nonuniform quantizers at all bit per symbol region. It has been shown that the proposed chaotic quantizer provides more constant and higher level of SQNR, which can be considered via the gains in the SQNR that range up to $3\ dB$ as illustrated in the results section. Finally, the quantized samples are encrypted with a chaotic sequence which has a key space of 2^{299}.

References

[1]. N. S. Jayant and P. Noll, Digital Coding of Waveforms, Prentice Hall, Upper Saddle River, N. J., 1984.

[2]. R. M. Gray and D. L. Neuhoff, "Quantization," IEEE Transactions on Information Theory, vol. 44, no. 6, pp. 2325-2383, Oct. 1998.

[3]. S. P. Lloyd, "'Least squares quantization in PCM," IEEE Transactions on Information Theory, vol. IT-28, no. 2, pp. 129-137, Mar. 1982.

[4]. J. Max, "Quantizing for minimum distortion," IRE Transactions on Information Theory, vol. IT-6, pp. 7-12, Mar. 1960.

[5]. ITU-T, Recommendation G.711, Pulse Code Modulation (PCM) of Voice Frequencies, International Telecommunication Union, 1972.

[6]. Z. Peric and J. Nikolic, "An adaptive waveform coding algorithm and its application in speech coding," Digital Signal Processing, vol. 22, no. 1, pp. 199-209, Jan. 2012.

[7]. Z. Peric and J. Nikolic, "High--quality Laplacian source quantization using a combination of restricted and unrestricted logarithmic quantizers," IET Signal Processing, vol. 6, no. 7, pp. 633-640, Nov. 2012.

[8]. J. Nikolic, Z. Peric, and A. Jovanovic, "Two forward adaptive dual--mode companding scalar quantizers for Gaussian source," Signal Processing, vol. 120, no. 3, pp. 129-140, Mar. 2016.

[9]. Z. Peric, M. D. Petkovic, J. Nikolic, and A. Jovanovic, "Support region estimation of the product polar companded quantizerfor Gaussian source," Signal Processing, vol. 143, pp. 140-145, Feb. 2018.

[10]. [M. Y. Valandar , P. Ayubi, M.J. Barani, "A new transform domain steganography based on modified logistic chaotic map for color images," Journal of Information Security and Applications , vol. 34, no. 2, pp. 142-151, Jun. 2017.

Iterative Time-Varying Filter Algorithm Based on Discrete Linear Chirp Transform

Osama A. S. Alkishriwo[1],Ali A. Elghariani[2], Aydin Akan[3]
[1]alkishriewo@yahoo.com, [2]elghariani_99@yahoo.com,[3]akan@istanbul.edu.tr
[1, 2]Department of Electrical and Electronic Eng., College of Eng., University of Tripoli, Libya
[3]Department of Electrical and Electronic Engineering, Istanbul University, Turkey

ABSTRACT

Denoising of broadband non--stationary signals is a challenging problem in communication systems. In this paper, we introduce a time-varying filter algorithm based on the discrete linear chirp transform (DLCT), which provides local signal decomposition in terms of linear chirps. The method relies on the ability of the DLCT for providing a sparse representation to a wide class of broadband signals. The performance of the proposed algorithm is compared with the discrete fractional Fourier transform (DFrFT) filtering algorithm. Simulation results show that the DLCT algorithm provides better performance than the DFrFT algorithm and consequently achieves high quality filtering.

Keyword— Discrete linear chirp transform, Filtering, Discrete fractional Fourier transform, Sparse signals.

1. Introduction

Non–stationary relates to the time--dependence of the statistics of a random process. As such, non-stationary signals display either time–varying mean, variance or evolving spectra, or a combination of some or all of these. It is thus why more sophisticated filtering approaches are needed for the representation and processing of non–stationary signals.

Noise is an unwanted component which acts as a source of error in the signal analysis and should be suppressed before data processing and interpretation. In many cases, therefore, noise mitigation is essential in order to extract useful information from the signal contaminated in noise.

The Fourier transform is one conventional signal denoising technique. However, due to the nonlinear and non–stationary properties of signals, this method is limited in the denoising capability to this kind of signals [1]. To overcome this shortcoming, several new approaches have been proposed in literature. In [2, 3] the least mean square adaptive algorithms are presented, but these algorithm are not able to track the rapidly varying non–stationary signals. Moreover, the wavelet transform (WT) based methods are widely used because of their abilities to remove Gaussian noise. However, the performance of the WT-based denoising methods depends on their selected mother wavelets [4].

To capture the variability with time of the non–stationary signal parameters, it is necessary to consider extensions of the Fourier–based representations capable of providing instantaneous–frequency information for multi–component signals. Although this can be achieved by considering

polynomial–phase transforms [5], second-order polynomial transforms [6, 7] are preferable due to computational viability.

In [7] the discrete linear chirp transform (DLCT) is introduced to represent a signal as a combination of linear chirps. The DLCT is an extension of the discrete Fourier transform (DFT) and provides a parametric modelling of the instantaneous frequencies of the components. Rather than joint time–frequency, the DLCT is a joint chirp–rate frequency transformation. It can be implemented efficiently using the fast Fourier transform (FFT) algorithm [7].

In this paper, a time–varying filtering algorithm based on the DLCT is proposed. The algorithm relies on the ability of the DLCT to decompose a signal iteratively into its components locally. Each of these components is filtered separately and then synthesized with the other filtered components to estimate the desired signal. Since each segment of the signal has different components with different bandwidths, the filter has to be time–varying. The performance of the proposed algorithm is compared with the discrete fractional Fourier transform (DFrFT) based filtering method [8, 9]. Simulation results of the proposed method show better performance on the denoising in comparing with major denoising schemes based on the DFrFT.

The paper is organized as follows. Section 2 shows how to obtain the DLCT and presents some of its properties. In section 3, we introduce the DLCT filtering algorithm. Simulation results are given in section 4, where we compare the DFrFT with the DLCT. In particular, we consider which of these two transforms is more efficient in transforming a non–sparse signal into a sparse–signal in time or in frequency, the resolution of the transforms, and the computational time required. Then, we evaluate the capability of the DLCT in filtering nonstationary signals. Finally, conclusions are summarized in section 5.

2. The Discrete Linear Chirp Transform (DLCT)

For a discrete–time signal $x(n)$, $0 \le n \le N-1$, its discrete linear chirp transform (DLCT) and its inverse are given by [7]

$$x(k,m) = \sum_{n=0}^{N-1} x(n)\, exp\left(-j\frac{2\pi}{N}(c\, m\, n^2 + k\, n)\right) \tag{1}$$

$$x(n) = \sum_{m=-L/2}^{L/2-1} \sum_{k=0}^{N-1} \frac{X(k,m)}{LN}\, exp\left(j\frac{2\pi}{N}(c\, m\, n^2 + k\, n)\right) \tag{2}$$

where c is the resolution of the transform,L and N are the number of samples in the chirp–rate, and in the frequency domain, respectively. The DLCT is a joint chirp–rate frequency transformation that generalizes the discrete Fourier transform (DFT): indeed

$$X(k,m) = \frac{1}{N} X(k) \odot DFT\left\{exp\left(j\frac{2\pi}{N}\, c\, m\right)\right\} \tag{3}$$

where $\odot$ is the circular convolution. Hence, If $m = 0$, then $X(k, 0)$ is the DFT of $x(n)$. Thus, the DLCT can be used to represent signals that are locally combinations of sinusoids, chirps or both.

3. The Proposed DLCT–Based Filtering Algorithm

For a signal $x(n)$ we can identify from its DLCT $X(k, m)$ the number of components Q, the chirp–rates $\beta_i = c\, m_i$, and frequency parametersk_i. The energy concentration is indicated by the peak values of $|X(k, m)|^2$ | as a function of k and m. Considering the region in the joint chirp–rate frequency plane where these peak values occur, we should find the values of the chirp–rates and frequencies that can be used to approximate the given signal locally as a sum of linear chirp components

$$x(n) = \sum_{i=1}^{Q} x_i(n) \tag{4}$$

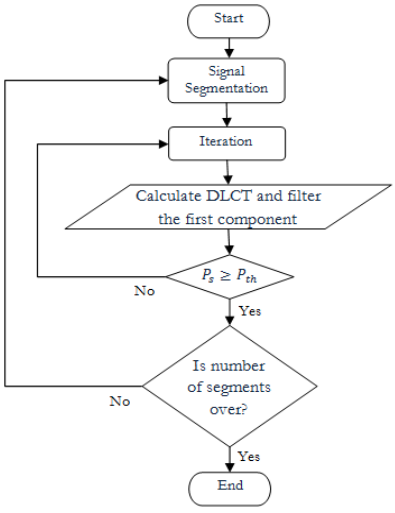

Figure 1: Filtering algorithm flowchart.

If we consider the case of a linear chirp contaminated in white Gaussian noise, filtering it directly without processing will permit for a large amount of noise to stay with the chirp since it has a broad bandwidth. However, if we implement the filtering process in the DLCT domain where the linear chirp has narrow bandwidth, then most of the noise will be removed.

The proposed DLCT filtering algorithm is performed over multiple iterations. Flowchart given in Figure 1 shows the step by step operation of the algorithm. The stopping criterion for the sub-iteration can be set manually by the expected number of components or adaptively based on a threshold P_{th} of the remaining energy P_s in the residual.

4. Simulation Results and Discussion

To evaluate the performance of the proposed algorithm, a simulation is performed to observe and compare the mean absolute error of the filtered signals with the DFrFT filtering algorithm. Both algorithms are applied to a synthetic signal as well as a real world signal. The synthetic signal is generated as follows,

$$x(n) = exp\left(j\frac{\pi}{256}(0.1\,n^2 + 10\,n)\right)$$

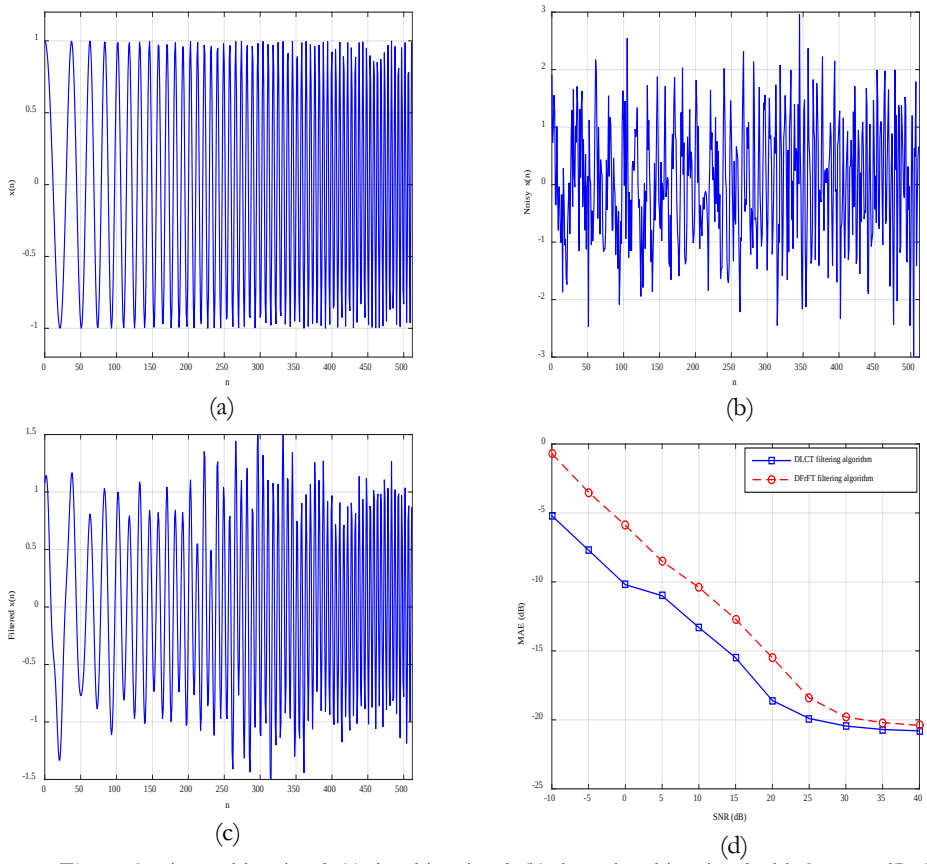

Figure 2: Linear chirp signal, (a) the chirp signal, (b) the noisy chirp signal with SNR= 0dB, (c) the filtered chirp signal using DLCT filtering algorithm, and (d) mean absolute error for the two algorithms.

If the noiseless signal is denoted by $x(n)$ and $\hat{x}(n)$ is the filtered signal, then the mean absolute error can be calculated as follows,

$$MAE = \frac{1}{N}\sum_{n=0}^{N-1}|x(n) - \hat{x}(n)| \qquad (5)$$

Figures 2(a),(b), and (c) show the chirp signal, the noisy chirp signal, and the filtered chirp signal using the DLCT filtering algorithm, respectively. In Figure 2(d), we provide the mean absolute error (MAE) for the two algorithms against signal–to–noise ratio (SNR). It can be seen that the DLCT filtering algorithm outperforms the performance of the DFrFT filtering algorithm, especially at low SNR. For instance, at 0 dB SNR, DLCT has a 5 dB improvement, while at 25 dB SNR, it has only about a 1 dB improvement over DFrFT.

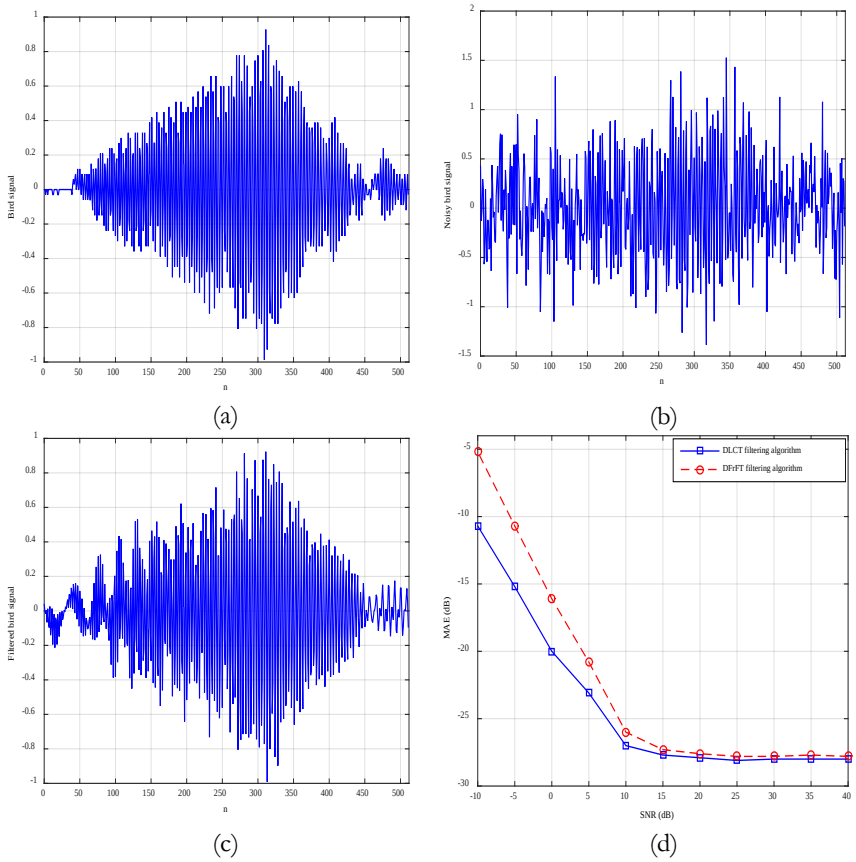

Figure 3: Real–world signal: (a) the bird chirping signal, (b) the noisy bird chirping signal with SNR= 0 dB, (c) the filtered birdchirping signal using DLCT filteringalgorithm, and (d) the mean absolute error for the two algorithms.

To quantify the MAE improvement, a real–world signal (Bird chirping signal) with varying noise level is also simulated. The noiseless and noisy bird chirping signals are presented in Figures. 3(a) and (b). The denoised bird chirping signal based on the DLCT filtering algorithm is shown in Figure 3(c) at SNR=0 dB. Similar to the previous case, Figure 3(d) depicts the MAE for the two algorithms as a function of the input SNR, where input SNR is varied from −10 dB (severely poor SNR) to 40 dB (high SNR).

The DLCT filtering algorithm greatly enhances the MAE by simply employing few iterations in the simulation. This gain occurs because the DLCT algorithm gives sparser signals than the DFrFT algorithm.

5. Conclusion

In this paper, an iterative time–varying filtering algorithm based on the DLCT transform is proposed. The method exploits sparsity structure of signals to improve denoising performance of non-stationary signals. The performance of the proposed algorithm is analysed and compared with the performance of the (DFrFT) based method. Simulation results show that the DLCT filtering algorithm gives lower mean absolute error results than the DFrFT filtering algorithm in both

synthetic and real–world signals. For instance, at SNR=0 dB, the proposed algorithm has a 5 dB improvement over the DFrFT filtering algorithm.

References

[1]. M. Alfaouri and K. Daqrouq, "ECG Signal Denoising By Wavelet Transform Thresholding ," American Journal of Applied Sciences, vol. 5, no. 3, pp. 276-281, 2008.

[2]. V. Almenar and A. Albiol, "A new adaptive scheme for ECG enhancement," Signal Processing, Vol. 75, no. 3, pp. 253-263, Jun. 1999.

[3]. L. Durak and S. Aldirmaz, "Adaptive fractional Fourier domain filtering,"Signal Processing, vol. 90, no. 4, pp. 1188-1196, Apr. 2010.

[4]. J. P. Amezquita-Sanchez and H. Adeli, "A new MUSIC-empirical wavelet transform methodology for time-frequency analysis of noisy nonlinear and non-stationary signals," Digital Signal Processing, vol.45, pp. 55–68, Oct 2015.

[5]. S. Peleg and B. Friedlander, "The discrete polynomial-phase transform," IEEE Transactions on Signal Processing, vol. 43, no. 8, pp. 1901-1914, Aug. 1995.

[6]. C. Candan, M. Kutay, and H. Ozaktas, "The discrete fractional Fourier transform," IEEE Trans. on Signal Processing, vol. 48, no. 5, pp. 1329-1337, May 2000.

[7]. O. A. Alkishriwo and L. F. Chaparro, "A Discrete Linear Chirp Transform (DLCT) for Data Compression," in Proc. of the IEEE International Conf. on Information Science, Signal Processing and their Applications, Montreal, Canada, Jul. 2012, pp. 1283-1288.

[8]. O. A. Alkishriwo, L. F. Chaparro, and A. Akan, "Signal separation in the Wigner distribution using fractional Fourier transform," European Signal Processing Conf., EUSIPCO, Spain, Sep. 2011, pp. 1879-1883.

[9]. P. Kumar and S. Kansal, "Noise removal in speech signal using fractional Fourier transform, " 2017 International Conference on Information, Communication, Instrumentation and Control, ICICIC, Indore, India, Aug. 2017.

Color Image Encryption in the Spatial Domain Using 3-D Chaotic System

Hanan Salem Alzreghi[1], Osama A S Alkishriwo[2]
hanansalem52@yahoo.com, alkishriewo@yahoo.com
[1, 2]Department of Electrical and Electronic Eng., Faculty of Eng., University of Tripoli, Libya

ABSTRACT

Users of Internet daily send and receive many images through social media. These images are vulnerable to hack by attackers. Therefore, it is necessary to develop methods to protect these images against attackers. A nontraditional encryption method for encrypting color images in the spatial domain is proposed. The main idea in this work is based on building strong encryption algorithm through implementing the permutation and diffusion operations on the pixels, where every pixel composed of three values red, green and blue. These operations are implemented depending on extracting three chaotic sequences from the 3-D chaotic system, where each chaotic sequence is used to shuffle and diffuse each color in the plaintext image. The proposed system is tested on well-known images like Lena and Mandrill. Experiments and security analysis prove that the algorithm has an excellent performance in image encryption.

Keyword— Color image encryption, spatial domain, 3-D chaotic system, permutation, diffusion.

1. Introduction

Nowadays information security is a vital problem in information communication. With the advancements of information technology, lots of digital contents are being stored and transmitted in various forms. As a result, the protection of digital contents data against irregular phenomena, such as illegal copying, and guarantee of their secure utility has become an important issue. In particular, compared to text data, some intrinsic features of image data, such as big size, high redundancy of data and strong correlation among neighbouring pixels are different with ordinary information. Therefore, an encryption method with fast speed and high security is needed. But the traditional block encryption being widely used now is found to be inefficient for real-time communication. Hence a lot of image encryption methods using chaotic maps with high sensitivity to their initial conditions and system parameter values and simple structures are proposed[1, 2].

2. Proposed Algorithm

The aim of this work is to design and implement a novel and highly secure method which is essential for confidentiality and to solve the problems of some previous chaotic image encryption schemes. Figure1

depicts the main algorithm executed in this paper and includes three operations which are permutation, diffusion, and linear transformation.

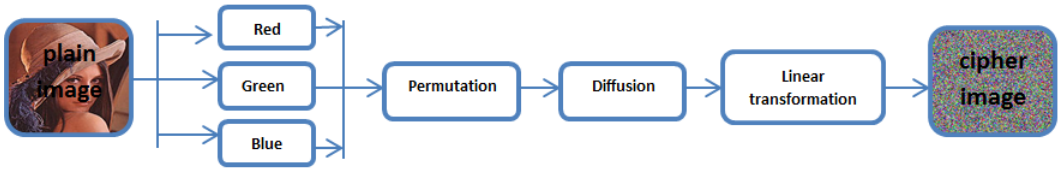

The original color images is divided into three images with Red ,Green and Blue channels,respectively. The encryption steps can be summarized as follows:

(1) permutation process by scrambling operation on all pixels in the image with chaotic sequence.

(2) diffusion process by a sequential XOR operation on all the bits of pixels in the image.

(3) linear transformation process by rotated the image to the left by amount of ℓ_p,where ℓ_p using as a security key, then we decrypte the image using inverse these process.These operations are implemented depending on extracting three chaotic sequences from the 3-D chaotic system, where each chaotic sequence is used to shuffle and diffuse each color in the plaintext image.

3. Chaotic System

The 3-D chaotic system used in this paper can be expressed as follows:

3.1. Logistic-Logistic map

$$x_{n+1} = u \times x_n \times (1 - x_n) \times 2^{14} - floor(u \times x_n \times (1 - x_n) \times 2^{14}) \quad (1)$$

3.2. Sine-Sine map

$$x_{n+1} = u \times \sin(\pi \times x_n) \times 2^{14} - floor(u \times \sin(\pi \times x_n) \times 2^{14}) \quad (2)$$

3.3. Chebyshev-Chebyshev map

$$x_{n+1} = \cos\left((u+1)\cos^{-1}(x_n)\right) \times 2^{14} - floor\left(\cos\left((u+1)\cos^{-1}(x_n)\right) \times 2^{14}\right) \quad (3)$$

where the control parameter $u \in (0, 10)$ and $x_n$is the initial value of the sequence.

4. Experimental Results and Performance Analysis

A good quality encryption scheme should be robust against all types of attack, involves security attack and statistical attack. The proposed procedure is implemented in some color images to demonstrate its efficiency. The results of encryption and decryption are shown in Figure 2.This shows that all encrypted images are noise-like ones and can be efficiently applied to images of various forms such as grayscale images, color images and binary images [3].

Figure 2: Encryption result of some images.

4.1. Histogram Analysis

Image histogram reflects the distribution of pixel values of an image. To resist statistic attacks, the image histogram should be flat. Figure3shows the histograms of the some images and the histograms of their encrypted images. The histogram of the encrypted image has a good uniform distribution, so that it is enough to resist statistical attacks[4].

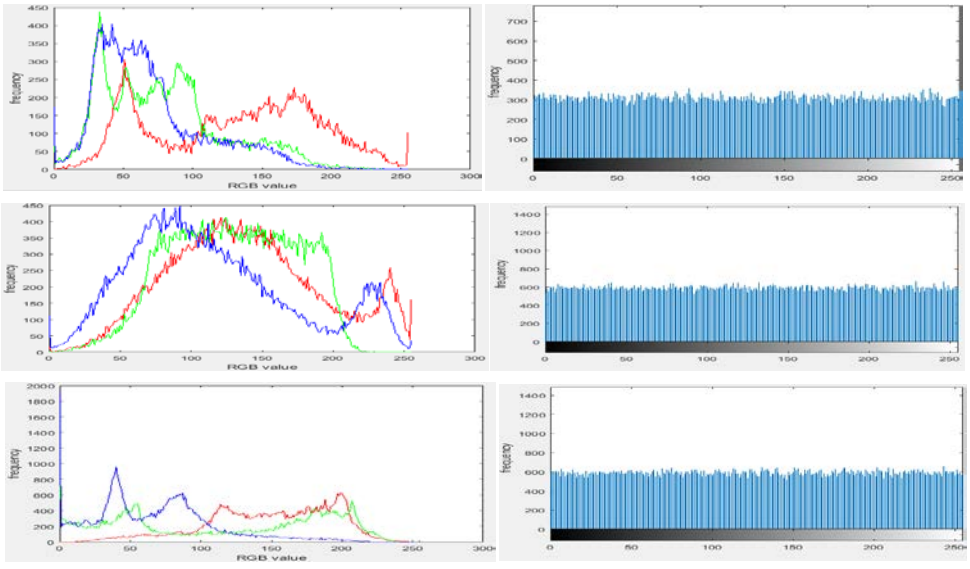

Figure 3: (a) the histogram of the original and encrypted Lena images; (b) the histogram of the original and encrypted Mandril images; (c) the histogram of the original and encrypted Pepper images.

4.2. Correlation of Two Adjacent Pixels

Image data generally has some intrinsic features. We analysed the correlations between two adjoining pixels of the plain-image and the cipher image at horizontal, vertical and diagonal directions for original and encrypted images[5]. The correlation coefficient is calculated by the following equations:

$$r_{xy} = \frac{cov(x,y)}{\sqrt{D(x) \times D(y)}}$$

where $cov(x,y) = \frac{1}{N}\sum_{i=1}^{N}(x_i - E(x))(y_i - E(y))$

$$D(x) = \frac{1}{N}\sum_{i=1}^{N}(x_i - E(x))^2 \quad \text{and} \quad E(x) = \frac{1}{N}\sum_{i=1}^{N} x_i$$

where x and y are color values of two adjacent pixels in the images.Figure 4shows the correlation analysis of Lena image.

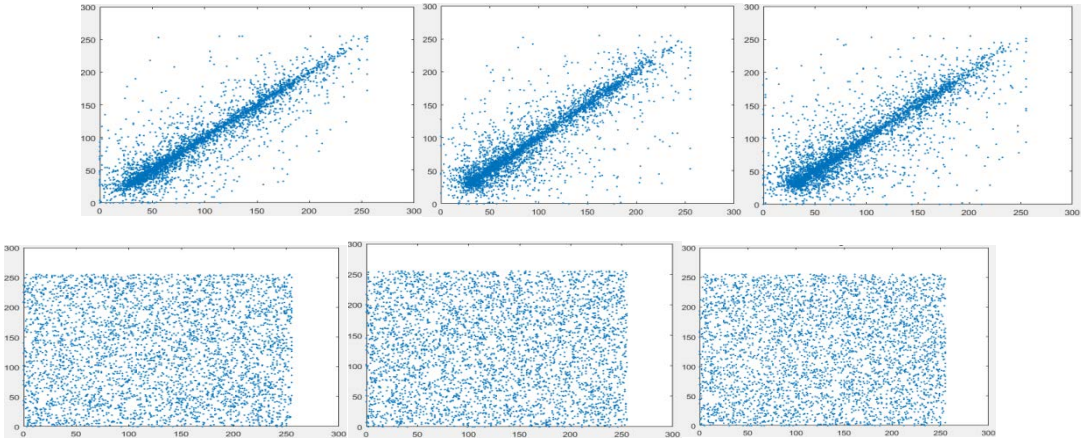

(a) (b) (c)

Figure 4: Correlation analysis of Lena image. (a) horizontal correlation of original and encrypted images; (b) vertical correlation of original and encrypted images; (c) diagonal correlation of original and encrypted images.

Table 1: Correlation coefficients of original Lena, Koala, Mandrill and Pepper images.

Image	Original image			Encrypted image		
	Vertical	Horizontal	Diagonal	Vertical	Horizontal	Diagonal
Lena	0.9062	0.8722	0.8387	0.0036	0.0012	0.00032
Mandrill	0.8592	0.8876	0.8360	0.00075	0.0016	0.0017
Pepper	0.9767	0.9696	0.9551	0.0004	0.0016	0.0025

As seen in Table 1, the correlation coefficient of the original images comes near to 1, but the correlation coefficient of the encrypted images comes near to 0.This means that the encrypted image has no correlation property with original image.

4.3. Data Loss and Noise Attack

Digital images can be easily influenced by noise and data loss during transmission through the network and storage in physical media. An image encryption algorithm should have an ability of resisting these abnormal phenomena. To test the ability of resisting the attack, we did some experiments on a data loss and a noise attack as shown in Figures 5 and 6.An original image is first

encrypted by our proposed algorithm. The encrypted image is attacked by a data cut of size 15%, 30% and 40% and with 3%, 10% and 20% "salt&pepper" noise, respectively. The decryption process is then applied to these encrypted images.

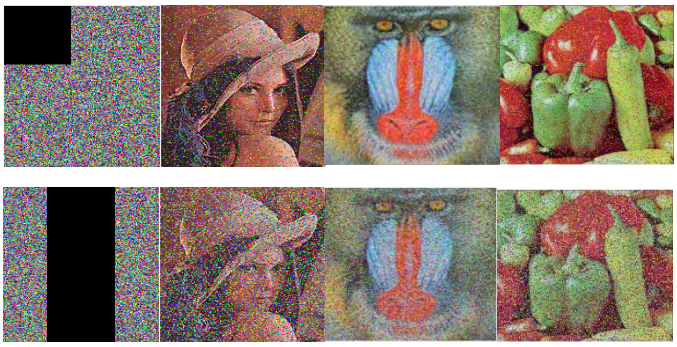

(a) (b) (c) (d)

Figure 5: Data loss. (a) The encrypted images with data loss; (b) the decrypted Lena image with different data loss; (c) the decrypted Mandrill image with different data loss; (d) the decrypted Pepper image with different data loss.

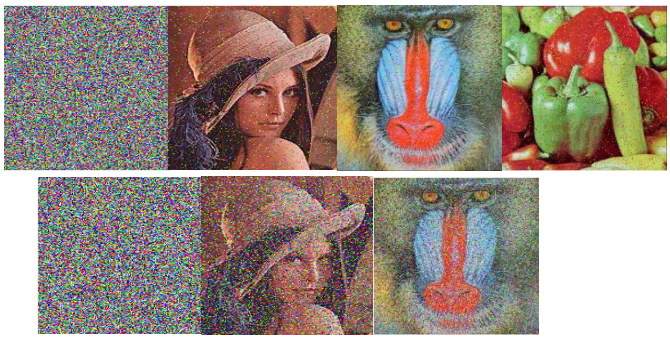

(a) (b) (c) (d)

Figure 6: Noise attack. (a) the encrypted images added with 'salt & pepper' noise; (b) the decrypted Lena image of (a); (c) the decrypted Mandrill image of (a); (d) the decrypted Pepper image of (a).

The restoring ability of an image is evaluated by peak signal to noise ratio (PSNR) as expressed in the followimg equation.

$$PSNR = 10 \times \log\left(\frac{255}{MSE}\right)(dB)$$

$$\text{where } MSE = \frac{1}{W \times H}\sum_{i=1}^{H}\sum_{j=1}^{W}(OI(i,j) - DI(i,j))^2$$

where $W \times H$ is the size of image, $OI(i,j)$ a pixel of the original image and $DI(i,j)$ a pixel of the decrypted image.Table 2 shows the PSNR values for some images.

Table 2: The peak signal to noise ratioof some encrypted images.

Image	Lena			Mandrill			Pepper		
	Red	**Green**	**Blue**	**Red**	**Green**	**Blue**	**Red**	**Green**	**Blue**
loss 15%	35.3900	37.7780	38.4302	35.2594	35.6046	36.2049	34.9495	36.1639	38.7565
loss 40%	31.0203	33.4110	34.2228	30.7908	31.0408	31.7175	30.3950	31.5676	34.2500
Noise 3%	39.5836	42.2247	42.3936	39.3673	39.8392	40.1186	38.9030	39.9778	42.5033
Noise 20%	31.7474	34.2945	34.8950	31.4815	31.8250	32.3980	31.2189	32.4015	35.0655

5. Conclusions

In this paper, a scheme for image encryption using 3D chaotic system is presented. The encryption method involves scrambling, diffusion, and linear transformation techniques to make it more confident. The experimental analysis and results of the proposed system includes histogram analysis, correlation analysis, and peak signal to noise ratio. The results show that the graphical shape of histogram for cipher image is uniformly distributed, so the proposed algorithm is protected from frequency analysis attack. Also, the low correlation coefficient of encrypted image is near to the ideal value zero. Thus the experimental results and statistical analysis demonstrate the security, flexibility, correctness, effectiveness, and robustness of the proposed cryptosystem.

References

[1]. C. Pak and L. Huang, "A new color image encryption using combination of the 1D chaotic map, "*Signal Processing*, vol. 138, pp. 129-137, Sep. 2017.

[2]. O. A. Alkishriwo, "An image encryption algorithm based on chaotic maps and discrete linear chirp transform," *Almadar Journal for Communications Information Technology and Applications*, vol. 5, no. 1, pp. 14-19, Jun. 2018.

[3]. B. Abugharsa, A. Basari, and H. Almangush, "A New Image Scrambling Approach using Block-Based on Shifted Algorithm," *Australian Journal of Basic and Applied Sciences*, vol. 7, no. 7,pp. 570-579, 2013.

[4]. Y. Zhang and X. Wang, "A symmetric image encryption algorithm based on mixed linear–nonlinear coupled map lattice," *Information Science*., vol. 273, pp. 329–351, Jul. 2014.

[5]. H. Huang and S. Yang, "Colour image encryption based on logistic mapping and double random-phase encoding," *IET Image Processing*, vol. 11, no. 4, pp. 211-216, Mar.2017.

Hearing Protection System By Using a Simple Noise Reduction Strategy

Izziddien Alsogkier
izziddien@yahoo.de
[1]Department of Electrical and Computer Engineering, College of Engineering, Elmergib University, Libya

ABSTRACT

In this paper, a very brief discussion and analysis of the noise problem are given particularly at the work environment, where the workers hearing system needs to be protected from an excessively loud noise source but at the same time the workers need to communicate with each other. Therefore, a simple strategy of noise reduction is introduced by means of isolation plus a noise filtered communication channel to keep the worker in contact with the work environment as well as the other co-workers with a minimum noise intervention as possible.

Keyword— Noise Reduction, Noise Isolation, Noise Filtering, Passive and Active Noise Control.

1. Introduction

There are a lot of noise sources that disturb the workers in the work environment, for example, machines driven by internal combustion engines such as cars, trucks and tractors also tool machines like generators, air compressors, drilling, cutting machines … etc. Moreover, heavy machineries in industrial fabrics generate very loud noise so that the workers or the operators need to be isolated but at the same time they need to communicate with each other. The same instance can be found in civil and military aviation like jet engine aircrafts particularly with propellers as helicopters, where the pilot, copilot and the passengers need to be protected and isolated from the excessive noise so that they can easily communicate with each other.

Therefore, the strategy is mainly to protect the workers or the operators' hearing system from the loud noise generated in the workplace, as well as, providing a communication channel with a minimum possible noise intervention. This, in most circumstances, is a very critical and fatal safety issue.

Usually, the noise problem take place or can be defined, whenever there are a *noise source*, which generates the noise, *noise transmission* or *propagation medium*, where the noise travels and expands, and *noise sink*, which is the target element that gets affected or disturbed by the noise.

Therefore, the noise problem can primarily be solved from the very beginning at the noise source which gives a very general and global solution to the problem, but this can be in some circumstances the most expensive solution (e.g. internal combustion engine exhaust system). Furthermore, a secondary solution can be done by preventing the noise to reach the noise sink by isolating the noise source from the noise sink this gives more local solution to the problem, but this can be in some circumstances the less expensive one.

Generally in the literature, there are two distinct classifications of noise control algorithms, which are passive and active noise control algorithms, passive is by implementing passive elements like isolating or absorbing materials to reduce the impact of the noise on the medium [1], active is by using active elements to generate an anti-noise to counteract the noise and reduce its impact on the targeted medium [2]. Moreover, sometimes in order to get maximum results, hybrid algorithms, a combination of passive and active methods can also be applied simultaneously [2].
In the following, a brief introduction to passive and active noise control techniques is given in Section 2, then the problem formulation of this paper and the experimental setup are given in Section 3. Experimental examples are presented in Subsection 3.2. Moreover, results analysis of the experiments and comments are given in section 4. Finally, conclusions and further work suggestions are given in Section 5.

2. Passive and Active Noise Control Techniques

Passive noise control technique is usually applied by using passive isolating and filtering elements. For example, noise isolation can be done by using sound isolating and absorbing(soundproof) materials like in civil buildings or an isolation compartment (as the case of cars, helicopter, bulldozer like machine) or at very smaller scale by implementing an isolating ear plugs, muffler headset or helmet, see Figure 1.

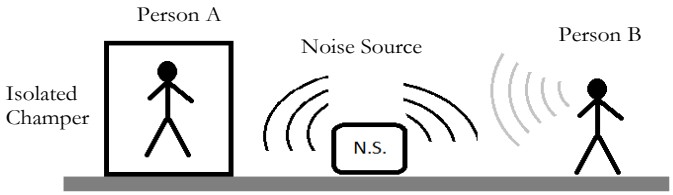

Figure 1: Passive noise control by using isolation.

The positive thing about this way of fighting the noise is that, it is very simple technically. On the other hand, apart from using intensive materials that leads to heavy weight solutions, which makes a big crucial problem particularly in the case of light weight applications like airplanes where the weight is an important factor. The negative thing about this technique is that the perfect isolation of an operator at a working place means that he will no longer receives information from the surrounding working place, which could be very fatal in most circumstances.
For example, in the case of helicopter where the pilot and the copilot need to be isolated from the excessive noise generated from the engine and the rotating blades but at the same time they need to communicate with each other without noise. This problem can be solved by using the setup shown in Figure 2 where both persons A and B are completely isolated from the noise and talk to each other via an isolated communication channel. This can be implemented also by using a soundproof helmet for each person with an electronic communication channel, as shown in Figure 3. Much simpler is by using ear protection system (ear muffs plus a communication system).

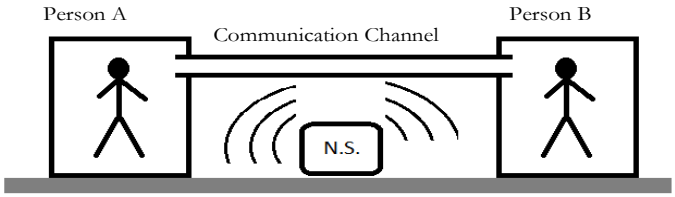

Figure 2: Two persons passive noise isolation with communication channel.

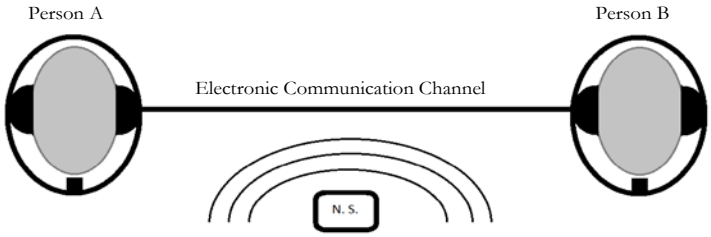

Figure 3: Two persons with head passive noise isolation and electronic communication channel.

Another example is the case of operators work beside a very loud noisy machine like an air compressor, internal combustion engine generator or any type of noisy rotational tool machines. Where, the communication channel could also be wireless based system so that the persons can move freely in their working area without any constant wire connection between them.

More specific situation regarded in this paper is when the workers need to be isolated but at the same time they need to communicate with each other. This can be done as in the helicopter case but with less expensive and simple technology by placing the operator in an isolated compartment, as shown in Figure 4, but still he receives noise filtered information from outside the isolated compartment, the communication channel is not noise isolated. Further simplification can also be achieved by using helmet or a headset ear protection system with noise filter set up as shown in Figure 5.

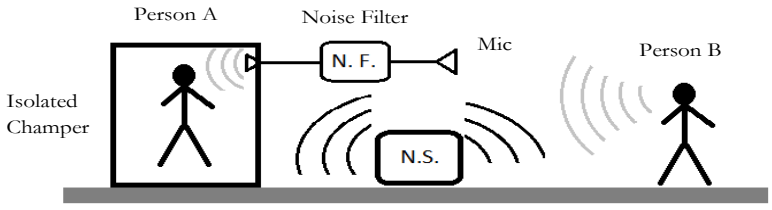

Figure 4: Passive and active noise isolation.

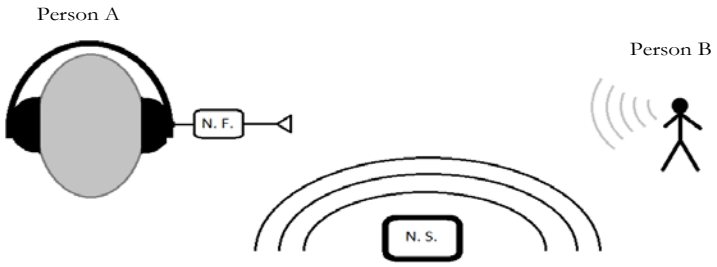

Figure 5: Passive and active noise control by using headset.

Alternatively, Active Noise and Control (ANC) is a technique that fights back the noise source by generating a counter action (anti-noise) against the noise actively [2]. In other words, it generates a counter action against the noise that cancels completely or partially the impact of the noise on the targeted environment. For example, in case of Figure 1, first the passive vibration control methods can be used to reduce the vibration generated at the source, where these vibrations are the source of the noise. Moreover, the ANC methods can be applied to cancel the noise generated from the noise source. Furthermore, ANC methods can be used to cancel actively the rest noise that penetrates the non-perfect isolation compartment as demonstrated in Figure 6 and the headset stereo active noise control as shown in Figure 7. There are a lot of robust and adaptive algorithms developed for active noise and vibration control applications, see for example [3-6].

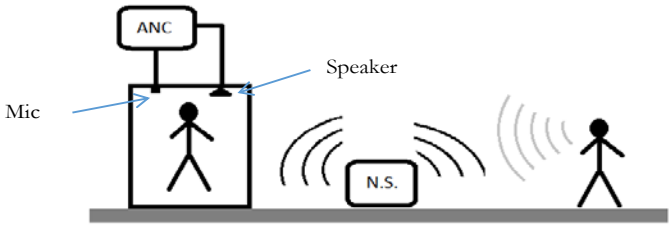

Figure 6: Active noise control system.

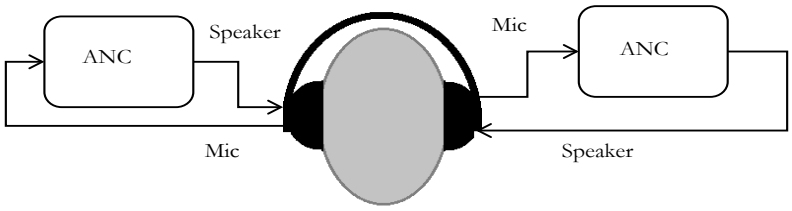

Figure 7: Stereo active noise control headset system.

3. Problem Formulation and Experimental Setup

As explained in sections (1 and 2), it is assumed that there is a noise source that disturbs the operators or the workers in the workplace, the goal is to reduce the effect of the noise by using

passive isolation as well as keeping the worker in contact with the other coworkers but with the possible minimum noise intervention. Therefore, the experiment setup will be as presented in Figure 4 and Figure 5. Moreover, the noise source considered in this experiment is assumed to be a single harmonic (sinusoidal) function. Therefore, a narrow band stop filter can be used as a noise filter to reduce the noise in the communication channel.

In this experiment, a notch filter will be designed and applied as narrow band stop filter. The notch filter can be implemented by using analog passive elements, a combination of R, L and C circuits, or active filters by using some sort of linear amplifiers with RLC elements. Furthermore, a digital filter can also be designed and implemented by utilizing a digital signal processor.

3.1. Notch Filter

In this work, an analog notch filter in form of second order transfer function is designed and applied to filter out a single harmonic noise source. Hence, the notch filter transfer function is defined by

$$G_N(s) = \frac{s^2+2\xi_N\omega_N s+\omega_N^2}{s^2+2\xi_D\omega_D s+\omega_D^2}, \quad (1)$$

where $\omega_N = \omega_D = \omega_{Notch}$ is the notch angular frequency, $\xi_N = 0, \text{or } \approx 0$ and $\xi_D \geq 1$.

Therefore, the notch filter transfer function becomes

$$G_N(s) = \frac{s^2+\omega_N^2}{s^2+2\xi_D\omega_D s+\omega_D^2}, \quad (2)$$

The following Figure 8 shows the frequency response of the notch filter for the parameters $\omega_{Notch} = 100$ [rad/s], $\xi_N = 0, 0.1, 0.01$ and $\xi_D = 1$.

3.2. Notch Filter Experiment

The experimental setup as mentioned earlier is as shown in Figure 4 and Figure 5, where the noise source is a 100 Hz single harmonic (sinusoidal) function. Therefore the noise filter is an analog notch filter in form of second order transfer function, which is designed and applied to filter out noise from voice in the communication channel.

The experiment data is gathered and presented in Figure 9, where the voice signal without noise is plotted by a blue line, while the voice signal with 100Hz noise is plotted by a green line and the filtered voice with noise signal is plotted by a red line.

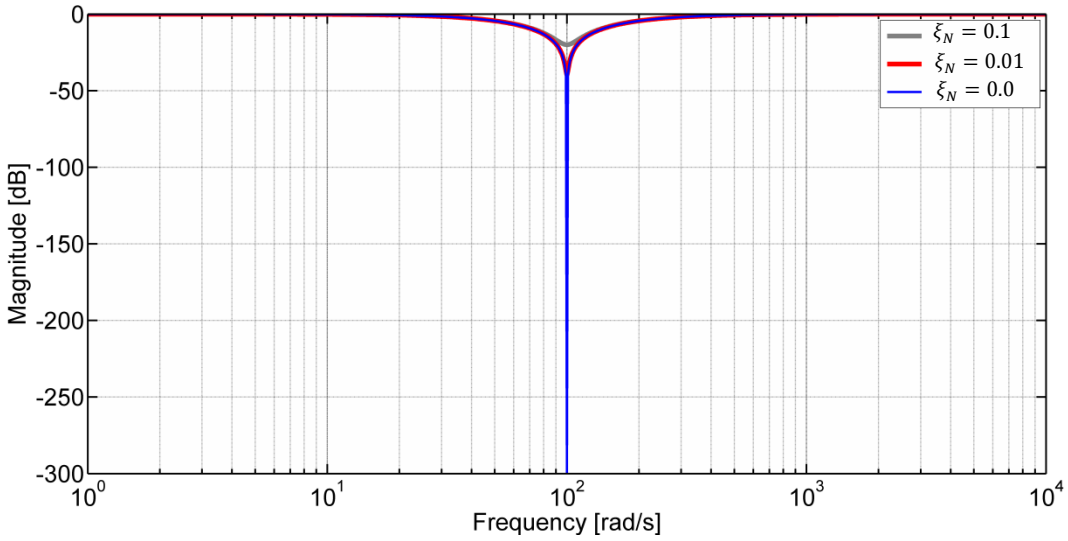

Figure 8: Notch filter frequency response.

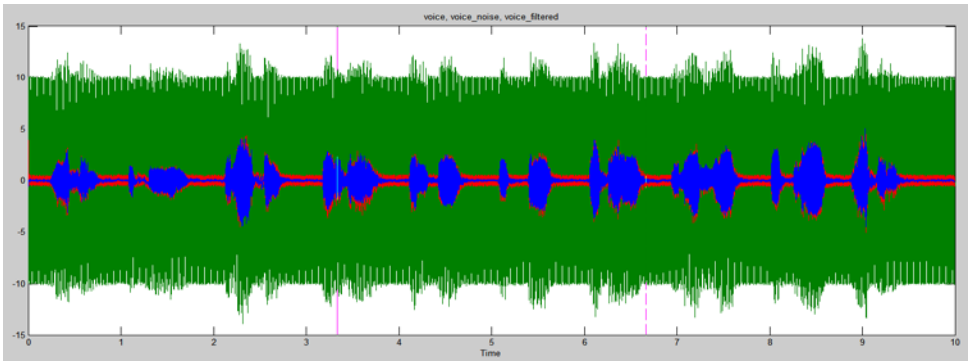

Figure 9: Original voice without noise (Blue), voice with noise (green) and filtered voice with noise (red).

4. Results Analysis and Discussion

Figure 9 shows the time plot of the original voice signal without noise, represented by the blue line, where the voice signal is simply a record of counting from one to ten in ten seconds. The green line is the plot of the voice signal corrupted with single harmonic noise at 100Hz frequency. Moreover, Figure 10 is time axis zoomin of Figure 9 between less than 3.9 and more than 4.4 seconds, where it shows clearly the filtered voice signal still has a rest noise component but it is much better than the voice signal with noise, in fact, the filtered signal became almost like the noise free voice signal. Furthermore, Figure 11 shows the plot of the frequency spectrum of corresponding signals in Figure 9 and Figure 10 with the same respective colors as well. Also this graph shows that the notch filter has managed to reduce the noise component at the frequency 100 Hz.

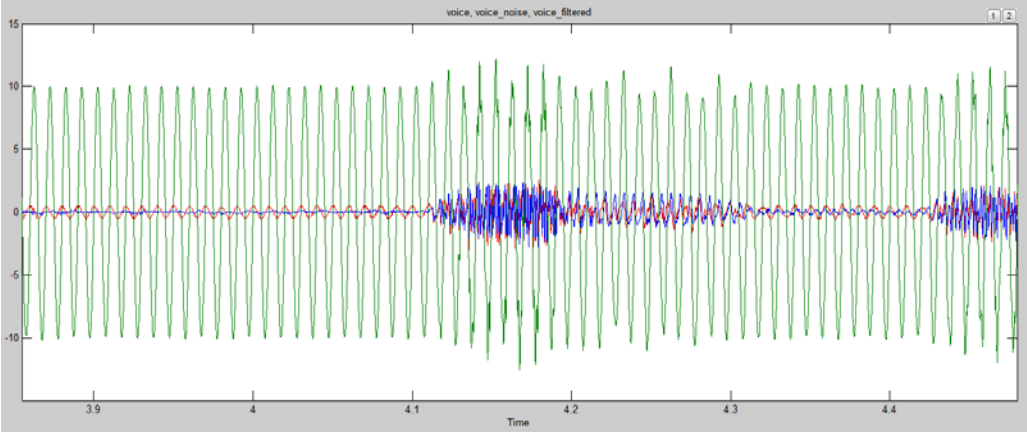

Figure 10: Original voice without noise (Blue), voice with noise (green) and filtered voice with noise (red).

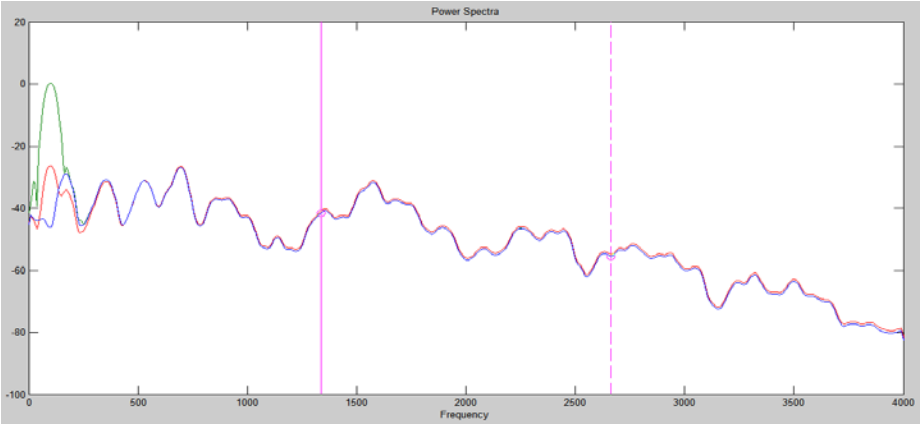

Figure 11: Frequency spectrum of original voice without noise (Blue), voice with noise (green) and filtered voice with noise (red).

5. Conclusions and Further Works

In this paper, instead of using isolation only to protect the workers or the operators against a very loud noise, which make them completely deaf in their working environment, a communication channel between the environment and the worker is applied with a band stop filter in form of a notch filter to reject or filter out the single harmonic noise, so that the worker can keep in contact with the work environment, this can improve the communication with the other coworkers as well as the environment which, in consequence, is a very important safety factor.

The application of this technique can be at its simplest, by adding (to a head set muffler) a communication channel microphone, low power audio amplifier with noise filter and very small speaker embedded in the head set muffler.

The noise filter can be designed as RLC band stop notch filter, or just an analog transfer function filter that can be built by using operational amplifiers, or can be built by using a digital signal processor utilizing a digital computer system. For small scale implementations, a suitable microcontroller based system can also be used to realize this strategy.

References

[1]. L. Ver and L. L. Beranek, "Noise and vibration control engineering principles and applications," John Wiley & Sons,2006.
[2]. C. H. Hansen, "Understanding active noise cancellation," Taylor & Francis e-Library, 2003.
[3]. B. Widrow and S. D. Stearns, "Adaptive signal processing," Prentice-Hall PTR, 1985.
[4]. C. R. Fuller, S. J. Elliott and P. A. Nelson, "Active control of vibrations," Academic Press,1996.
[5]. S. Elliott, "Signal processing for Active Control," Academic Press, 2001.
[6]. B. Widrow and E. Walach, "Adaptive inverse control a signal processing approach," John Wiley & Sons, 2008.

Enhancement of Bandwidth of U-shape Loaded Microstrip Patch Antenna According to 802.11b Standard

Fadel A. M. Alaswad[1*],Marai M. Abousetta[2*], Mohamed A. S. Alshushan[3*]
[1]fadel.abu83@gmail.com, [2]m.abousetta59@yahoo.co.uk, [3]mohammedsaad1318@gmail.com
[1]Department of Communication, Collage of electronic technology, Bani Walid, Libya
[2]Libyan Academy, Tripoli , Libya
[3]Department of Electric and Electronics, College of engineering, Sabratha University, Libya

ABSTRACT

The bandwidth of microstrip antennas is proportional to the thickness of the substrate that used. Since most substrates are very thin in terms of wavelengths, the bandwidth is usually small. To enhance the bandwidth, a new design of rectangular microstrip patch antenna is presented. The proposed geometry consists of a rectangular shaped ground plane structure with a U- slot loaded patch layer. The aim of this is to design a single, double and triple U slotted rectangular patch antenna and compare its performance with non-slotted rectangular microstrip patch antenna. The antennas were designed and simulated using advanced design software. The design has been worked out according to 802.11b IEEE standard.

Keyword— Microstrip antenna, Feed point, Bandwidth, return loss.

1. Introduction

Microstrip antennas were first proposed in 1952. This concept had to wait until 1974 when that microstrip antenna got a lot of attention and began being used for military applications. So far, these antennas have mainly been used on aircraft, missiles, and rockets. Just recently, they have been expanded to commercial areas such as mobile satellite communication, the direct broadcast satellite (DBS), and the global position system (GPS) [1].With the wide spread proliferation of communication technology in recent years, the demand for compact, low profile and broadband antennas has increased significantly. A number of new developed techniques to support high data rate wireless communication for the next generation technologies have been rapidly increasing.
802.11b is one of many Institute of Electrical and Electronics Engineers (IEEE) standards that govern wireless networking transmission methods. They are commonly used today to provide wireless connectivity in the home, office and some commercial. It operates on a 2.4 GHz band and allows for wireless data transfers up to 11 Mbps. Several techniques have been proposed to enhance the bandwidth in the state-of-the art antenna research for microstrip patch antenna. In this research, our design is forwarded a rectangular shape that contains a single, double and triples U, concentered accordingly.

2. Design procedure

The basic design uses a rectangular U-slot microstrip patch antenna on suitable microwave substrates [1]. The new antenna is a probe-fed rectangular microstrip patch antenna on a permittivity substrate with an internal U- slot as shown in Figure 1. In the second design, Another U –slot is added,and the

dimension of the second U-solt will be the half length of the first U-solt as shown in Figure 2.In the final design, a third U-slot is formed and its dimension will be the half length of the second U-solt see Figure 3.

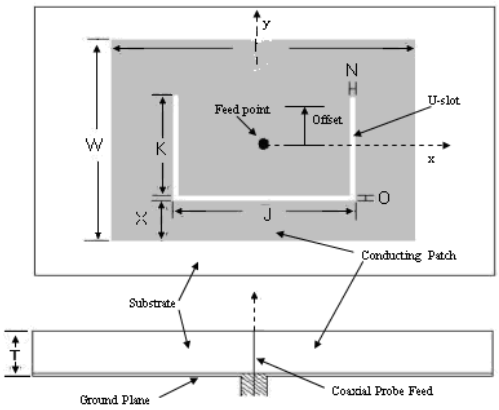

Figure 1: Geometry of the rectangular U-slot microstrip patch antenna

This design procedure is a set of steps for the rectangular U-slot mircostrip patch antenna. Specify the center frequency and 2:1 VSWR bandwidth of the desire antenna. Approximate the center frequency as (fres3) and the lower and upper frequency bounds of the bandwidth as (fres2) and (fres4) respectively. Select a substrate permittivity (ε_r) and a substrate thickness h.According to the following relationship [2]:

$$h \geq 0.06 \frac{\lambda_{res3}}{\sqrt{\varepsilon_r}} \quad (1)$$

where λ_{res3} wavelength at the center frequency in air.
Calculate the width of the patch W as:

$$W = \frac{c}{2.f_{r3}} \sqrt{\frac{2}{\varepsilon_r+1}} \quad (2)$$

where c speed of light in free space.
Calculate the effective permittivityε_{eff} as:

$$\varepsilon_{eff} = \frac{\varepsilon_r+1}{2} + \frac{\varepsilon_r-1}{2}\left(1+\frac{12h}{W}\right)^{-1/2} \quad (3)$$

Then the length due to the fringing field ΔL

$$\Delta L = 0.824h \frac{(\varepsilon_r+0.3)\left(\frac{W}{h}+0.262\right)}{(\varepsilon_r-0.258)\left(\frac{W}{h}+0.813\right)} \quad (4)$$

Calculate the length of the patch L as:

$$L = \frac{c}{2f_{r3}\sqrt{\varepsilon_{eff}}} - 2\Delta_L \quad (5)$$

Select a starting value of slot thickness E,F using following:

$$E = F = \frac{\lambda_{res3}}{60} \quad (6)$$

Calculate the Slot width J as:

$$J = \frac{c}{f_{r2}\sqrt{\varepsilon_{eff}}} - 2(L + 2\Delta_L - E) \quad (7)$$

Select the Slot height K such that

$$\frac{K}{J} \geq 0.7 \text{ and } \frac{K}{W} \geq 0.3 \quad (8)$$

Calculate the effective permittivity and effective length extension of the pseudo patch $\varepsilon_{eff(pp)}$ of the fourth resonance with the effective patch width $J - 2F$

$$\varepsilon_{eff(pp)} = \frac{\varepsilon_r+1}{2} + \frac{\varepsilon_r-1}{2}\left(1 + \frac{12h}{J-2F}\right)^{-1/2} \quad (9)$$

$$2\Delta L_{L-E-H} = 0.824H\frac{(\varepsilon_{eff(pp)}+0.3)\left(\frac{J-2F}{h}+0.262\right)}{(\varepsilon_{eff(pp)}+0.258)\left(\frac{J-2F}{h}+0.813\right)} \quad (10)$$

Calculate the Height of slot from base H as:

$$H \approx L - E + 2\Delta_{L-E-H} - \frac{1}{\sqrt{\varepsilon_{eff(pp)}}}\left(\frac{c}{f_{res4}} - (2K + J)\right) \quad (11)$$

When The optimized lower band frequency, fres2= 1.8GHz, upper bound frequency, fres4=3.1GHz ,Resonant Frequency fres3=2.45Ghz, εr = 4.2, and substrate Height = 10 mm are selected, The computed results are shown in Table1 as:

Table 1: Dimensions of single U slot antenna

L (mm)	W (mm)	K (mm)	J (mm)	O (mm)	N (mm)	X (mm)	H (mm)	T (mm)	Offset (mm)	ε_r	f_3 (GHz)	f_2 (GHz)	f_4 (GHz)
24.7	37.9	13.4	28.1	2.0	2.0	10.0	7.6	10	0.0	4.2	2.45	1.8	3.1

The second design" the double U–slot patch microstrip antenna" is depended on the first design and the dimensions of the second U shape$J', K'H'$ are the half length of first design. The next Table 2 summarizes the dimensions of the double U –slot patch microstrip antenna.

Table 2: Dimensions of double U slot antenna

L (mm)	W (mm)	K' (mm)	J' (mm)	O (mm)	N (mm)	X (mm)	H' (mm)	T (mm)	Offset (mm)	ε_r	f_3 (GHz)	f_2 (GHz)	f_4 (GHz)
24.7	37.9	6.7	14.05	2.0	2.0	10.0	3.8	10	0.0	4.2	2.45	1.8	3.1

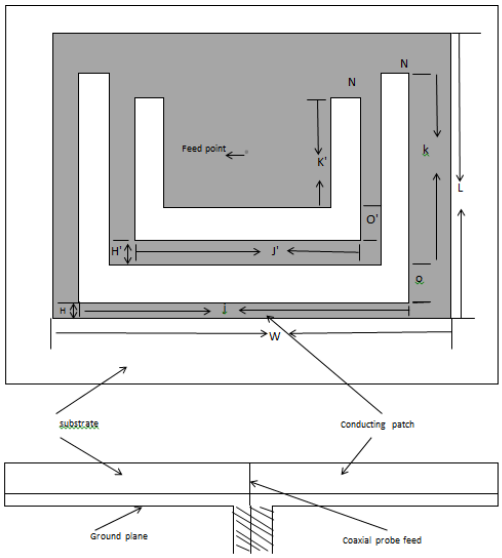

Figure 2: Geometry of the rectangular double U-slot microstrip patch antenna

In the same manner, the third design" the triple U–slot patch microstrip antenna "is depended on the second design and the dimensions of the third U shape J'', K'', H'' are the half length of second design. The next Table 3 summarizes the dimensions of the triple U –slot patch microstrip antenna.

Table 3: Dimensions of triple U slot antenna

L (mm)	W (mm)	K" (mm)	J" (mm)	O (mm)	N (mm)	X (mm)	H" (mm)	T (mm)	Offset (mm)	ε_r	f_3 (GHz)	f_2 (GHz)	f_4 (GHz)
24.7	37.9	3.35	7.02	2.0	2.0	10.0	1.9	10	0.0	4.2	2.45	1.8	3.1

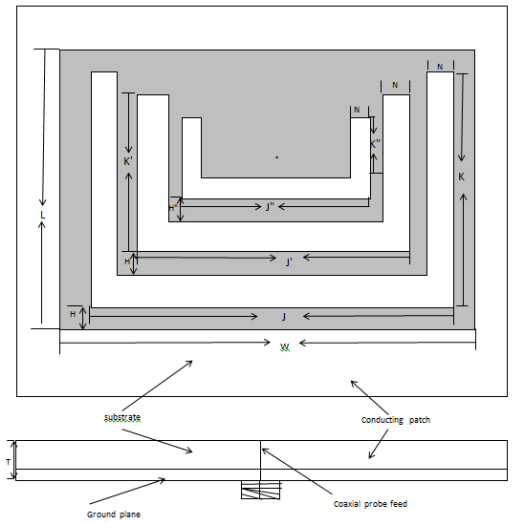

Figure 3: Geometry of the rectangular triple U-slot microstrip patch antenna

3. Result and discussion

3.1. Design of a rectangular patch microstrip antenna

Figure 4 illustrates a rectangle patch microstrip antenna which does not contain any slot in order to compare these results with the other designs to see how much improvement in the bandwidth.Figure5 shows simulated results of the variation of return loss versus the frequency of the proposed antenna. There is a resonant frequency which is located at the desired values of 2.45 GHz with return loss of (-22) dB and 13% bandwidth. The Bandwidth (BW) % can be calculated as follow:

$$BW(\%) = \frac{f_h - f_l}{f_c} * 100 \quad (12)$$

Where f_h,f_l are the upper and lower frequency at the point -10dB,f_c is theresonant frequency.

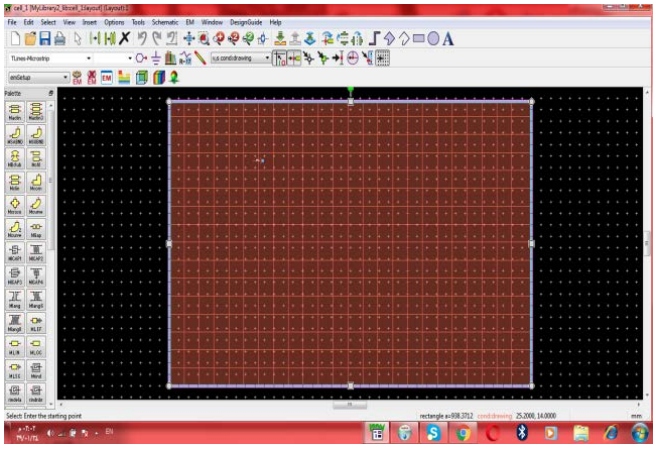

Figure 4: Rectangular patch microstrip antenna

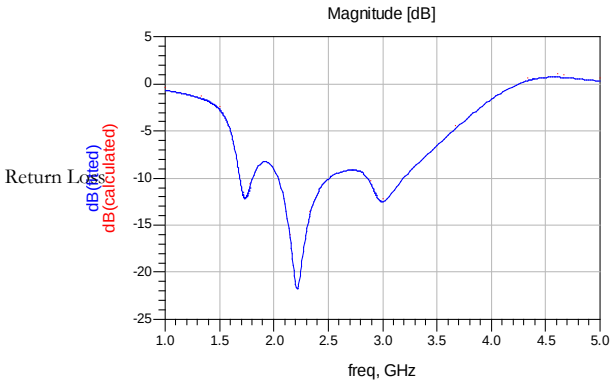

Figure 5: Return loss of the rectangular patch microsrtip antenna

3.2. Design of a rectangular U –slot patch microstrip antenna.

Figure6 shows a rectangle U-slot patch microstrip antenna.Figure7 shows the resonant frequency at 2.2GHz with return loss of -21dB. In addition, a bandwidth of 51.36% was achieved.

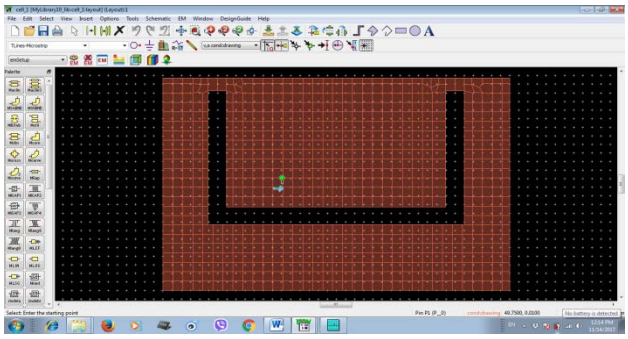

Figure 6: Design of the rectangle U-slot patch micro strip antenna

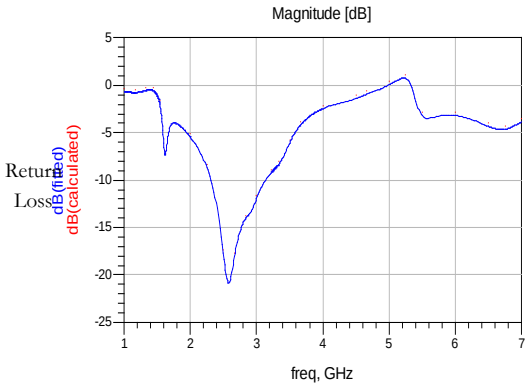

Figure7: Return loss of the rectangle U-slot patch micro strip antenna

3.3. Design of a rectangular double U –slot patch microstrip antenna.

A rectangle double U-slot patch microstrip antenna is illustrated in Figure8. From Figure9, the antenna was found to be resonating at 2.47GHz with a return loss of -26 dB, and a bandwidth of 52.63% was achieved.

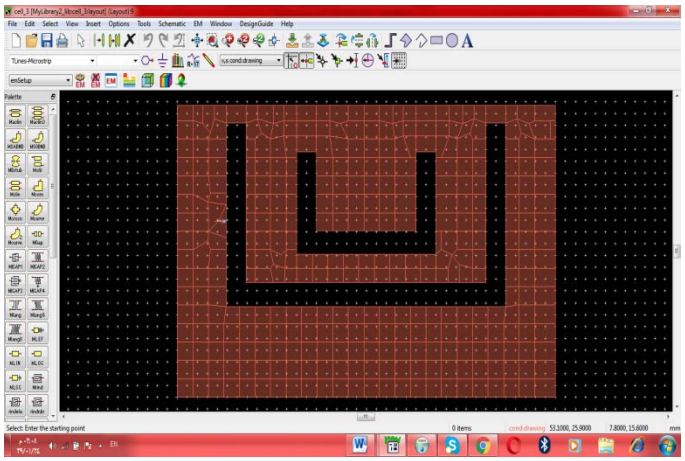

Figure8: Design of therectangle double U-slot patch microstrip antenna,

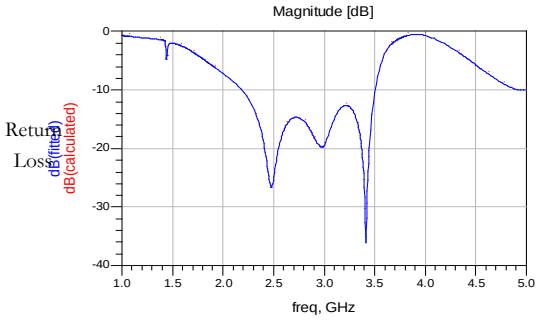

Figure 9: Return loss of the rectangle double U-slot patch microstrip antenna,

3.4. Design of a rectangular triple U –slot patch microstrip antenna.

Figure10 shows a rectangle Triple U-slot patch microstrip antenna. Figure11 shows a resonant frequency at 2.47GHz with a return loss of -22 dB. a bandwidth was found 52.63%, which is approximately the same as in a rectangle double U-slot patch microstrip antenna.

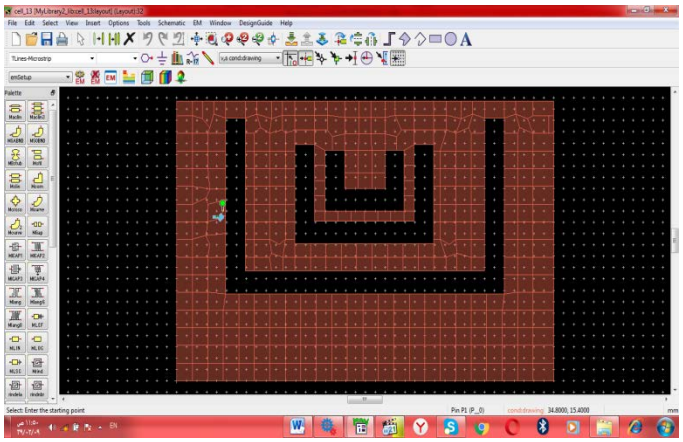

Figure 10: Design of the rectangle triple U-slot patch microstrip antenna,

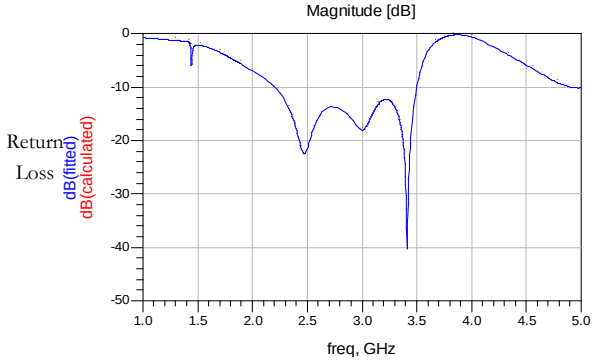

Figure11: Return loss of the rectangle triple U-slot patch microstrip antenna,

Table 4 summarizes the data from all designs. The three designs give bandwidth enhancement above 50%.The double U-solt and Triple U-slot patch micro-strip give slightly higher bandwidth enhancement of 52.63% covering from 2.2 to 3.50 GHz frequency. It should be considered that the bandwidth specification changes according to the feed point location.

Table 4: summarizes the data from all designs

	$f_{c(GH_z)}$	$f_{u(GH_z)}$	$f_{l(GH_z)}$	dB_i	Feed point position	bandwidth
Rectangular patch antenna	2.2	2.5	2.05	-26	(9.80,19.60)	13%
Single U-slot	2.2	3.13	2	-21	(7.60,20.00)	51.36%
Double U- slot	2.47	3.50	2.2	-26	(4.70,14.90)	52.63%
Triple U-slot	2.47	3.50	2.2	-22	(4.60,14.50)	52.63%

4. Conclusion

In this research, a rectangular shaped microstrip antenna has been designed that contains a single, double and triple U shape using ADS software. A single U shape has been designed and tested for the sake of increasing bandwidth at operating frequency 2.45 GHz. The achieved bandwidth was 51.36% at return loss equal to 21dBi. A double U shape microstrip antenna has also been tested with bandwidth equal to 52.63% at return loss equal to -26 dB. In addition, a triple U shape has also been undertaken to give bandwidth equal to52.63% at return loss equal -22 dB. In general, the results are considered very satisfactory where most designs give bandwidth enhancements above 50%at very acceptable levels of return loss.

Reference

[1] P. Bhattacharjee, V. Hanumante, S. Roy," Design of U-Slot Rectangular Patch Antenna for Wireless LAN at 2.45GHz", *9th International Conference on Microwaves, Antenna, Propagation and Remote Sensing*, 2013.

[2] Aruna Rani, R.K. Dawre," Design and Analysis of Rectangular and U Slotted Patch for Satellite Communication", *International Journal of Computer Applications*, Volume 12– No.7, December 2010

[3] Runa Rai, A. K. Gautam," improvement in gain and bandwidth of rectangular and U slot loaded patch", *International Journal of Computer Science Issues*, Vol. 8, Issue 6, No 2, November 2011

[4] H. Khidre, Kai-Fong Lee, A. Z. Elsherbeni, F. Yang, "Wide Band Dual –Beam U-Slot Microstrip Antenna", *IEEE*, Vol. 61, No. 3, March 2013.

[5] J. Bahl, P. Bhartia ,"Design and Performance Evaluation of Microstrip Antenna for Ultra-Wideband Applications Using Microstrip Feed", *American Journal of Electrical and Electronic Engineering*, Vol. 3 No. 4, 93-99, 2015

Bandwidth Optimization Through Hybrid Codecs G.711 and G.729 for VoIP Ethernet, FR and MP Networks

Mohamed Alahemar, Abdullah Masrub, AbdulSalam Addeeb
mohammed13111992@gmail.com, a.masrub@elmergib.edu.ly, dr.aaddeeb@gmail.com
Department of Electrical &Computer Engineering, Elmergib University, Libya

ABSTRACT

With the rapid growth in both internet and telecommunication technologies, VoIP has become more and more popular and expected to replace the traditional telephony services. The main issues in communication of real time application on IP networks, however, are providing high Quality of Service (QoS), security and appropriate capacity of transmission medium. Therefore, one of the most important factors to consider when designing packet voice networks is the capacity. This paper focuses on the capacity problem and attempts to determine the minimum bandwidth (BW) that can support in each transmission rate based on different speech codecs. In precise, this paper discusses an overhead problem in VoIP transmission and studies the extent of which the required BW is affected by the type of used network and the dependency on the codec type used for the VoIP encoders. The study devises the variation payload size in two codec techniques (G.711and G.729) to optimize the BW utilization. The study concluded that increasing the payload size and using the cRTP protocol would reduce bandwidth requirements to more than 50%.

Keyword— VoIP; Overhead Problem; Codec Techniques; Capacity.

1. Introduction

Voice over Internet Protocol (VoIP) is a technology that used widely in both internet and telecommunication fields to make voice calls and expected to replace the traditional telephony services. Nowadays, using VoIP services users are not only allowed to call other users using the same service, but they may allowed to call anyone who has a subscribe number connected to a VoIP adapter. The idea of this technology is to convert the user voice into a digital signal to be transmitted using the Internet connection. The idea behind such technology is a number of protocols that organize and control connection establishment over different network layers. As the voice packet is moved over different network layers, some additional information needs to be added to the packet. Real-time Protocol (RTP), Datagram Protocol (UDP), and Internet Protocol (IP) header address represent more than 70% of the added information to such packets. The formed (RTP/UDP/IP) packet represent about 54 bytes of information. The main components of a VoIP system are CODEC (Coder-Decoder), Packetizer and playout buffer [1].

The most critical components of a VoIP system is the voice codec. It is the process of converting the speech signal into digital form, transmit it through the medium to the receiver and reconstruct the received information to form the original signal. different algorithms are run on both sides, the sender and the receiver sides, to ensure the success deliver of the packetized voice data. Different

codecs have different bit-rate, packet length, speech quality, algorithmic delay, complexity are used to enable optimization of bandwidth utilization. Bit rate is a very important parameter of codec which affects the quality of encoded speech. Therefore, to obtain the best quality of voice with the lowest bandwidth requirements, it is important to select the appropriate codec for a particular voice network [2] [3][4].

However, the main issues in communication of real time application on IP networks are providing high Quality of Service (QoS), security and appropriate capacity of transmission medium. Choosing the appropriate codec for a particular bandwidth of the network is also a little difficult. Using other internet application such as web browsing, file transfer, … etc in the same time with VoIP service is affect the performance of the connection of the VoIP session because it is affect the network bandwidth. Due to popularity of both the common hybrid codecs (G.711 and G.729), they have been studied in this paper to optimize the bandwidth utilization.

2. Background

1. Voice Codecs

With VoIP, the voice traffic is carried through the transport medium over an IP network, requiring a source, destination, User headers. Voice codec samples the waveform at regular intervals and generates a value. Samples are taken 8000 times/s (i.e. 8 kHz sampling rate) or 16000 times/s (i.e. 16 kHz sampling rate).The values are quantized in order to map it into discrete-finite value which can be represented using digital bits, which forms the voice data frame being transmitted over the network. To achieve such process, codec provides compression capabilities to save network bandwidth. The rapid development of VoIP technology has driven to deep advancement in designing of voice codecs which provide better QoS management capabilities. As mentioned above, choosing a proper codec is an important factor because it can affect the voice quality and bandwidth utilization together. Then the philosophy is, having higher compression codecs leads to lower bit rate which means lower bandwidth. From another point of view, high-quality voice codecs with high degree of compression require very low bandwidths for transmission, and thus have better performance in network congestion situations [2][5][6].

Formally, voice codecs are standardized by the International Telecommunication Union (ITU-T). The most common voice codecs specified by ITU-T include G.711 with 64 kbps
and G.729 with 8 kbps bit rate. Both versions are widely used. G.729 utilizes one eighth of the bandwidth compared to G.711. This means that G.729 supports more calls but they have less quality. G.711 codec doesn't have licensing fee so it can be used in VoIP applications freely. In contrary, G.729 is a licensed codec. Most phones that support VoIP have implemented this codec in their chipset. G.711codec use Pulse Code Modulation (PCM) of voice frequencies at a standard bit rate of 64 Kbps. Typically 12..14 bit samples, sampled at 8 KHz sample rate, are compounded to 8 bit for transmission over a 64 Kbps data channel. This codec requires low computation complexity and provides very good voice quality with negligible delay. However, it consumes 64 Kbps of audio bandwidth per direction, which is high in comparison to other codecs. On the other hand, G.729

codec samples the voice band at 8 KHz with a 16 bit resolution. This codec provides significant bandwidth savings. It has 8:1 compression and requires just 8 Kbps of audio bandwidth [2][4]. Main characteristics of both codecs are shown in Table 1.

Table 1: Main characteristics of the G711, G729

Codec	Data Rate (kbps)	Coding Type	Comments
G.711	64	PCM	Delivers precise speech transmission. produces audio uncompressed
G.729	8	CS-ACELP	Excellent bandwidth utilization. produces audio compressed

2. Related Work

The issue of voice performance are widely studied and the most research have been done in this area focus on codec selection. The aim is to select the appropriate sampling method for suitable codec to provide better voice performance. The Quality of Service (QoS), network traffic, and bandwidth requirement are topics of interest in the research field [5]. However, not many work have been done on specific type of network and bandwidth optimization. For example, different voice codecs were employed to investigate VoIP traffic with silence suppression technique where no packets are generated in silence period [6]. Simulation methods were also used to investigate the performance of VoIP using different coding schemes [7]. As multi rate make different transmission rate and hence, different bandwidths possible. In this context, if the number of calls exceed the allocated bandwidth, the quality of perceived voice can be affected by packet loss, jitter and delay [8].

While Constant Bit Rate (CBR) traffic with different codec schemes were considered by many researchers, others suggest that G.729 codec generates smaller packets and is more error resilient than G.711 [9][10]. In such case, G.729 codec with Voice Activity Detection (VAD) enabled was used to produce the Variable Bit Rate (VBR) characteristics. Accordingly, it is more suitable for use in wireless network where there are higher channel errors [11]. Both codecs G.711 and G.729 were compared over 802.11 Distributed Coordination Function (DCF) protocol in infrastructure mode. Results have shown that the output bit rate of the G.729 encoder being eight times less than that of the G.711 encoder [12]. Moreover, to improve quality of service capabilities, it have shown that the header overhead for voice traffic can be reduced [13] and can also be compressed during multiplexing to increase the bandwidth efficiency [14].

3. Bandwidth Calculation

In order to be moved over the IP network layers, the IP packet is wrapped by the physical transmission medium. The overhead introduced in VoIP communication links by the RTP/UDP/IP headers is quite high: Consider a scenario where a G.729 codec operating at a rate of 8Kbps, sending frames every 20 msec. This will result in a voice payloads of 20 bytes for each packet. However, to transfer these voice payloads using RTP/UDP/IP, the following headers must be added: an Ethernet header of 14 bytes (18 bytes if VLAN is used), IP header of 20 bytes, UDP header of 8 bytes and an additional 12 bytes for RTP. This is a whopping total of 54 bytes (58 with VLAN) overhead to

transmit a 20-byte payload. Transmission of IP over other mediums will result in different overhead calculations. These protocol header assumptions can be summarized as follows:

40 bytes for: IP (20 bytes) / User Datagram Protocol (UDP) (8 bytes) / Real-Time Transport Protocol (RTP) (12 bytes) headers.

Compressed Real-Time Protocol (cRTP) reduces the IP/UDP/RTP headers to 2 or 4 bytes (cRTP is not available over Ethernet).

6 bytes for Multilink Point-to-Point Protocol (MP) or Frame Relay Forum (FRF).

1 byte for the end-of-frame flag on MP and Frame Relay frames.

18 bytes for Ethernet L2 headers, including 4 bytes of Frame Check Sequence (FCS) or Cyclic Redundancy Check (CRC).

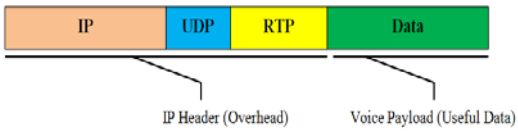

Figure 1: IPheader forms a significant part of small Voice over IP packets

The amount of bandwidth required to carry voice over an IP network is dependent upon a number of factors such as Codec (coder/decoder) and sample period, IP header, Transmission medium, Silence suppression. The term 'IP header' is used to refer to the combined IP, UDP and RTP information placed in the packet, see fig. 1. The payload generated by the codec is wrapped in successive layers of information in order to deliver it to its destination. RTP is the first, or innermost, layer added. This is 12 octets. RTP allows the samples to be reconstructed in the correct order and provides a mechanism for measuring delay and jitter. UDP adds 8 octets, and routes the data to the correct destination port. It is a connectionless protocol and does not provide any sequence information or guarantee of delivery. IP adds 20 octets, and is responsible for delivering the data to the destination host. It is connectionless and does not guarantee delivery of packets [4][5].

Overall, the IP/UDP/RTP headers add a fixed 40 octets to the payload. With a sample period of 20 ms, the IP headers will generate an additional fixed 16 kbps to whatever codec is being used. The payload for the G.711 codec and 20 ms sample period calculated above is 160 octets, the IP header adds 40 octets. This means 200 octets, or 1,600 bits are sent 50 times per second resulting in 80,000 bits per second. This is the bandwidth needed to transport the VoIP only, it does not take into account the physical transmission medium.

There are other factors, which can reduce the overhead incurred by the IP headers, such as compressed RTP (cRTP). This can be implemented on point-to-point links and reduces the IP header from 40 to just 2 or 4 octets. The codec determines the actual amount of bandwidth that the voice data will occupy. It also determines the rate at which the voice is sampled. The IP/UDP/RTP header can generally be thought of as a fixed overhead of 40 octets per packet, though on point-to-point links RTP header compression can reduce this to 2 to 4 octets (RFC 2508). The transmission medium, such as Ethernet , will add its own headers, checksums and spacers to the packet. Finally, some codecs employ silence suppression, which can reduce the required bandwidth by as much as 50 percent [2] [15].

Total packet size = (layer 2 header: MP or FR or Ethernet) + (IP/UDP/RTP header) + (voice payload size) (1)

Packet Per Second (PPS) = (codec bit rate) / (voice payload size) (2)

Bandwidth = total packet size * PPS (3)

4. Results and Discussion

The programming language used in this work is the Matlab, for its speed of data processing and ease of use, and the possibility of displaying the results in graphical form so that it can be easily understood. Bandwidth requirement for transmission VoIP is calculated using codecs G711, G729. We examine the effect of the used network type and the variation payload size on bandwidth requirement. In this work, we consider the types of networks (Ethernet, Frame Relay (FR), Multilink Point-to-Point Protocol (MP)), and for Payload size when using the codec G711 it was (5, 10, 20, 30, 40) ms while when using the codec G729 it was (10, 20, 30, 40, 50, 60) ms.

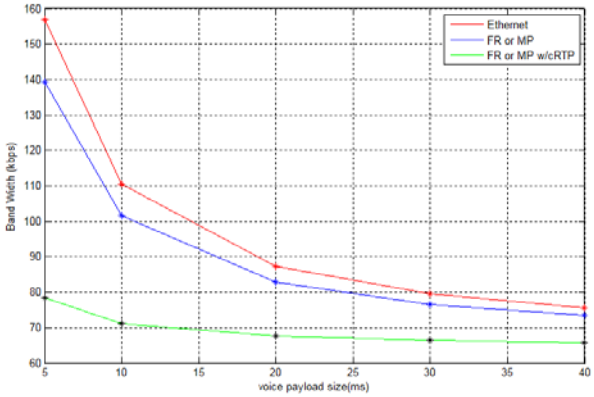

Figure 2: Bandwidth Requirement of Codec G711

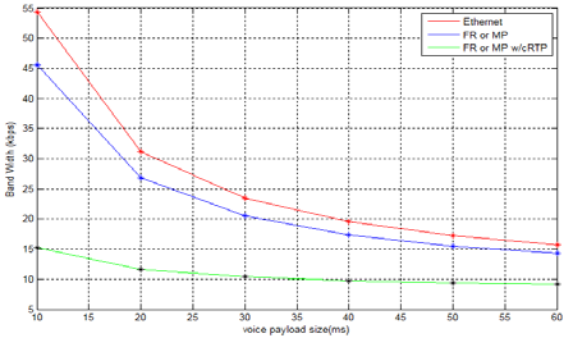

Figure 3: Bandwidth Requirement of Codec G729

From Fig. 2 and Fig. 3, it is noticed that as payload size increases the BW decreases. The network that requires the widest bandwidth is clearly the Ethernet network. This is due to not utilizing cRTP protocol which responsible for decreasing the header. On the other hand, the type of network system that requires less bandwidth is the Frame Relay (FR) and Multilink point-to-point (MP) networks. Again, this is due to cRTP function that is reduceing the header and therefore condensing the bandwidth requirements. Fig. 4 and Fig. 5 show the percentage of the header size with respect to

the total load size.When increasing the voice payload size the VoIP bandwidth reduces and the overall delay increases.

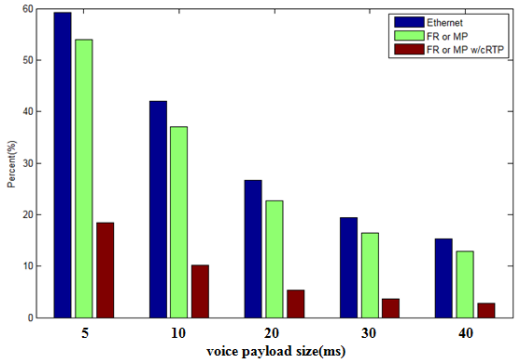

Figure 4: Packet Overhead of Codec G711

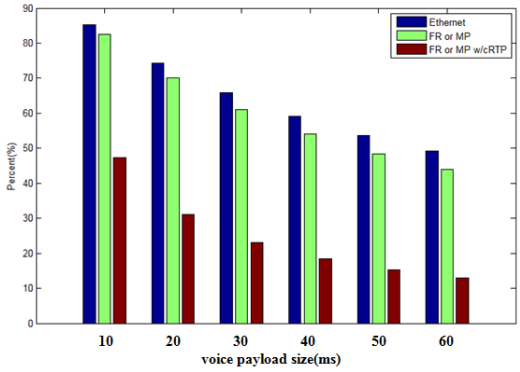

Figure 5: Packet Overhead of Codec G729

5. Conclusions

All VoIP packets are made up of two components: voice samples and IP/UDP/RTP headers. Although the voice samples are compressed by the Digital Signal Processor (DSP) and can vary in size based on the codec used, the headers are a constant of 40bytes in length. With cRTP, these headers can be compressed into two or four bytes. This compression offers significant VoIP bandwidth savings. When increasing the voice payload size the VoIP bandwidth reduces and the overall delay increases.

There are many factors that influence the amount of bandwidth required to transmit a voice call over an IP network. By approaching the problem one element at a time, the final calculation becomes relatively feasible. Other factors may influence the use of the actual bandwidth, such as RTP header compression, silence suppression and other techniques are still under development. The study concluded that increasing the payload size and using the cRTP protocol would reduce bandwidth requirements to more than 50%.

References

[1]. H. Kazemitabar, S. Ahmed, K. Nisar, A.Said, and H. Hasbullah, "A Comprehensive review on VoIP over Wireless LAN networks, "ISSR Journal, Vol. 2, No. 2, September 2010, pp. 1-16.

[2]. Haniyeh Kazemitabar and Abas Md. Said, "Capacity Analysis of G.711 and G.729 Codec for VoIP over 802.11b WLANs" International Conference, ICIEIS 2011, November 14-16, 2011, Kuala Lumpur, Malaysia.

[3]. S. Rattal, A. Badri, M. Moughit, "Performance Analysis of Hybrid Codecs G.711 and G.729 over Signaling Protocols H.323 and SIP" international journal of Computer Applications, Vol. 72, No. 3, May 2013.

[4]. M. Sulovic, D.Raca, M.Hadqialic and N. Hadziahmetovic "Dynamic codec selection algorithm for VoIP". The sixth international conference on digital telecommunications, ICDT 2011

[5]. H.A. Ifijeh, F.E. Idachaba, and I.B. Oluwafemi, "Performance Evaluation of The Quality of VoIP Over WLAN Codecs" Proceedings of the World Congress on Engineering , July 1 – 3, 2015, London, UK.

[6]. Broadcom Corporation, "Critical Steps for Successful VoIP Deployment" available at http://www.broadcom.com/ (April 2005) last visited February 2013.

[7].] K. Salah & A. Alkhoraidly, "An OPNET-based Simulation Approach for Deploying VoIP" International Journal of Network Management, Volume 16 Issue 3, Pages 159-183, John Wiley & Sons, Inc. New York, NY, USA, (May 2006).

[8]. M. Meeran, P. Annus, M. Alam, Y. Moullec, "Evaluation of VoIP QoS Performance in wirelessMesh Networks" Journal of information, 2017, 8, 88; doi:10.3390/info8030088.

[9]. Jiango Cao & Mark Gregory, "Performance Evaluation of VoIP Services Using Different CODECs Over A UMTS Network" Telecommunication Networks and Applications Conference, 2008.ATNAC 2008. Australasian ISBN: 978-1-4244-2602-7 pp 67 –71.

[10]. Abu Sayed Chowdkery, Mark Gregory "Performance Evaluation of Heterogeneous Network for Next Generation Mobile" 2009 12th International Conference on Computers and Information Technology (ICCIT 2009)Dhaka, Bangladesh, IEEE Catalog Number:CFP0917D-PRT ISBN: 978-1-4244-6281-0 pp 100-104.

[11]. Bowei Xi, Hui Chen, William S. Cleveland, Thomas Telkamp, "Statistical Analysis and Modeling Of Internet VoIP Traffic for Network Engineering" Electronic Journal of Statistics Vol. 4 (2010) pp58–116 ISSN: 1935-7524 DOI: 10.1214/09-EJS473

[12]. Carlos Ign´acio de Mattos, Eduardo Parente Ribeiro and Carlos Marcelo Pedroso, "A New Model For VoIP Traffic Generation" The 7th International Telecommunications Symposium (ITS 2010)

[13]. AT & T, "Critical Steps for Successful VoIP Deployment" (2005).

[14]. Di Wu, "Performance Studies of VoIP over Ethernet LANs" A Master Degree dissertation submitted to Auckland University of Technology (2008).

[15]. R. Dimova, G. Georgiev, Z. Stanshev "Performance Analysis of QoS Parameters for Voice over IP Applications in a LAN Segment "International Scientific Conference Computer Science" 2008.

Modeling and Performance Evaluation of MapReduce in Cloud Computing Systems Using Queueing Network Model

Guzlan Miskeen
Dept of Computing, Faculty of Education Brack, University of Sebha, Sebha, Libya
Guz.Miskeen@Sebhau.Edu.Ly

ABSTRACT

MapReduce is a two -stage information processing technique and it is common concept for big data. Map and Reduce procedures are distributed among some processors within a cluster in the cloud. The performance modeling and analysis of MapReduce execution times has been a challenging task. Analytic performance models provide reasonably accurate job response time estimation with significantly lower cost compared with experimental experiments. Queueing theory is one the modeling and analysis tools of such systems since it enables efficient analysis of the performance, availability and some other key metrics of a data processing system. In this paper, an M/G/1/K performance model with first come first serviced (FCFS) discipline of MapReduce is proposed. More specifically, it will present a queueing model with two stages hypoexponential service time and finite queue. This model has a cloud server with two stages to investigate the performance of the MapReduce technique subject to heavy traffic conditions. The system is analyzed via discrete-event simulation (DES). Key numerical examples are presented for varying number of mappers, reducers and the mean arrival rates to assess their effect on the system mean response time, loss probability and mean queue length. The results are expected to be useful for predicting MapReduce under various workloads and operating conditions of big data processing.

Keyword— Cloud computing, MapReduce, Performance Modeling, Queuing Theory, Hypoexponential distribution

1. Introduction

MapReduce is a well- known programming model that process in parallel large data on cloud clusters [1]. This model is composed of map and reduce functions, "Map" function processes a key/value pair to generate a set of intermediate key/value and a "Reduce" function merges all intermediate values associated with the same intermediate key [2].

In big data cluster, a MapReduce job is divided into several tasks that are executed on parallel on multiple virtual machines (VMs), which significantly reduce the job execution time. The operating concept of a MapReduce is depicted in Figure 1. The Hadoop Distributed File System (HDFS) is an open source System that is responsible for storing replicated data fashion and run in a distributed way on a cluster of servers [1].

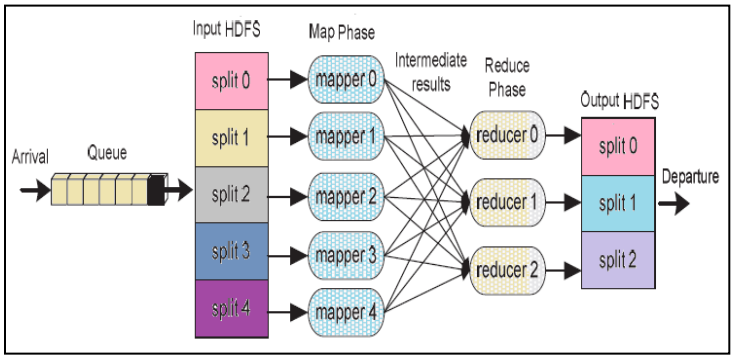

Figure 1: The operating concept of MapReduce process (adopted from [1])

For a cloud MapReduce cluster, a cloud node is a VM which can have several mappers and reducers [1]. MapReduce functionality can be described as following: upon arrival, MapReduce jobs are queued for processing at the cloud cluster which has hundreds of nodes. The job is scheduled by the load balancer which plays an important role in dispatching, monitoring, and tracking the availability of nodes at the cloud data center. Then, the input data of a MapReduce job is split into multiple data set. As a result, the map phase is initiated where each data set is processed by one mapper node to produce intermediate key/value pairs or results. After all data sets have received the required service, the reduce phase starts where each reducer can process and aggregate the intermediate results to form the final output results [3].

The ratio of the total mappers to reducers can be specified by the user and the job tracker, with additional controlling functionality, is responsible for provisioning the correct number of slave nodes (which host the mappers and reducers) to meet the QoS conditions. There is a tradeoff between cloud cluster's performance and the cloud usage cost since allocating fewer resources than required will affect the cloud's performance while allocating more nodes will increase the cost to the cloud user due to the over- provisioning[1].Therefore, knowing the correct number of nodes can be implicitly made via determining the number of mappers and reducers needed to execute a MapReduce job and then resolving the cloud MapReduce performance-cost tradeoff.

The rest of the paper is organized as follows. Section 2 reviews the key studies on the performance evaluation of map reduce technique. Section 3 presents the proposed queueing mode to capture the MapReduce node's behaviour. Section 4 presents DES and numerical examples to show how to utilize the proposed model in predicting the performance of the node. Feasible extension of the proposed model is presented in Section 5 and finally Section 6 concludes the study and suggests directions for future work.

2. Related work

There has been some prior work on the performance of MapReduce node. A queueing network model with hypoexponential service time and finite queue was proposed to study and analysis the performance of MapReduce and multi-stage big data processing [4]. In [5] MapReduce model

behaviour was captured via a Triple-Queue Scheduler based where MapReduce workloads were classified into three types based on their CPU and I/O utilization under heterogeneous workloads. A network of queues model was proposed in [6] to model MapReduce and it was evaluated via simulation. Only the execution time of MapReduce jobs with varying cluster size was estimated. While a closed queuing networks model was proposed in [7] to model the map phase. More specifically, a mathematical model was constructed for predicting the execution time of the map phase of MapReduce single class jobs. The model results were validated by experiments on a single as well as a 2-node Hadoop environment.

The work in [3] presented an analytical model based on finite queueing system M/G/1/K to model MapReduce algorithm and to determine, at any time and under current workload conditions, the minimal number of cloud resources needed to satisfy the Service Level Objective SLO response time. The queueing model' server has three stages in tandem, namely: "job scheduling" delay centre, parallel n delay centre "VMs worker", and "result aggregating" delay centre.An analytic solution and a DES were developed to solve the system and the work considered only light- to- medium traffic. The work in [3] was extended in [1] where the model has a three- phase service time namely: delay centre scheduler (load balancer), parallel m delay centre mappers and parallel n delay centre reducers. An analytic solution and a DES were developed to solve the system that has three phases where the second and third phases arewith mand n servers with exponential service rate respectively.

The above mentioned studies did not take into consideration the MapReduce operation under heavy traffic conditions. Moreover, to the best of the author's knowledge, the heavy traffic approximation for multiple server queueing system was not utilized to simplify the queueing model analysis. The paper aims to simplify a model similar to those proposed in [1] and [3] according to this theory. In this context, i.e., at heavy traffic, multiple server queueing systems can be approximated by single server queues with total mean service rate, $\mu_t = C\mu$. Using a heavy traffic approximation, multiple server systems can be approximated to single server queueing systems, as approved in [8],[9].

3. The Proposed Model

3.1. The Queueing Model

A queueing model for executing big data MapReduce tasks is proposed, as depicted in Figure 2. Three performance metrics are considered for the mean service time, mean queue length and the loss probability. In order to simplify the simulation of the MapReduce node model proposed in [1], the approximation based on the theory of heavy traffic condition is adopted where both parallel m and n delay centres were replaced in the proposed model by single delay server with $n\mu$ and $m\mu$ rates respectively.

The model assumptions and the analysis methods are justified as following: arrivals are assumed to have Poisson distribution, since it was shown that arrival of HTTP requests for documents under a heavy load closely follow the Poisson process (According to [1] and [3]). Service times are hyperexponentially distributed, as in reality, service times are not always exponential, but they are generally distributed. In this case, these models become difficult to be analytically solved when

considering bursty traffic and non- Poisson arrivals. Therefore, simulation is an effective alternative to capture the system behaviour.

It is worth mentioning that the impact of buffer size variation on the node's performance was not taken into consideration in this study.

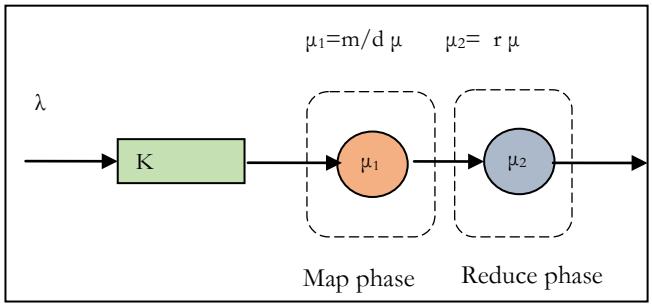

Figure2: M/G/1/K model for a big data server running m mappers and r reducers

3.2. Performance Metrics

The performance metrics adopted in this study are briefly described below[10]:

1. Mean Response time (W)

It is the time a server takes to process a job (i.e., it is the time between receiving a job at the server node and its departure from the node).

2. Loss Probability (LP)

This is the percentage of jobs that get lost on arrival when they found the server queue full.

3. Mean queue length (Wq)

It is the number of jobs waiting in the queue to be served by the server.

These performance metrics are chosen to explicitly reflect the system behaviour when the MapReduce is overloaded in the event of queue saturation (at heavy traffic conditions).

4. Simulation and Numerical Results

4.1. Simulation Analysis

Discrete-event simulation was implemented using a java package to simulate M/G/1/K /FCFS for MapReduce process with m mappers and r reducers where m > r. The performance was assessed in terms of the MapReduce node's mean response time, mean queue length and loss probability. These performance metrics were compared to assess the effect of increasing the number of m and r on the performance.

where the service time has hypoexponential distribution. The simulation is implemented according to [11].The built-in pseudorandom number generator was used to generate uniformly distributed random variables, U on [0,1] interval. (RVs) which were employed to generate exponential and hypoexponential RVs, are expressed in equations1 and 2:

$$\text{Exponential RV}=\frac{-1}{\lambda}\,.\,\ln(U) \qquad (1)$$

Hypoexpoential = $\sum_{i=1}^{n} \frac{-1}{\mu_i} \ln(U_i)$ (2)

whereλ is the mean rate of the exponential RV,$\mu_i$is the mean rates for the hypoexponential stages of the RVs and U is a uniform RV.

since hypoexponential RVs are the sum of n exponential RVs. The rates of exponential RVs can be equal or different from each other. In the context of this work, the rates are assumed to be different and the simulation algorithm of 2-sytages hypoexponential RV is depicted in Figure 3.

Algorithm:
Generating 2-stages hypoexponential RV, X, using the inverse transform method to generate two exponential RVs, the following steps as followed:
Begin
Step 1: Input the value of the mean rate λ_1, λ_2 of the Exponential RV;
Step 2: Generate two uniform RVs $U_1[0,1]$, $U_2[0,1]$ and
Step 3: Let X= $\sum_{i=1}^{2}[-\frac{1}{\lambda_i} \ln (U_i[0,1])]$;
End.

Figure 3: Algorithm of generating 2-stages hypoexponential RV

In order to improve the accuracy of simulation output, the number of the simulated events was made 10^6.. The values of the simulation parameters are listed in Table 1.

Table 1: The Parameters of The Simulation Experiments

Parameter	*Value*
K	100
Λ	200-1400 job /sec
μ	1200 job /sec
μ_1	μ_1=m/d μ
μ_2	μ_2= r μ
D	5
M	6,9,12,15
R	2,3,4,5

4.2. Numerical Results

Figures 4-7 show the relations between the adopted performance metrics for the MapReduce as a function of the mean arrival rate in order to check the effect of increasing of mappers and reducers subject to heavy traffic conditions. While Figures 6 and 7 show mean response time and loss probability against the number of both mappers and reducers. Figure 4 to 6 illustrate the effect of the number of mappers and reducers on the MapReduce performance metrics.
Figure 4 depicts the mean response time. The higher the mappers and reducers the better the performance will be (with the lowest mean response time). Clearly, this improvement is achieved because more workers operate in parallel so that any incoming job that finds the first CPU core is busy will be more probably to receive service by other workers. Figure 5 shows the performance comparison in terms of loss probability. It is verified that the loss probability for m=15 and r=5 is

much smaller than that of a m=6 and r=2. This is expected as the server capacity is around twice as the original one. As a result, the queue will have less number of jobs and this will reduce the possibility of being full that causing job loss. Figure 6 illustrates the mean queue length. It is obvious that the increase of m and r will delay the full occupation of the queue till the moment when the mean arrival rate = 800 job/sec and this is almost close to the theoretical value when the server utilization ρ=1. On the contrary, when m=6 and r=2 the queue is more probable to be full. Due to the low service rate which is a function of both m and r.

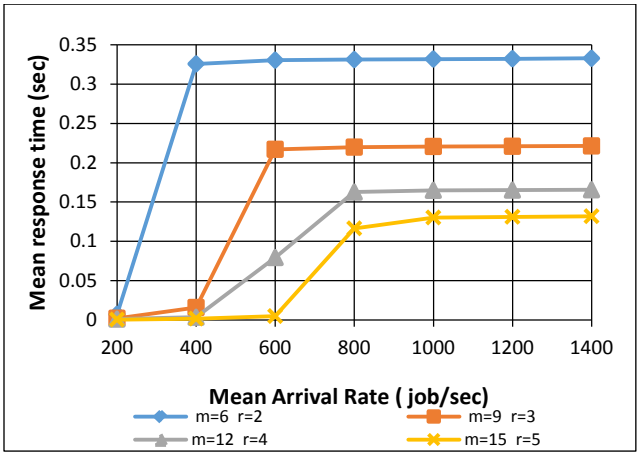

Figure 4: Mean response time Vs mean arrival rate with varying mappers(m) and reducers (r)

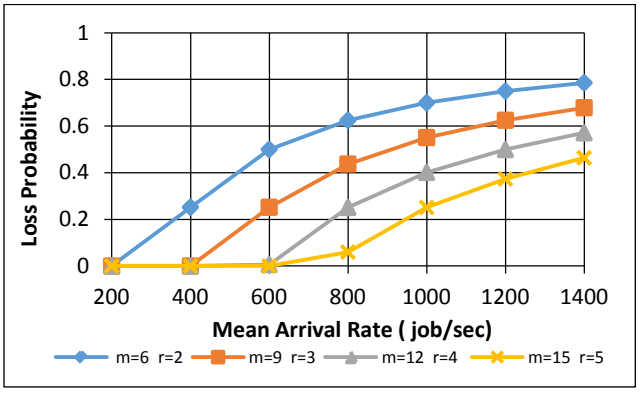

Figure. 5: Loss probability Vs mean arrival rate with varying mappers(m) and reducers (r)

In order to make a decision on the number of mappers and reducers according to specific workload conditions, Figure 7 can be employed for this purpose by taking the mean response time as a key performance metric. When the sum of m and r are equal to 12, for example, the corresponding mean response time is around 0.22 sec.

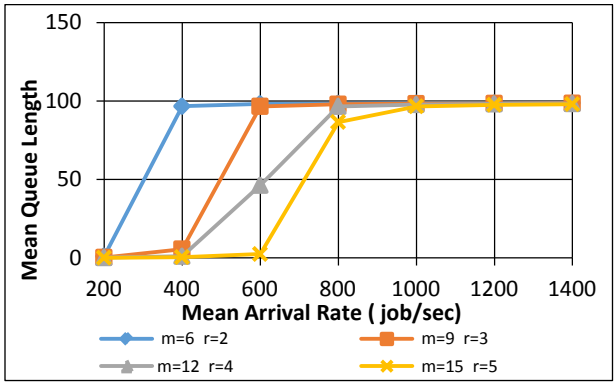

Figure. 6: Mean queue length Vs mean arrival rate with varying mappers(m) and reducers (r)

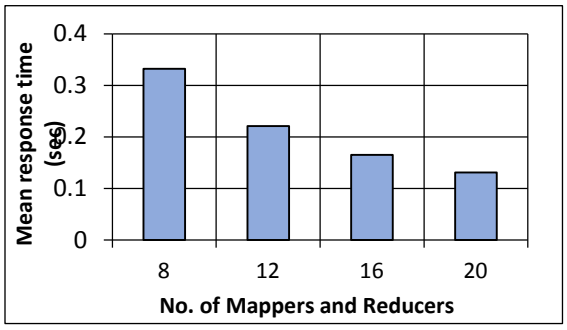

Figure. 7: Mean response time Vs. the sum of mappers and reducers (m+r) (when λ =1200 jobs/ sec)

5. A Model Extension Employing a QNM with Multiple Servers

In this section, a more general queueing model, depicted in Figure 8, is suggested to examine the performance of Map-reduces algorithm for a cluster has N servers utilizing the model proposed in [12]. This involves the use of the universal maximum entropy (ME) algorithm for arbitrary open QNMs with finite capacity (c.f., [8],[9]).

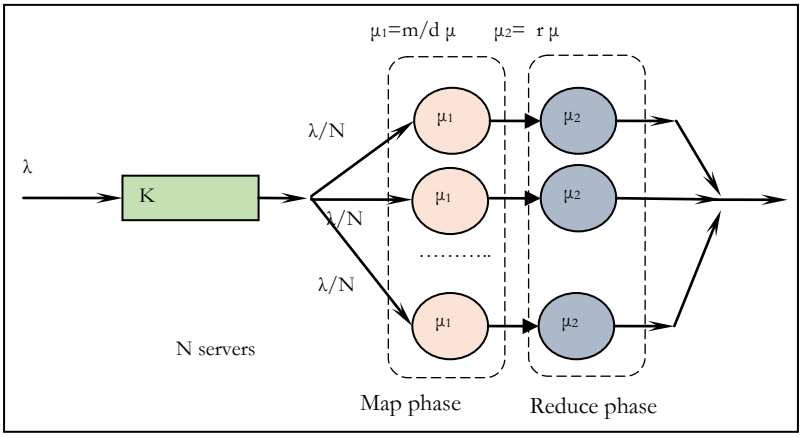

Figure. 8: Possible extension of the proposed model

6. Conclusions

The performance for big data map reduce process is investigated by assessing the impact of the number of mappers and reduces on the MapReduce system performance, in terms of the node mean response time, mean queue length and the loss probability, when fixing the buffer size. The results showed that the increase of the mappers and reducers in big data cluster node improve the overall performance. This improvement was quantified via DES.

The proposed model can be used as an effective tool to determine the number of mappers and reducers to meet specific operating conditions. This study is an attempt towards investigating the performance of MapReduce procedure using a simple QNM as a quantitative tool for the design and possible development of MapReduce process under heavy traffic workloads.

Extensions of the work may address the modelling of a big data cluster that composed of N servers running MapReduce on parallel. In this context, one or more classes can be taken into consideration to reflect realistic operating conditions. The accuracy of the proposed queueing model can be improved by taking into account the scheduling delay at the load balancer, as suggested in [1],[3].

References

[1]. K. Salah, J. M. A. Calero, "*Achieving Elasticity for Cloud MapReduce Jobs*", IEEE International Conference on Cloud Networking (CloudNet 2013), 2013, pp 195-199.

[2]. J. Dean and S. Ghemawat, "*MapReduce: Simplified Data Processing on Large Clusters*", 2004, pp. 1-13.

[3]. K. Salah, "A Queueing Model to Achieve Proper Elasticity for Cloud Cluster Jobs," Proceedings of the 2013 IEEE Cloud Conference, Santa Clara, CA, June 27, 2013, pp. 755-761.

[4]. S. Zapechnikov, N. Miloslavskaya and A. Tolstoy "Analysis *of Hypoexponential Computing Services for Big Data Processing*",2015 3rd International Conference on Future Internet of Things and Cloud, pp 579-584.

[5]. C. Tian, H.Zhou,Y. He , L. Zha, "*A Dynamic MapReduce Scheduler for Heterogeneous Workloads*", 2009 Eighth International Conference on Grid and Cooperative Computing

[6]. S. Ahn and S. Park, "An *Analytical Approach to Evaluation of SSD Effects under MapReduce Workloads*", Journal of Semiconductor Technology And Science, Vol.15, No.5, October, 2015 Issn(Print) 1598-1657.

[7]. S. Bardhan, D. A. Menasce, "Queuing Network Models to Predict the Completion Time of the Map Phase of MapReduce Jobs", In the Proc. of International Computer Measurmenr Group Conference, Las Viga, NV, 3-4th of December 2012, PP. 146-153.

[8]. D. D. Kouvatsos, I. U Awan, "*Entropy Maximization and Open Queueing Networks with Priorities and Blocking*", Elsevier, Performance Evaluation, 51, 2003,pp.191-227.

[9]. Y. Li, "*Performance Modellingand Evaluation of Cellular Networks*", Phd thesis, University of Bradford, UK (2005)

[10]. D. D., Chowdhury, "*HighSpeed LAN Technology Handbook*", Springer, USA (2000).

[11]. M. Law , W. D. Kelton, "*Simulation Modelling and Analysis*", Mc Grow-Hill , 3rd ed., 2000

[12]. S. El Kafhali, K. Salah Stochastic,"*Modelling and Analysis of Cloud Computing Data Cente"*, IEEE, 2017.

Combined Image Encryption and Steganography Algorithm in the Spatial Domain

AyaH.S. Abdelgader1 ,Raneem A. Aboughalia2, Osama A. S. Alkishriwo3
[1]A.Abdelgader@uot.edu.ly,[2]Raneem.abg@gmail.com, [3]alkishriewo@yahoo.com
[1, 2, 3] Department of Electrical and Electronic Eng., College of Eng., University of Tripoli, Libya

ABSTRACT

In recent years, steganography has emerged as one of the main research areas in information security. Least significant bit (LSB) steganography is one of the fundamental and conventional spatial domain methods, which is capable of hiding larger secret information in a cover image without noticeable visual distortions. In this paper, a combined algorithm based on LSB steganography and chaotic encryption is proposed. Experimental results show the feasibility of the proposed method. In comparison with existing steganographic spatial domain based algorithms, the suggested algorithm is shown to have some advantages over existing ones, namely, larger key space and a higher level of security against some existing attacks.

Keyword— Steganography, data hiding, cover image, stego image.

1. Introduction

The growing of digital communication technologies has caused a substantial increment in data transmission. When sensitive information such as bank account numbers is being shared between two communicating parties over a public channel, security of such data becomes necessary. Cryptography and steganography are two important tools for providing security and protecting sensitive information. Cryptography provides features such as confidentiality and integrity of data. For instance, confidentiality is achieved via an encryption algorithm which scrambles/mixes the private information so that it becomes unreadable to any party other than the intended recipient. However, steganography provides data security by hiding the information in a cover medium so that even the existence of a hidden message is not known to an intruder. Secret messages are embedded in cover objects to form stego objects. These stego objects are transmitted through the insecure channel. Cover objects may take the form of any digital image, audio, video and other computer files. Digital images are widely used as cover object of hidden information because of the high level of redundancy in them which is caused by the low sensitivity of the human visual system to details. The success of steganography lies in transmission of stego objects without suspicion [1].

A large number of image steganographic techniques have appeared in the literature, for example [2-7]. These techniques can be classified into two main classes: spatial domain and transform domain techniques. In spatial domain techniques, private message is embedded in the intensity of image pixels directly [2-4]. In transform domain techniques, the privatemessage is embedded in the cover by

modifying coefficients in a transform domain such as discrete cosine transform (DCT) and integer discrete wavelet transform [5-6].

Although transform domain based algorithms are more robust to steganalytic attacks, the spatial domain based algorithms such as least significant bit (LSB) algorithms are much simpler and faster. Several versions of the LSBs embedding algorithms have appeared in the literature. However, many steganalysis tools that reveal the insecurity of some LSBs replacement algorithms have been reported. For example, in [7] authors suggested a steganalytic attack that can estimate the length of information embedded in a host image for various LSBs algorithms. Nevertheless, the high embedding capacity and low computational complexity of these algorithms have encouraged researchers to further participate in this area.

Chaotic maps are well known for their sensitivity to initial conditions and control parameters. These properties make them suitable for building blocks in the design of many cryptographic and steganographic algorithms [3, 8]. In this paper, we propose a new LSBs spatial domain algorithm that is based on mixing two 2-D chaotic maps. The proposed algorithm encrypts the secret message using mixed chaotic map and uses LSB for data hiding.

The rest of the paper is organized as follow: Section 2 presents the used 2-D chaotic maps. In Section 3, we give a detailed description of the proposed algorithm and a flowchart. In Section 4, simulation results are presented and discussed. The conclusions are given in Section 5.

2. Two Dimensional Chaotic Maps

In the proposed steganography method, we have used a combination of two 2D chaotic systems which are logistic and duffing maps defined in [8, 9] as given in (1) and (2).

$$x_{n+1} = \mu\, x_n\ (1 - x_n)$$
$$y_{n+1} = \lambda y_n\ (1 - y_n) \quad (1)$$

where, μ, λ, x and $y$are the control parameters and state values, respectively. When $\mu\ and\ \lambda\ \epsilon\ [3.57,4]$, the system is chaotic. The Duffing map depends on the two constants a and b. These are usually set to $a = 2.75$ and $b = 0.2$ to produce chaotic behaviour. It is a discrete version of the Duffing equation.

$$z_{n+1} = w_n$$
$$w_{n+1} = -b\, z_n + aw_n - w_{n+1}^3 \quad (2)$$

3. The Proposed Steganographic Algorithm

The steganographic scheme proposed in this article embeds a binary message according to the least significant bit technique as shown in Figure 1. This helps imperceptibility since the more significant bits of the cover image are not altered. Data embedded is done using the following steps:

- Step 2: Read both of cover image and secret image, the cover image most be equal or larger than the secret image.
- Step 3: use chaotic maps to encrypt secret image.

- Step 3: Select the block size for the encryption algorithm and generate random initial conditions for the chaotic maps.
- Step 4: Using the initial conditions to generate chaotic maps key streams X and Y.
- Step 5: Secret image is divided into blocks of same size ($m \times m$), scrambled using the encryption key stream and recombined into a single image.
- Step 6: Pixel wise XOR operation is done on the scrambled image using the key stream to get the encrypted image.
- Step 7: Extract the pixels of the cover image and encrypted secret image.
- Step 8: Choose first pixel of the cover image and pick first pixel of the encrypted secret image then place it using LSB algorithm, one pixel of the encrypted secret image have 8 bits, using for example 8bpp all this bits will be hidden inside one pixel of the color image.
- Step 10: Repeat step 9 till all the pixels of the encrypted secret image has been embedded.

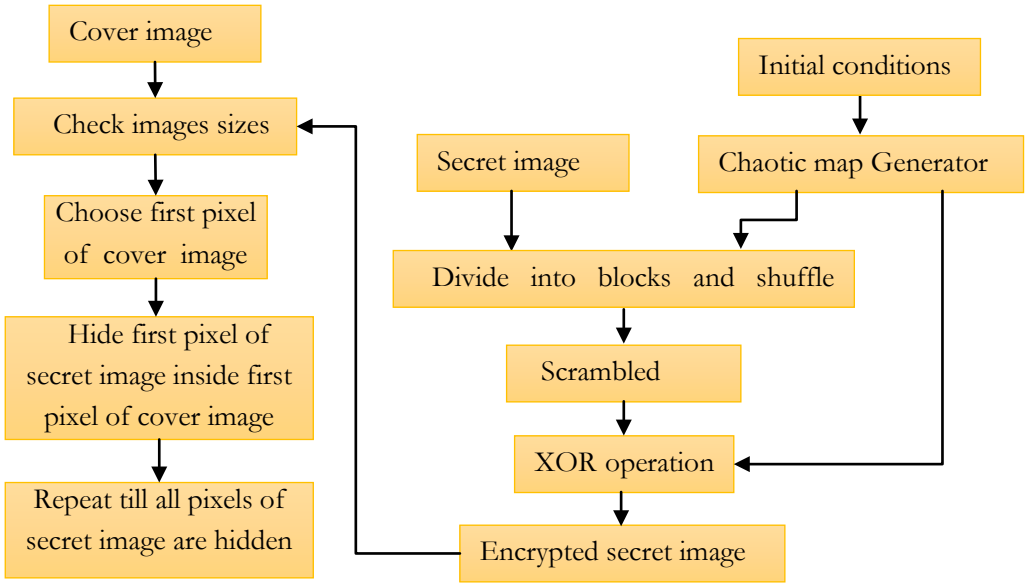

Figure 1: Block diagram of proposed steganography algorithm.

When applying LSB techniques to each byte of a 24 bit image, we can take the binary representation of the hidden data and overwrite the LSB of each byte within the cover image. If the LSB of the pixel value of cover image $C(i,j)$ is equal to the next message bit SM of secret massage to be embedded, $C(i,j)$ remain unchanged; if not, set the LSB of $C(i,j)$ to SM.

4. Performance Analysis and Experimental Results

In this section, experimental results are given to demonstrate the performance of the proposed algorithm. Comparative experimental studies are also presented to show the superiority of the proposed algorithm over typical existing ones. Four standard $512 \times 512 \times 3$colored images,

namely, Airplane, Fruits, pool, and girl are used as cover images for hiding sensitive information of length 524288 bit.

4.1. Visual Attack

Visual attacks, regarded as the simplest type of steganalysis, aim at revealing the presence of hidden information through visual inspection by the naked eye. The presentedalgorithm is designed to be robust against visual attacks. Figure 2 presents a cover image ($512 \times 512 \times 3$ Airplane), a secret-image carrying of size(256×256), an encrypted secret image, and a stego-image carrying an encrypted secret image. A visual inspection of the coverand the stego-image does not reveal any difference between the two images.

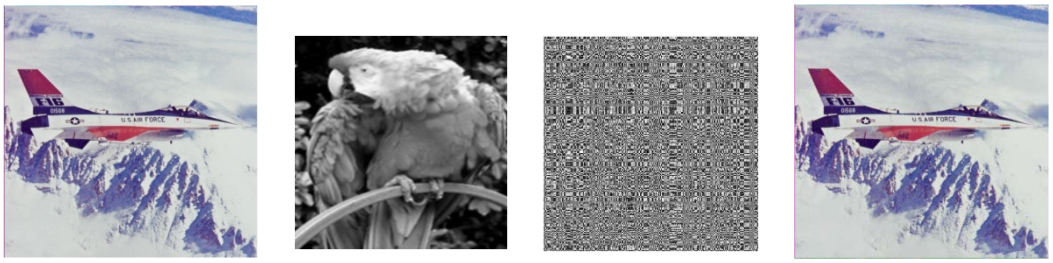

[1]. (b) (c) (d)

Figure2: (a) cover image, (b) secret image, (c) encrypted secret image, (d) stego image.

4.2. Imperceptibility and Payload

For data hiding in images, hiding capacity and visual quality of the scheme play important roles. So, increasing hiding capacity adversely affects the visual quality of the stego-image. The embedding rate is the number of bits that can be embedded into one pixel, and it is measured by bits per pixel (bpp). It is known that human visual system cannot detect the distortion of a stego-image, when the peak signal to noise ratio (PSNR) is higher than 30 dB. To compare between each of 3, 6, 8 bits per pixel, we measure PSNR for all stego-images as shown in Table 1, the highest PSNR values means the stego-image is similar to cover image.

Table 1:PSNR comparison in dB.

bpp	Airplane	Fruits	Pool	Girl
3	53.0	53.6	53.8	53.6
6	48.2	48.5	48.2	48.6
8	41.5	41.8	42.7	41.5

In Table 2, PSNR (dB) is calculated with different payload capacity of 3 bpp on a stego- image using Lena as a cover image , and the results are compared with similar steganography schemes for the same cover image.

Table 2: Comparison of the proposed algorithm to existing work in terms of PSNR (dB).

bpp	Proposed	[4]	[10]	[11]
3	53.0	37.9	37.3	37.8

4.3. Image Histogram

In Figure 3, we present the histograms of the cover image Lena and the resulting stego-image produced by our algorithm with a message of size 3bpp, 6 bpp, and 8 bpp. It can be observed that the two histograms are very similar. This test shows a comparison between the cover image and the stego image, using the histogram as a visual comparison tool.

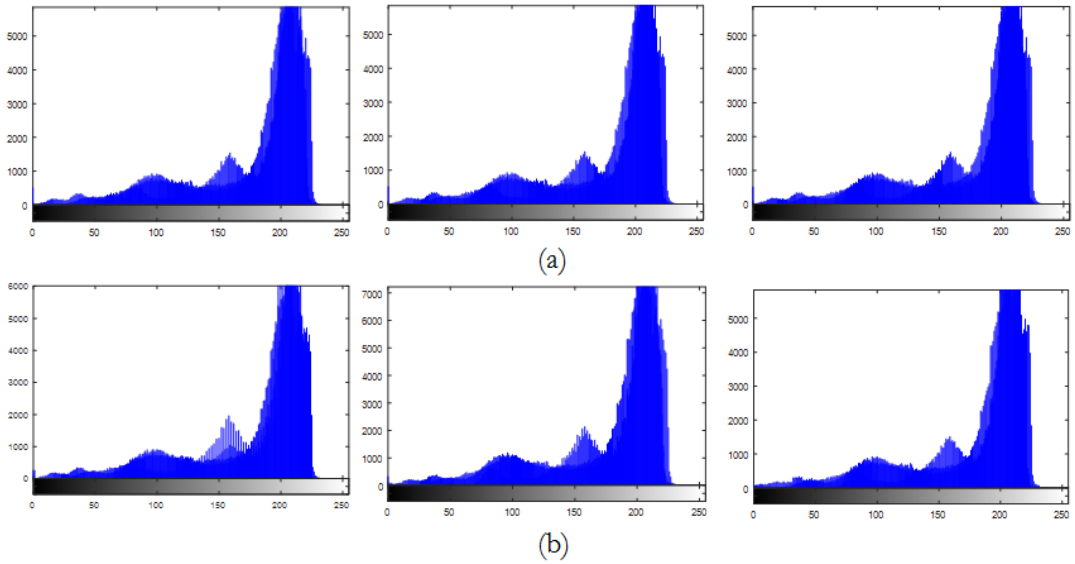

Figure 3:(a) Histogram of cover image, (b) Histogram of stego-image from left to right 3 bpp, 6 bpp, and 8 bpp.

4.4. Key Space Analysis

The key space of an encryption algorithm should be large enough to resist brute–force attacks. In the proposed algorithm, the secret key contains seven real numbers (two control parameters and four initial states). If we assume the computation precision of the computer is 10^{-15}, then the key space is about $10^{90} \approx 2^{299}$. Such a large key space can ensure a high security against brute–force attacks.

5. Conclusions

In this paper, a steganographic algorithm based on two 2-D chaotic maps has been introduced. This algorithm embeds the encrypted sensitive information using chaotic maps into the cover image according to the least significant bit technique. The LSB algorithm effectively allows the embedding of secret information at higher level frequencies, which are not visible to the human eye. The

presented simulation results show the resistance of the suggested algorithm against some existing steg analytic attacks. Furthermore, the results show its advantages over some existing algorithms.

References

[1]. Kanso and H. S. Oun, "Steganographic algorithm based on a chaotic map," Commun Nonlinear SciNumerSimulat, vol.17, pp. 3287-3302, 2012.

[2]. Chan and L. Cheng, "Hiding data in images by simple LSB substitution," Pattern Recognition, vol. 37, no. 3, pp. 469–474, 2004

[3]. Battikh, S. El Assad, B. Bakhache, O. Deforges, and M. Khalil, "Chaos-based spatial steganography system for Images," International Journal of Chaotic Computing, vol. 3, no. 1, pp. 36–44, Jun. 2014.

[4]. G. S. Yadav and A. Ojha, "Chaotic system-based secure data hiding scheme with high embedding capacity," Computers and Electrical Engineering, pp. 1-14, 2018.

[5]. R. El Safy, H. Zayed, and A. El Dessouki, "An adaptive steganographic technique based on integer wavelet transform," In IEEE International conference onnetworking and media convergence (ICNM 2009), pp. 111–117, 2009.

[6]. Lin and P. Shiu, "High capacity data hiding scheme for DCT-based images," J Inf Hiding Multimedia Signal Processing, vol. 3, no. 1, pp. 220–240, 2010.

[7]. J. Fridrich and M. Goljan, and D. Rui, " Detecting LSB steganography in color and grayscale images," IEEE Multimedia, vol. 8, no. 4, pp. 22-28, 2001.

[8]. N.K. Pareek, V. Patidar, and K.K. Sud, "Image encryption using chaotic logistic map," Image and Vision Computing, vol. 24, pp. 926-934, 2006.

[9]. Y. Abanda1 and A. Tiedeu, "Image encryption by chaos mixing," IET Image Processing, vol. 10, no. 10, pp. 742–750, 2016.

[10]. Q. Wu, C. Zhu, J. Li, C. Chang, and Z. Wang, "A magic cube based information hiding scheme of large payload," J. Inf.Secur. Appl., vol. 26, pp. 1–7, 2016.

[11]. Z. Eslami and J. Ahmadabadi, "Secret image sharing with authentication-chaining and dynamic embedding," J. Syst. Softw., vol. 84, no. 5, pp. 803–809, 2011.

Experimental Evaluation of the Humans' Health Hazards' Potential Due to Exposure to the Microwaves' Radiations in Garaboulli City-Libya.

Abdurahman Alsonosy Altawil[(1)], (aaaltawil@elmergib.edu.ly), Mohamed Youssef Ahmed Abou-Hussien[(1)], (myabouhussein@elmergib.edu.ly), Abdelbaset Karem Omran[(1)], (Abdelbaseto91@gmail.com).
Majdi Masoud Alrajhi [(1)], (magdimassud99@gmail.com).
[(1)]Department of Electrical and Computer Engineering, Faculty of Engineering – Garaboulli, Elmergib University, Libya.

ABSTRACT

There is a high concern worldwide about the effects of the high level of energy of the transmitted electromagnetic radiations for the wireless communications on the humans' health. So, the purpose of this study is to experimentally evaluate the human health safety related to the exposure to the highest energy of the transmitted microwave radiations (highest radiation risk) at the highest operating frequency 2450 MHz of all operating frequencies (850, 900, 950, 2450 MHz) within the range of 30 MHz-3GHz of the tested AL-MADAR mobile phone base station in the population area for the first time in Garaboulli City - Libya. The specific absorption rate (SAR) value is used as a measure of the rate of absorption of microwave radiation energy in the human tissues on the basis of exposing to the highest radiation risk which is considered asthe worst case scenario. The SAR values are evaluated at predetermined distances (5, 40, 80, 120 and 160 meters) by using MATLAB program. The power density and the electric field measurements of the microwaves radiation of the antenna of the selected of AL-MADAR mobile phone base station, were experimentally measured by utilizing the spectrum analyzer devise (Spectrum HF-6065), in addition to the mass density and the medium conductivity values for the investigated human tissues (eye (Sclera), brain (Grey Matter), nerve and blood) at 2450 MHz frequency. The numerical results indicate that the highest SAR value is $205.4 * 10^{-6} W/kg$ of the human blood at the shortest distance (5 meters). This SAR value is significantly lower than the international recommended safe radiation level standards. So, for the first time, these results show that the microwave equipments which use AL-MADAR network in the Garaboulli city-Libya can be considered safe on the humans' health.

Keyword— Microwaves Radiations, Specific Absorption Rate (SAR), MATLAB Program, Health Hazards & Garaboulli City-Libya.

1. Introduction

People nowadays commonly use several applications of the microwave communication technology which are constitutively emitting microwaves radiation such as modern mobile telephone services (text messaging ; messaging multi services (MMS) ; email ; internet access ; short range communications (infrared , Bluetooth) ; business application ; gaming and photography), which use the cellular wireless network architecture ; whereas it's work depends on mobile phone base stations (these are also known as base transceiver stations or telecommunication structures). These

telecommunication structures are multi-channel two ways radio for transmitting and receiving signals, and have antennas which produce microwaves radiation whereas they are mounted on transmission towers that need to be of at a certain height order to have a wider coverage [1].

The microwaves radiation has the potential to interact with the human biological system and could cause hazards on people's health. The microwaves radiation of all frequencies between 30MHz to 3GHz is classified as non-ionizing and can potentially lead to irreparable damages in the exposed human biological tissues [2].

On the basis of the exposure to the highest microwaves radiations (EMRs) energy (the highest radiation risk which is considered as the worst case scenario); by using the SAR measure in different human tissues, for the first time in Garaboulli City-Libya, this study is designed and conducted aiming to experimentally assess the potential radiation risks on the human health related to the exposure to the highest microwave radiation energy at the highest operating frequency 2450 MHz of all operating frequencies (850, 900, 950, 2450 MHz) which is included in the internationally recommended operating very high (VHF) and ultra high frequencies (UHF) range of 30 MHz to 3 GHz according to the stratification specified by International Telecommunication Union (ITU).

2. Materials and Methods

Firstly, due to the availability of many different designs of the mobile phone base stations that vary widely in their power, characteristics, and their potential for exposing people to the microwaves radiation [1] and secondly, based on the highest radiation risk, which is fulfilled requirement by the highest experimental values of each of the power density and the electrical field received at the population area of the tested site, the MATLAB program is used to experimentally evaluate the exposure to the highest microwaves radiation energy atthe highest operating frequency 2450 MHz of all operating frequencies (850, 900, 950, 2450 MHz) , within the operating VHF and UHF range of 30 MHz to 3 GHz, of the antenna of the selected AL-MADAR mobile phone base station, which is located near Garaboulli City's bridge. This selected mobile base station uses modern mobile telephone services, and its antenna's radiation is received by the population area in tested site (Garaboulli city centre).

The selection of the highest operating frequency 2450 MHz of all operating frequencies of the tested mobile base station was done with full consideration of the direct relationship between the calculated SAR values and the different operating frequencies.

The calculation of the SAR value which is used as the evaluating measure tool at pre determined distances (5, 40, 80, 120 and 160 meters) , was done using the correspondent information of the power density and the electric field of each investigated human tissues. The calculated SAR value is measured in watt per kilogram (W/kg).

The experimental measurements of the highest radiation energy at each earlier mentioned different distances, were done by utilizing the spectrum analyzer devise (Spectrum HF-6065), in addition to the medium conductivity (σ) values of each of the investigated human tissue [eye (Sclera), Brain(Grey

Matter), nerve and blood]that have the highest values at the highest operating frequency 2450 MHz of all operating frequencies (850, 900, 950 and 2450 MHz) which is included in the internationally recommended operating VHF and UHF range of 30 MHz to 3 GHz according to the stratification published by ITU[3].

3. Theory and Calculation

This study is conducted to experimentally assess the possible health hazards on the humans due to the exposure to the highest microwaves radiation energy at the highest operating frequency 2450 MHz of all operating frequencies (850, 900, 950 and 2450 MHz), which is emitted by the selected AL-MADAR mobile phone base station that is located in Garaboulli City-Libya for the first time on the basis of considering the exposure to the highest radiation risk in the population area at the tested site; by using the SAR measure in each investigated human tissue [3, 4, 5].

3.1. Mathematical Expressions and Symbols

The MATLAB program is used to evaluate the SAR values, by applying the equation number (3) which is obtained from the equations number (1) and (2) as following:

For a sinusoidal steady state electromagnetic field, the SAR value is calculated as given in equation (1), [5];

$$SAR = \left(\sigma + \omega\varepsilon_o\varepsilon''\right)\frac{{E_{rms}}^2}{\rho} \quad \ldots\ldots\ldots\ldots\ldots\ldots\ldots\ldots\ldots\ldots\ldots\ldots\ldots\ldots\ldots\ldots \quad (1)$$

And by using the power density equation through applying the following formula [6];

$$P = \omega\varepsilon_o\varepsilon''{E_{rms}}^2 \quad \ldots\ldots\ldots\ldots\ldots\ldots\ldots\ldots\ldots\ldots\ldots\ldots\ldots\ldots\ldots\ldots\ldots \quad (2)$$

Accordingly, the equation (1) can be expressed as following;

$$SAR = \frac{(\sigma{E_{rms}}^2 + P)}{\rho} \quad \ldots\ldots\ldots\ldots\ldots\ldots\ldots\ldots\ldots\ldots\ldots\ldots\ldots\ldots\ldots\ldots \quad (3)$$

Where:

SAR: The evaluated specific absorption rate$[watt/kilogams(W/kg)]$.

E_{rms}: The measured value of the electric field$[Volt/meter(V/m)]$.

p: The measured value of the power density$[watt/square\ meters(w/m^2)]$.

σ: The medium conductivity$[Siemen/meter(S/m)]$.

ρ: The mass density$[Kilograms/Cubic\ meters(kg/m^3)]$.

ε'': Out of phase loss (unit less).

ε_o : The vacuum permittivity$[Farad/meter\ (F/m)]$.

ω: The angular frequency (radians / second).

The ρvalues andσ values for each of the under studied human tissues [Eye (Sclera), Brain (Grey Matter), nerve and blood) at 2450MHzfrequency, are given in Table 1.

Table 1: Clarified the difference values of Mass density (ρ), and the medium conductivity (σ) for different parts of human body at 2450MHz frequency [3, 4].

Human Tissues	Mass Density (ρ) (kg/m³)	Medium Conductivity(σ) (S/m)
Nerve	**1075**	**1.0886**
Brain (Grey Matter)	**1045**	**1.8077**
Eye (Sclera)	**1032**	**2.0332**
Blood	**1050**	**2.5448**

4. Results and Discussion

Table 2 shows that the maximum electrical field (V/m) and the maximum power density ($\mu W/m^2$) were detected at 5 meters distance, however the minimum electrical field (V/m) and the minimum power density ($\mu W/m^2$) were detected at 160 meters distance. It also demonstrates the calculated SAR values in the tested human tissues [Nerve, Brain (Grey Matter), Eye (Sclera), Blood] at the predetermined different distances at which all the study variables were measured.

It has been well noted in Table 1that the Blood which has the maximum SAR value, has also the maximum Medium Conductivity(σ) of 2.5448 S/m value and the nerve which has the minimum Medium Conductivity(σ) of 1.0886 S/m value, has also the minimum SAR value.

Table 2 shows also the maximum SAR value of 205.4X10$^{-6}W/kg$was measured at 5 meters distance in the blood and the minimum SAR value of 5.7X10$^{-6}W/kg$was measured in the Nerve biological tissue at the distance of 160 meters.

Table 2: The measures power density, electric field values and the calculated SAR values of the investigated human tissues at 2450 MHz frequency at different distances.(*GM=Grey Matter)

Distance (m)	Electric field (V/m)	Power density ($\mu W/m^2$)	$SAR(\times 10^{-3}W/kg)$ Human tissue			
			Eye (Sclera)	Brain (GM*)	Nerve	Blood
5	0.291	221.2	0.1670	0.1467	0.0860	0.2054
40	0.281	210.2	0.1558	0.1368	0.0802	0.1916
80	0.192	85.94	0.0727	0.0639	0.0374	0.0894
120	0.144	55.44	0.0409	0.0359	0.0211	0.0503
160	0.075	15.21	0.0111	0.0097	0.0057	0.0136

The results given above indicate that the highest SAR value is 205.4×10^{-6} W/kg of the blood human tissue that has been calculated at the shortest distance (5 meters) and at 2450 MHz frequency. Comparatively, this SAR's value is much lower than the international recommended safe radiation level standard's values. These standards are regulated by world authoritative bodies include the following with their correspondent safe SAR limits; 1.6 W/kg during 30 minutes according to the Federal Communications Commission (FCC) and2 W/kg during 6 minutes according to the European recommendations.

It is important to note that the average time exposure of 30 minutes according to FCC and 6 minutes according to the European recommendations have a significance only in the cases that are exposed to the power or the electromagnetic fields which are higher than the allowed ones according to the related international standards. However, in the inhabitant residential populated areas similar to the tested site in this study, the FCC recommends not to apply the average time exposure parameter, so, the calculated SAR values which do not exceed the allowed ones according to the international standards, are considered as the allowable values to a continuous exposure for indefinite time period [7].

5. Conclusion

This study shows clearly that on the basis of the exposure to the highest microwaves radiation energy (the highest radiation risk which is considered as the worst case scenario) in the population area at the tested site and by considering the direct relationship between the calculated SAR values and the different operating frequencies, the obtained practical results prove that microwaves radiation for all operating frequencies that are emitted by AL-MADAR wireless communication system networks in Garaboulli City-Libya can be considered safe to the people's health.

Acknowledgment

The authors are very grateful and highly thankful to all members of the developing and the investigation office in AL-MADAR Company for providing the spectrum analyzer devise (Spectrum HF-6065) and their extensive professional indispensible assistance throughout the study.

References

[1]. Girish Kumar ," *Cell Tower Radiation* ", Electrical Engineering Department ,IIT Bombay, Poway, Mumai - 400-076, December 2010. Access online on 28th August 2018 at https://www.scribd.com/doc/44736879/Cell-Tower-Radiation-Report-sent-to-DOT-Department-of-Telecommunications

[2]. "Exposure from mobile phones, base stations and wireless networks" A statement by the Nordic radiation safety authorities, 17 .12. 2013. Access online on 28th August2018 at https://www.gr.is/wp-content/media/2013/12/absolute-final-version-EMF-statement-logo.pdf

[3]. Website of the Italian National Research Council-Institute for Applied Physics "Nello Carrara"-Florence (Italy)-2018. Access online on 28th August2018 at http://niremf.ifac.cnr.it/tissprop/htmlclie/htmlclie.php

[4]. Website of the Foundation for Research information Technologies in Society (IT'IS)-Zurich Switzerland. Tissue properties→Database→Density. Access online on 28th August2018 at https://www.itis.ethz.ch/virtual-population/tissue-properties/database/density/

[5]. Riadh W. Y. Habash, Electromagnetic Fields and Radiation: Human Bioeffects and Safety, New York, NY: Marcel Dekker, 2001. ISBN 0-8247-0677-3. Access online on 28th August2018 at https://books.google.com.mt/books?hl=en&lr=&id=NEXgsO_y9ssC&oi=fnd&pg=PA1&ots=NgKtFf4vZR&sig=6imurgf2Ww1aGkmIif_tc3ucbaY&redir_esc=y#v=onepage&q&f=false

[6]. B. M. Tareev, "Electrical and Radio Engineering Materials-Dielectric Loss"-*MIR Publishers*, Page – 154-169. Access online on 28th August2018 at http://www.ursi.org/proceedings/procGA05/pdf/KP.26(01122).pdf

[7]. FCC OET Bulletin No.65, 1997, Evaluating Compliance with FCC Specified Guidelines for Human Exposure to Radiofrequency Radiation. Access online on 28th August 2018 at www.fcc.gov/oet/rfsafety

Capability of Modified SIFT to Match Stereo Imagery System

Omar Abusaeeda1*, Salah Naas2, Nasar Aldian Shashoa3
1 abossada1@gmail.com, 2naas.salah@gmail.com, 3dr.naser.elec@gmail.com
[1] Department of Computer Networks, Faculty of Information Technology, Azzaytuna University, Libya
[2, 3] Department of Electrical & Communication Engineering, Faculty of Engineering, Azzaytuna University, Libya

ABSTRACT

This paper presents an improved version of SIFT method for extracting invariant features from images that can be used to solve the correspondence problem between different views of an object or scene in an image. Scale invariant feature transform (SIFT) has recently gained substantial attention in the computer vision community to address the problem. Corresponding features in sequential pairs of images, at various different angular separations, were identified by applying a scale invariant feature transform (SIFT). Due to limitation in the standard SIFT; some of matches are considered false matches. Epipolar-line and disparity window criteria were introduced to enhance the performance of SIFT. Experiments revealed that considerable number of unfaithful matches were removed when new criteria are introduced. Future work will focus on improving the SIFT technique; to rectify the negative matches in order to obtain better matching result.

Keyword— SIFT, Image matching, positive matches.

1. Introduction

A typical image matching method begins with detecting points of interest, then selects a region around each point, and finally associates a descriptor with each region. Correspondences between two images may then be established by matching the descriptors of both images. SIFT is proposed by David Lowe in 2004[1] to extract features of interest from images that can be used for reliable matching between different views of an object. The features are invariant to image scaling and rotation and partially invariant to change in 3D viewpoint and additional noise. Over recent years, SIFT has played a significant role in various computing applications such as object recognition, 3D modelling and video tracking.

Feature matching can be defined as the process of matching corresponding points between two or more images of the same scene. Feature based methods match special features of two images, such as corners or edges to produce a sparse disparity map [2,3]. This method matches more features, rather than matching textured regions in the two images [4,5]. Feature based methods provide more precise positioning for the matching results and are more reliable than correlation-based matching when good image features can be extracted from the scene [6]. Feature based methods are widely used in wide-base stereo image matching [7,8]. Correspondences between two images is established by matching the descriptors of both images. Numerous variations exist on the computation of interest points matching. It can be traced back to the work of stereo matching using a corner detector [9,10], which was later improved by Harris and Stephens [11,12]. Consequently, the Harris corner detector has since been extensively used for various other image-matching tasks. The approach was presently expanded to match Harris corners over a large image range by using a correlation window around

each corner to select likely matches. Moreover, Harris corners were used to select interest points, but rather than matching with a correlation window, they used a rotationally invariant descriptor of the local image region. This allowed the matching of features under arbitrary orientation change between the two images. Additionally, it was demonstrated that multiple feature matches could accomplish general recognition under occlusion and clutter by identifying consistent clusters of matched features [1].The local feature approach was extended to achieve scale invariance and more distinctive features whilst being less sensitive to local image distortions such as 3D viewpoint change [13]. In recent times, there has been an inspiring body of work on extending local features matching. Most recently, there has been an impressive effort on expanding the approach of local feature descriptor [14,15]. While this method is not completely affine invariant, a different approach is used in which the local descriptor allows relative feature positions to shift extensively with only small changes in the descriptor[16]. This approach produces descriptors, which are consistently matched across a substantial range of affine distortion. It also makes the features more robust against changes in 3D viewpoint. This approach not only has the advantages of extracting more efficient feature, but it also able to identify larger numbers of features. Furthermore, Principal Components Analysis SIFT (PCA-SIFT) was introduced. This technique accepts the same input as the standard SIFT descriptor. The advantage of this approach is the size of the descriptor. It produces a more compact descriptor in comparison to standard SIFT. On the other hand, it tends to blur the edges around the objects[17]. Another local feature descriptor named, Speeded-Up Robust Features (SURF) was proposed [18]. SURF is mainly designed for real time application where the speed is the main concern. SURF performance is similar to SIFT but it is not invariant to rotation and illumination changes [5]. The choice of methods is informed by the computer vision application under consideration. It has been demonstrated recently that features identified by SIFT are highly distinctive and invariant to image scales and rotations, and partially invariant to a change in illumination [19]. It is indicated that using multiple images might help to solve some problems associated with stereo matching. However, more information may also carry the risk of increased uncertainties. Repeating features is a common problem encountered by stereo matching algorithms that apply feature-based method for visible light images.

1.1. Repeating Features

The images in Figure1presenta good example of repeated features, which are commonly found in stereo pairs, where Left view and Right view are the images obtained at different views. To study the effect of local similarity, consider the repeating features Object 1 and Object 2, illustrated in the two views in Figure1.

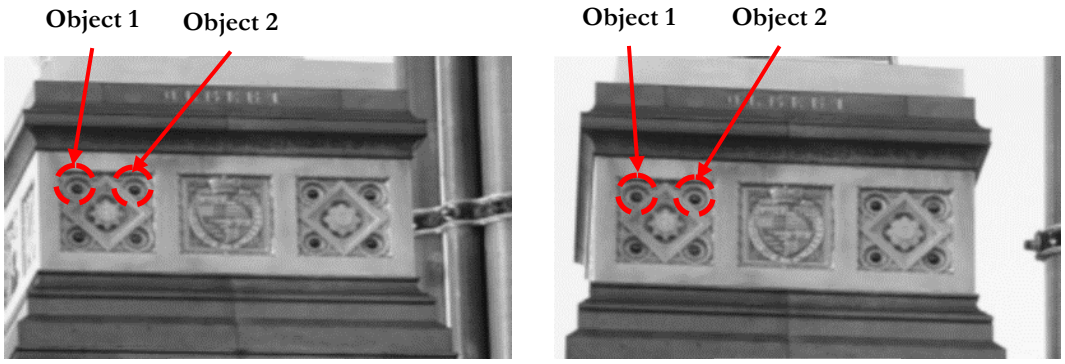

Figure 1: Repeating features extracted from two different views

By applying the stereo matching criterion on this pair of images, on one hand, and as these features are obvious and strong, the opportunity to match them is significant. On the other hand, unless special care is taken, Object 1 in the Left view would have an equal opportunity to match with Object 1, Object 2 or other similar features in the Right view. As a result, an error in matching could occur. This finding is exacerbated when considering overlapping structures commonly found in cluttered visible light images.

1.2. Keypoint Matching

The SIFT algorithm adopts the fast nearest-neighbour method to identify the best match for a particular feature from a database of features. Since the keypoint is described by its descriptor, the nearest neighbour is defined as the keypoint with minimum Euclidean distance for the invariant descriptor vector [20]. Nevertheless, numerous features from an image will not match correctly in the derived keypoints database for the reason that they were not detected in the training images. Lowe [1] mentioned to discard all matches in which the distance ratio between closest neighbour to that of the second closest neighbour is greater than 0.8. This ratio removes 90% of the false matches on the other hand it discards less than 5% of the correct matches. Even though 90% of false matched are discarded, the remaining 10%of false matches might be a problematic for a particular image application. To maximise the potential applicability of SIFT, additional boundary conditions of search for corresponding are proposed. These added criteria will tighten the support of the standard SIFT.

2. Materials and Methods

In our work, additional bounding criteria of a disparity window and an epipolar line constraint are employed. The former is defined as the intersection of the epipolar plane with the image plane, while the latter concerns the nominally zero vertical disparity. i.e. the epipolar line is along the image y-axis (vertical in the display), while the disparity window is along the image x-axis (horizontal in the display). Both criteria are shown in Figure 2.

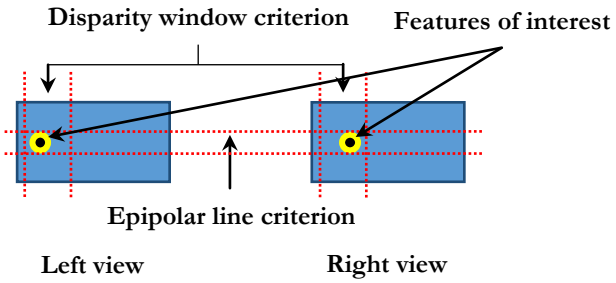

Figure 2: Two perspective views and their corresponding features of interest

Taking into account various practical fluctuations a tolerance of ±1 pixel deviation in the y-axis coordinate position (vertical in the display) is employed to accommodate a practical epipolar line criterion [19]. To further limit the search space a disparity window criterion is introduced. The window size in pixels is determined by the angle separation between views.

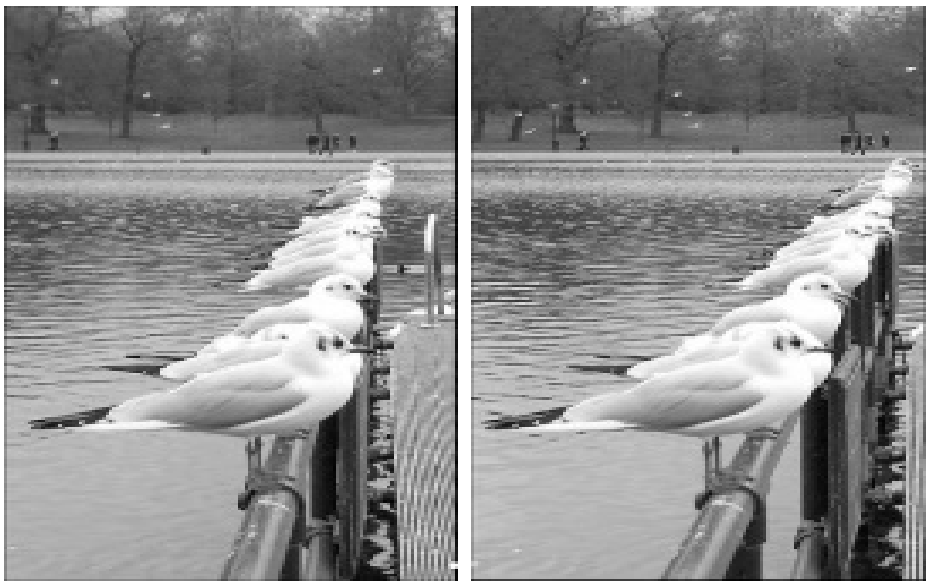

Figure 3: Corresponding pair of images employed in this study

It should be noted that for comparative purposes the new criteria are applied to corresponding pairs that have already satisfied the standard SIFT criteria. Care was taken when stereo images were selected to ensure overlapping. Repeating features were also taken into consideration to ensure that the standard SIFT is supported by the new added criteria. An example of stereo image are shown in Figure 3.

3. Results and Discussion

Matched features are categorised into two groups; negative and positive matches. The positive matches are the matches that satisfy the standard SIFT, epipolar and disparity window criteria while

the negative matches satisfy the standard SIFT criterion but violate either the epipolar line or disparity window criteria. Figures 4 represents the positive matches indicated by horizontal green colour lines connecting the corresponding pairs, while the negative or erroneous matches are presented in Figure5 and are shown as red colour lines.

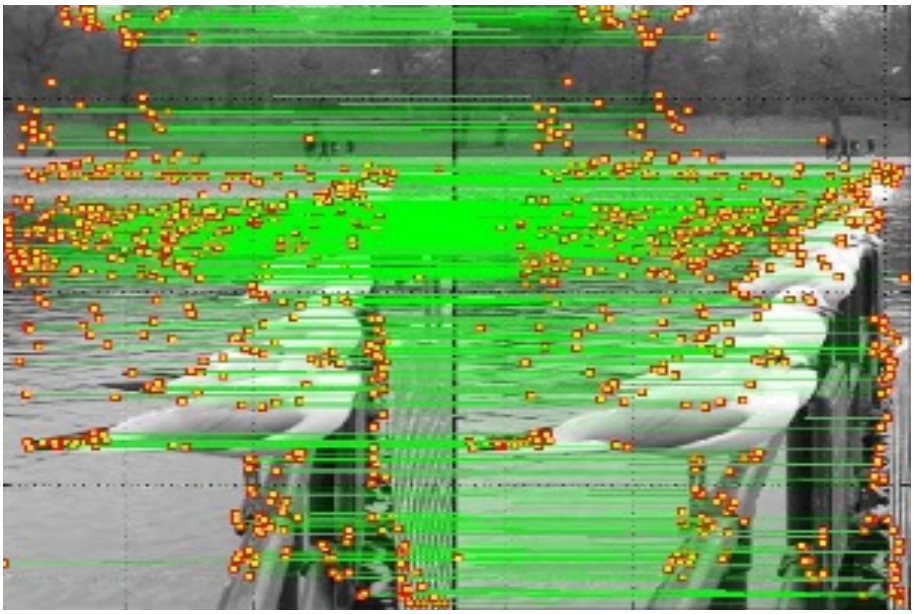

Figure 4: Proposed matching criteria results positive matches only

The application of the criteria tighten the support of standard SIFT. The increase in negative matches (and the corresponding decrement in positive matches) is the expected consequence of logically „ANDing" the criteria. It is important to note that only the matches in Figure 4(shown as green bars)which meet standard SIFT, epipolar line and disparity window criteria are considered as positive matches. The matching procedure described above has been repeated for 180stereo pairs and the numbers of positive and negative matches for each matching criterion are presented in Figure 6.

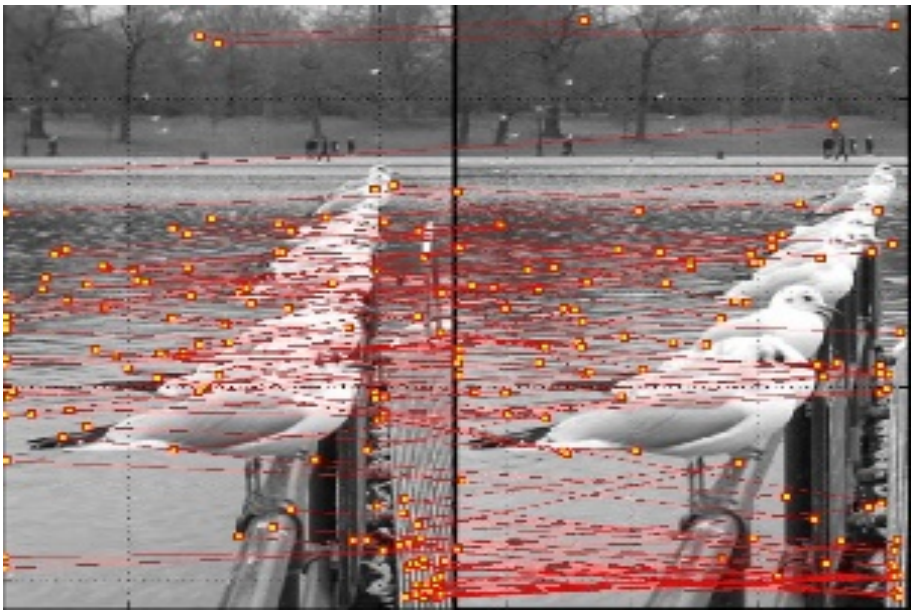

Figure 5: Proposed matching criteria results negative matches only

The bar chart in Figure6 has been plotted to demonstrate the effectiveness of new criteria in rejecting incorrect matches. The first bar in black represents the average number of matches generated by the 180 stereo pairs, which corresponds to matches that have met the standard SIFT criteria.

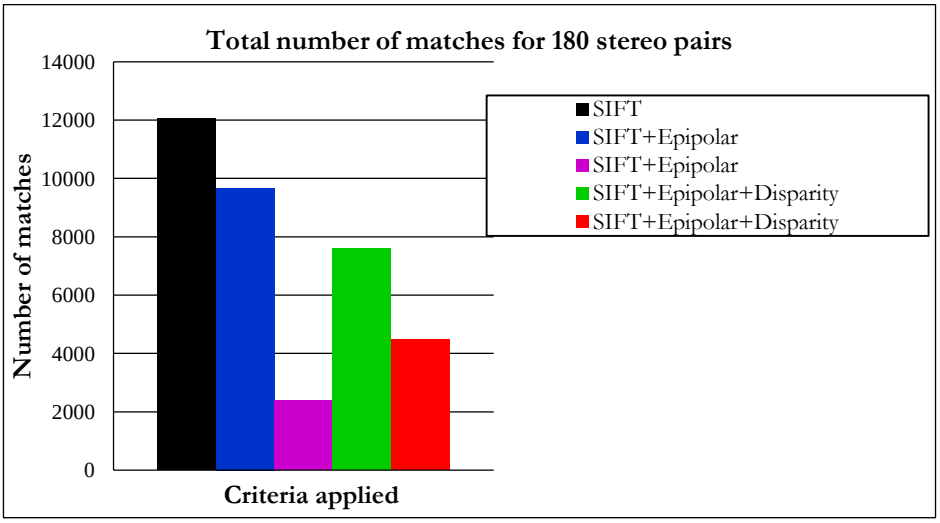

Figure 6: Total number of matches for 180 stereo pairs

Similarly, matches that have satisfied the epipolar line criterion, matches that have failed the epipolar line criterion, matches that have fulfilled the epipolar and disparity window criteria, and matches that have violated either or both new added criteria have been computed and plotted sequentially in the bar chart revealed in Figure 6.The proposed criteria have demonstrated that they can remove 37.2%

of unfaithful matches i.e. 19.8% are attributed to the epipolar line criterion and a further 17.4% attributed to the disparity window criterion.

4. Conclusions and Future Work

The material presented in this paper assessed the performance of optimized SIFT when dealing with stereo pairs. The potential of SIFT to locate correspondences in stereo pairs is established and quantified for 180 stereo pairs. The performance of SIFT is significantly enhanced by applying two additional criteria namely; a disparity window and an epipolar line constraint.. Each pair of images is analysed twice to accommodate either perspective view as the reference view. Experiments revealed that around 37% of unfaithful matches were removed. The appropriateness of the additional criteria is supported by the matching results organised in Figure 4, 5 and 6.

Solving the correspondences problem is an ill posed problem in computer vision applications. It has been established that performance of optimized SIFT significantly reduces when presented with spatially simple images. Therefore, a rigorous analysis of the SIFT parameters to increase the robustness and density of keypoints would enhance the fidelity the matching result. Also, it might be worthwhile to combine the optimized SIFT algorithm with other feature matching techniques so more keypoints are generated.

References

[1]. D.G. Lowe, "Distinctive image features from scale-invariant keypoints," *International Journal of Computer Vision,* vol. 60, no. 2, pp. 91-110, 2004.

[2]. Y. Chen and J. Z. Wang, "A region-based fuzzy feature matching approach to content-based image retrieval," *Pattern Analysis and Machine Intelligence, IEEE Transactions on,* vol. 24, pp. 1252-1267, 2002.

[3]. M. Brown, R. Szeliski and S. Winder, "Multi-image matching using multi-scale oriented patches," *in Computer Vision and Pattern Recognition, IEEE Computer Society Conferenceon*, vol. 1, pp. 510-517,2005.

[4]. D. Bespalov, W. C. Regli and A. Shokoufandeh, "Local feature extraction and matching partial objects," *Comput. -Aided Des.,* vol. 38, pp. 1020-1037, 2006.

[5]. Baumberg, "Reliable feature matching across widely separated views," *in IEEE Computer Society Conference on Computer Vision and Pattern Recognition*, 2000.

[6]. K. Mikolajczyk and C. Schmid, "An affine invariant interest point detector," *in European Conference on Computer Vision,*vol. 4, pp. 128–142, 2002.

[7]. Klaus, M. Sormann and K. Karner, "Segment-based stereo matching using belief propagation and a self-adapting dissimilarity measure," *International Conference on Pattern Recognition,*vol. 18, pp. 15-18, 2006.

[8]. J. Matas, O. Chum, M. Urban and T. Pajdla, "Robust wide-baseline stereo from maximally stable extremal regions," *Image Vision Comput,* vol. 22, pp. 761-767, 2004.

[9]. K. Mikolajczyk and C. Schmid, "A performance evaluation of local descriptors," *IEEE Trans. Pattern Anal. Mach. Intell.*, pp. 1615-1630, 2005.

[10]. C. B. Perez and G. Olague, "Learning invariant region descriptor operators with genetic programming and the f-measure," *in International Conference on Pattern Recognition*, 2008, .

[11]. C. Harris, "Geometry from visual motion," 1993.

[12]. C. Harris and M. Stephens, "A combined corner and edge detector," *in Alvey Vision Conference*, pp. 50, 1988.

[13]. D. G. Lowe, "Object recognition from local scale-invariant features," *in Iccv*, pp. 1150,1999.

[14]. P. Scovanner, S. Ali and M. Shah, "A 3-dimensional sift descriptor and its application to action recognition," *in Proceedings of the 15th International Conference on Multimedia*, pp. 357-360, 2007.

[15]. P. Moreno, A. Bernardino and J. Santos-Victor, "Improving the SIFT descriptor with smooth derivative filters," *Pattern Recog. Lett.,* vol. 30, pp. 18-26, 2009.

[16]. Z. Qi, R. Ting, F. Husheng and Z. Jinlin, "Particle Filter Object Tracking Based on Harris-SIFT Feature Matching," *Procedia Engineering*, vol. 29, pp. 924-929, 2012.

[17]. Y. Ke and R. Sukthankar, "PCA-SIFT: A more distinctive representation for local image descriptors," *in IEEE Computer Society Conference on Computer Vision and Pattern Recognition*, 2004, .

[18]. H. Bay, A. Ess, T. Tuytelaars and L. Van Gool, "Speeded-up robust features (SURF)," *Comput. Vision Image Understanding*, vol. 110, pp. 346-359, 2008.

[19]. Z. Feng, B. Yang, Y. Chen, Y. Zheng and T. Xu, "Features extraction from hand images based on new detection operators," *Pattern Recognit*, 2010.

[20]. Fusiello and L. Irsara, "Quasi-euclidean uncalibrated epipolar rectification," in *International Conference on Pattern Recognition (ICPR),* 2008.